NASA CONTRACTOR REPORT

NASA CR-1086

NASA CR-1086

DUAL RADIOMETER ASSEMBLY FOR PROJECT SCANNER

by Stillman C. Chase

Prepared by
SANTA BARBARA RESEARCH CENTER
Goleta, Calif.
for Langley Research Center

NATIONAL AERONAUTICS AND SPACE ADMINISTRATION • WASHINGTON, D. C. • JULY 1968

NASA CR-1086

DUAL RADIOMETER ASSEMBLY FOR PROJECT SCANNER

By Stillman C. Chase

Prepared under Contract No. NAS 1-3827 by
SANTA BARBARA RESEARCH CENTER
Goleta, Calif.

for Langley Research Center

NATIONAL AERONAUTICS AND SPACE ADMINISTRATION

For sale by the Clearinghouse for Federal Scientific and Technical Information
Springfield, Virginia 22151 – CFSTI price $3.00

CONTENTS

ILLUSTRATIONS

ILLUSTRATIONS (Cont)

TABLES

Section 1

INTRODUCTION

This report concludes the work performed by the Santa Barbara Research Center for the Langley Research Center under NASA Contract NAS 1-3827.

The intent of the report is to summarize the design and performance of the Dual Radiometer Assembly, essentially with information that has already been written in other project reports, and to describe the areas of difficulty encountered during the procurement, fabrication, assembly, and test phases of the program. Many of these areas, not apparent at the outset of the program, should be of particular interest to the reader, not so much because it may be necessary to reproduce more instruments of this design but because the information may be useful for future projects.

ACKNOWLEDGMENT

The writer welcomes this opportunity to thank H. Curfman, W. Dixon, J. Dodgen, and T. McKee of the Langley Research Center for their technical direction of the project. Their help and perseverance contributed greatly to the success of the Scanner program.

The writer especially thanks G. Bunson, D. Errett, H. Hatzenbeler, B. Olson, F. Panel, J. Reed, A. Schofield, and J. Young, all of the Santa Barbara Research Center, who helped design and test the Dual Radiometer instruments.

Section 2

GENERAL DESCRIPTION

The radiometer assembly depicted in Figure 1 is part of a spin-stabilized sub-orbital space probe payload that was used to make measurements in two far-infrared wavelength bands of the earth's horizon radiance profile. The equipment consists essentially of two vertical telescopes with flat object space scan mirrors to scan across the horizon as the vehicle spins.

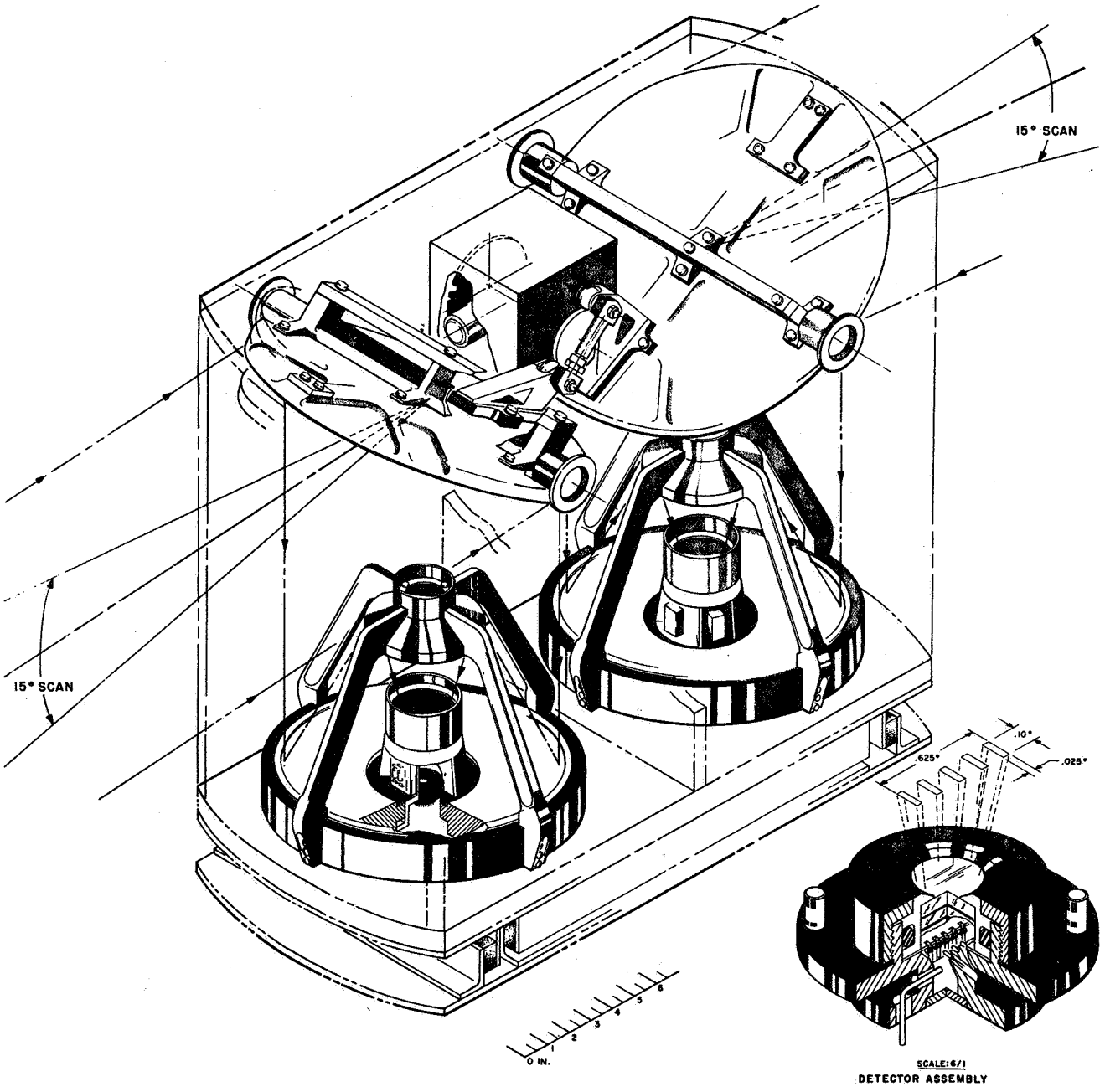

Figure 1. Dual Radiometer for Project SCANNER

The telescopes are 9-inch diameter reflecting types using true aspheric surfaces on both the primary and secondary mirrors. Diffraction limited, the resolution is limited to 0.025° in the longer wavelength band. The instantaneous field of view (IFOV), 0.62° in elevation and 0.1° in azimuth, is covered by a five-element bolometer detector array. Each immersed element has a FOV of 0.025° in elevation and 0.1° in azimuth, and they are spaced 0.15° apart in elevation.

Each of the two telescope assemblies covers a different spectral band determined by spectral bandpass filters; in one case 14 to 16 microns and in the other 20 to 35 microns. Two scan mirrors, one for each telescope, are driven in synchronism by a common gear train linkage assembly. The 15° sawtooth scan is accomplished at 10°/sec. The scan is centered about a predetermined horizontal depression angle of 22° to 26°.

The electronics consist of amplifiers for the ten detector channels, and position pickoff circuitry to define the scan position. There are temperature sensor circuits for each telescope assembly.

PERFORMANCE SPECIFICATIONS

The performance specifications, summarized in Table 1, are taken from the Langley Research Center Specification L-3771, dated 17 April 1964. Actual performance of the systems compared to these requirements is discussed in Section 5.

Table 1. Performance Specifications Summary

OPTICS	
Focal Length:	14.7 in.
Aperture:	9 in.
Resolution:	$<0.025^\circ$ at 50%. $<0.008^\circ$ between 5% and 50%.
Field of View:	0.025° elevation x 0.1° azimuth.
FILTERS	
Radiometer A:	Centered at $15\mu \pm 0.2\mu$. $<2\mu$ wide at 50% response. $<3\mu$ wide at 1% response.
Radiometer B:	A band $<20\mu$ wide at the 50% response points situated between 20μ and 40μ. $<1\%$ response beyond 18μ and 44μ.
DETECTORS	
Array Optical Field of View:	Five elements — each 0.025° elevation x 0.1° azimuth. Spaced in elevation $0.15^\circ \pm 0.005^\circ$.
Frequency Response:	1 to 500 radians/sec (1/6 to 80 Hz).
ELECTRONICS	
Frequency Response	
Low Frequency:	3 db point, 1 ± 0.1 radian/sec (1/6 Hz) — positive slope 6 db/octave.
Plateau:	Flat to 0.25 db.
High Frequency:	6 db point, 500 ± 25 radians/sec (80 Hz) — negative slope 12 db/octave.

Table 1. Performance Specifications Summary (Cont)

ELECTRONICS (Cont)	
Signal Levels	
Radiometer A:	2.5 ± 0.1 volts, alternately viewing 240°K and 100°K.
Radiometer B:	2.5 ± 0.1 volts, alternately viewing 240°K and 100°K.
Linearity:	±5%.
Stability:	±1.5%.
Noise:	< 50 mv.
Outputs:	100K to 200 pf, biased +2.5 volts (FM-FM IRIG stnd) (0 to 5 volts).
SCANNER	
Plane of Motion:	X-Y plane to within ±3 minutes (±0.05°).
Scan Angle:	15°, +0.5° -0°, centered about depression angle to ±0.1°.
Depression Angle:	22° to 26° accuracy, ±0.1°, below Y axis. (Scan angle is nominally 26°, but can be adjusted by modification kit.)
Scan Motion:	15° sawtooth; 0.25° turnaround in 100 msec.
Scan Repeatability:	±0.01° using four designated position references. (Total allowable post-flight position determining error, 0.015°.)
Scan Motion Between Radiometers:	Synchronized to < 1°.
Scan Rate:	10° ± 0.25°/sec — possible modification to 5° ± 0.13°/sec.

Table 1. Performance Specifications Summary (Cont)

POSITION READOUT	
Position Readout:	Combined with channels No. 1 and No. 6. The four position readout points will be coded as follows: Zero output for 1 msec rise to coded outputs in 0.1 msec. Maintain each code output for 2 msec. Coded outputs will be 1, 2, 3, and 4 volts, the rise time being the time reference. When combined with channel No. 1 or No. 6, there will be <4 msec loss of channel signal information.
TEMPERATURE READOUT	
Temperature Range:	50°F to 100°F.
Slope:	0.1 volt/degree.
Accuracy:	± 1°F.
Output Format:	0 to 5 volts, IRIG stnd.
Output Impedance:	10 kilohms.
INTERNAL CALIBRATOR:	+2.0 ± 0.1 volt pulse during scan reversal (low elevation).
OPERATING TEMPERATURE/ HUMIDITY RANGE:	50°F to 90°F at 95% relative humidity.
STORAGE TEMPERATURE/ HUMIDITY RANGE:	10°F to 130°F at 95% relative humidity.
WEIGHT:	92 lb ± 3 lb.
INTEGRATION	
Available Power:	+28 volts dc.
Launch Power:	Not to exceed 0.5 amp. (Scan phase must not exceed 0.90 amp.)
RADIO INTERFERENCE:	5.7 kmHz, 400 watts peak – 600 milliwatts average.

Section 3

DESIGN AND ANALYSIS

This section contains the analysis upon which the design was based.

SYSTEM ANALYSIS

Signal-to-Noise Calculations

Irradiance at Aperture. - The irradiance in the wavelength band $\Delta\lambda$ arriving at the aperture of the radiometer from a blackbody source at temperature T which fills the FOV can be written as:

$$H(T, \Delta\lambda) = W(T)\, F(T, \Delta\lambda)\, \Omega \text{ watt/cm}^2$$

where $W(T)$ is the radiance being emitted from a blackbody source at temperature (T) (watts cm^{-2} $steradian^{-1}$)

$F(T, \Delta\lambda)$ is the fractional amount of radiance being emitted in the wavelength band $\Delta\lambda$ from a blackbody source at a temperature T

Ω is the FOV of the radiometer (steradians)

For the blackbody temperatures 240°K and 100°K:

$$W(240°K) = 5.9 \times 10^{-3} \text{ watt cm}^{-2} \text{ ster}^{-1}$$

and

$$W(100°K) = 1.8 \times 10^{-4} \text{ watt cm}^{-2} \text{ ster}^{-1}$$

For Radiometer A

$$\Delta\lambda = 14 \text{ to } 16 \text{ microns}$$

$$\Omega = 7.6 \times 10^{-7} \text{ steradians } (0.025° \times 0.1°)$$

The spectral utilization factors are:

$$F(240°K, 14\text{-}16\mu) = 0.10$$

$$F(100°K, 14\text{-}16\mu) = 0.012$$

The difference in irradiance arriving at the radiometer aperture from a 240°K blackbody and a 100°K blackbody is, therefore,

$$\Delta H_A = 4.5 \times 10^{-10} \text{ watt/cm}^2$$

For Radiometer B:

$$\Delta\lambda = 20 \text{ to } 35 \text{ microns}$$

$$\Omega = 7.6 \times 10^{-7} \text{ steradians } (0.025^\circ \times 0.1^\circ)$$

and

$$F(240^\circ K, 20\text{-}35\mu) = 0.26$$

$$F(100^\circ K, 20\text{-}35\mu) = 0.38$$

Therefore:

$$\Delta H_B = 1.11 \times 10^{-9} \text{ watt/cm}^2$$

Radiometer Noise Equivalent Irradiance (NEI). - The NEI of the radiometer using an immersed bolometer detector can be written as:

$$NEI = \frac{4CK\gamma\sqrt{\Delta f}}{\pi R d^2 t_o}$$

where C is the factor necessary to convert the quoted bolometer responsivity for a single flake to one which will apply to a practical system and includes:

1. A factor of 2 to account for signal loading by the compensating flake.
2. A factor of 1.14 to account for immersion losses; i.e., compared to an unimmersed bolometer having a KRS-5 window.
3. A factor of 1.1 due to operating the bolometer at less than the maximum recommended bias voltage.

K is the bolometer bridge-noise voltage for a 1-Hz bandwidth (volts $Hz^{-1/2}$).

γ is the preamplifier degradation factor.

Δf is the effective noise bandwidth of the system (Hz). $\Delta fn = \frac{\pi}{2} fc$ where fc is the corner frequency for a -6 db/octave low-pass filter.

R is the quoted responsivity for a single flake bolometer (volts/watt).

d is the free aperture diameter (cm).

t_o is the effective transmission factor of the optics.

Table 2 gives the values of the above quantities used for the original design. The right hand side of the table gives those values actually obtained for the final systems (F-3 in this case). Section 5 explains the reasons for the differences.

Table 2. System Parameters

Proposed	Actual
$C = 2.5$	$C = 2.85$
$K = 1.65 \times 10^{-7}$ volts $Hz^{-\frac{1}{2}}$ (2.5 megohm)	$K = 2.4 \times 10^{-7}$ volts $Hz^{-\frac{1}{2}}$ (4-megohm flake with $N_B/N_o = 1.2$)
$\gamma = 1.26$ (2 db preamplifier)	$\gamma = 1.26$ (2 db preamplifier)
$\Delta f = 80$ Hz (500 radians/sec)	$\Delta f_A = 94$ Hz for Rad A (14-16μ) $\Delta f_B = 110$ Hz for Rad B (20-40μ)
$R_A = 4.3 \times 10^3$ volts/watt (0.1 mm x 0.1 mm bolometer) $R_B = 2.86 \times 10^3$ volts/watt (0.15 mm x 0.15 mm bolometer)	$R_A = R_B \cong 7500$ volts/watt (0.1 mm x 0.1 mm "thin" bolometer)
$d = 20.5$ cm (9-inch aperture with 20% obscuration loss)	$d = 20.5$ cm (9-inch aperture with 20% obscuration loss)
$t_o = 0.315$ for Channel A (0.33 average filter transmission, 0.95 reflectance - three mirror surfaces) $t_o = 0.33$ for Channel B (0.35 average filter transmission, 0.95 reflectance - three mirror surfaces)	$t_{oA} \cong 0.275$ average for Channel A between 14 and 16μ $t_{oB} \cong 0.23$ average for Channel B between 20 and 35μ
Therefore,	Therefore,
$NEI_A = 1.05 \times 10^{-11}$ watt/cm^2	$NEI_A = 1.23 \times 10^{-11}$ watt/cm^2
$NEI_B = 1.5 \times 10^{-11}$ watt/cm^2	$NEI_B = 1.59 \times 10^{-11}$ watt/cm^2

Radiometer Signal/Noise Output. - The signal-to-noise ratio developed at the output of a channel of the Dual Radiometer for a ΔH change in irradiance at the aperture of the radiometer can be written as;

$$S/N = \frac{\Delta H}{NEI}$$

Using the previously calculated values of NEI,

Proposed	Actual
$S/N_A = 45$	$S/N_A = 37$
$S/N_B = 74$	$S/N_B = 69.5$

when the radiometers alternately view a 240°K and a 100°K extended blackbody source.

With the gains in Radiometers A and B adjusted so that the radiometer signal is equal to 2.5 volts, the noise output voltage, Vn, was

$$Vn_A = 0.067 \text{ volt rms}$$

$$Vn_B = 0.036 \text{ volt rms}$$

It should be borne in mind, however, that the peak-to-peak noise is more significant than the rms value since when calibrating it is the peak-to-peak noise that is seen on the scope face from which an rms value must be determined. A factor of approximately 3 between peak-to-peak and rms noise is not unreasonable. The S/N ratios actually achieved are a result of design tradeoffs discussed on page 82.

Scan Rate Versus Frequency and Phase Response Tradeoffs

The scan rate and electrical bandwidth are both limited by the available S/N ratio. The result of this is that a compromise must be reached between the amount of data taken (scan speed) and the fidelity of the output to an ideal trapezoidal horizon gradient input.

The actual case is somewhat as depicted in Figure 2. The decay in amplitude is a result of the differentiation of the low-frequency cutoff RC network. The integration action on the leading edge of the trapezoidal input is due to the upper-frequency cutoff and is shown for both a 0.5° and a 1° infrared horizon edge. Because the limited bandwidth causes electrical delays which represent displacement of the apparent horizon edge, it is necessary to evaluate the delays carefully. The method describing this

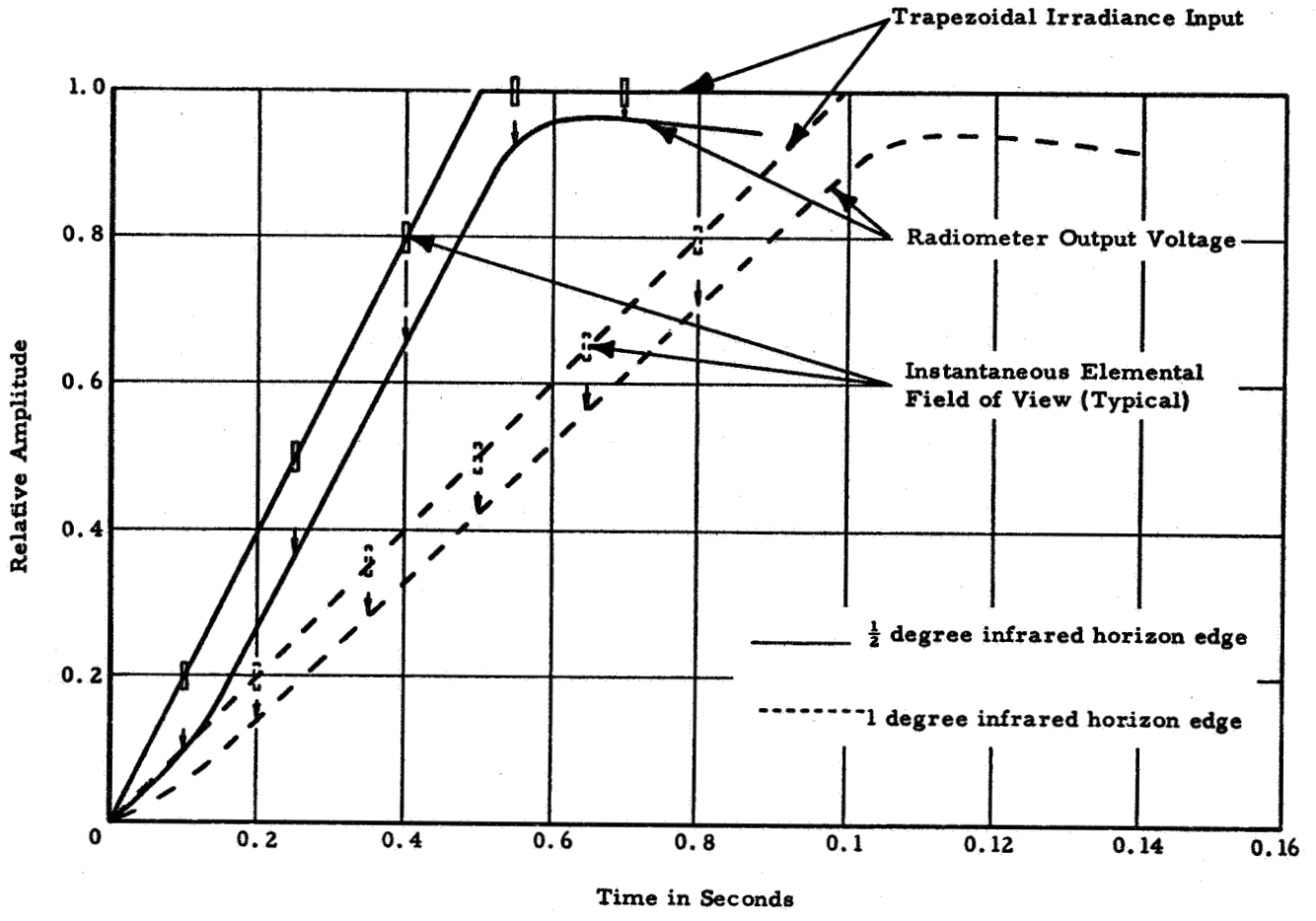

Figure 2. Effect of Radiometer Bandwidth on Leading Edge of Trapezoidal Irradiance Pulse

technique is discussed in Section 5. Typical measured delays are about 3.5 msec which if not corrected for would produce an apparent angular displacement of about 0.035° or roughly twice the maximum allowable error for the experiment.

MECHANICAL ANALYSIS

Frame/Isolation Mount

Since considerable effort was spent obtaining a suitable isolation mount, both through liaison with the vendor and work in-house, this subject is discussed separately in Section 4, under "Procurement of Mechanical Items."

Scan Drive Mechanism

The scan mirrors are driven by a cam and follower mechanism shown schematically in Figure 3. Followers G and K are rigidly attached to scan

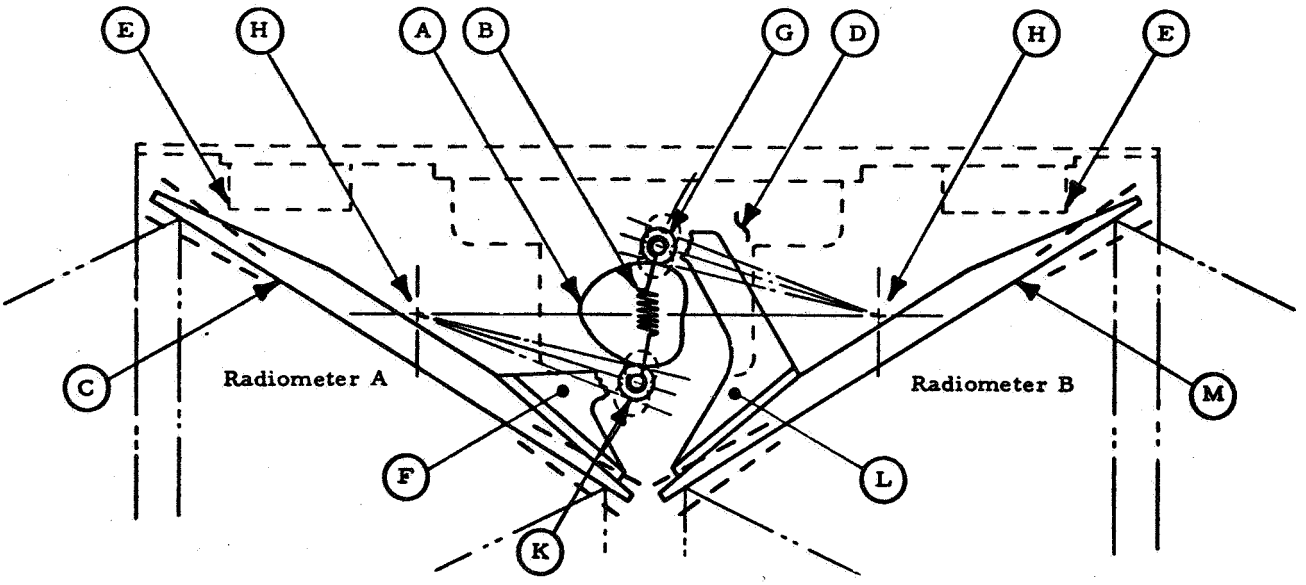

A. Cam - 1 revolution = 1 mirror scan cycle

B. Tension Link - Supplys constant spring load for positive drive motion

C. M. Scan Mirror - Beryllium material, interchangeable

D. Drive Housing - Contains motor, gear train position readout mechanism

E. Caging Mechanism - Located in this area, provides lock at end of mirrors

F. L. Follower Arms - Adjustable for centering scan motion and to change depression angle.

G. K. Cam Followers

H. Flexural Pivots

Figure 3. Scan Mirror Mechanism Schematic

mirrors M and C, respectively, by supports L and F. Hence, as the cam rotates its change in profile produces a rotation of the scan mirrors about their pivot axes. The tension link B connects the two followers G and K and ensures a positive rolling contact between the followers and the cam profile under all conditions.

It was originally anticipated that the scan mirror pivots would be of the Bendix flexure type. However, a point-by-point analysis of factors involved led to the selection of bearings in this location. The use of flexural pivots would require an additional adjustment mechanism to return the pivot to its relaxed position for every depression angle setting and/or adjustment. Also, the factor of safety under the environmental loadings is higher using the bearings, and the torque required is substantially lower.

Since the bearing is selected primarily on the basis of the environmental stresses (i. e., shock), it will be greatly derated under operating conditions. This, coupled with the relatively short life requirements, makes use of a bearing for oscillating movement feasible.

Centering of the scan range and adjustment of the depression angle are both determined by the angular position of the scan mirror surface relative to a line through the centers of the mirror pivot and the cam follower. Hence, both may be adjusted readily by inserting an appropriate spacer between the cam follower support and the scan mirror. Spacers made to normal fabrication tolerances will permit this adjustment to be made in increments of ±0.01°.

Since, as indicated previously, the scan mirrors complete one cycle for each revolution of the camshaft, the sweep rate is directly dependent upon the camshaft speed. Using a sweep rate of 10° per second, a 15° sweep range, and a reversal time of 0.1 second results in a scan cycle period of 3.2 seconds or a camshaft speed of 18.75 rpm.

The camshaft is driven through a gear reduction by a 26-volt, 100-cps hysteresis, synchronous motor. The motor synchronous speed is 6000 rpm. The gearing consists of two stages and an idler. The motor pinion drives through the idler to a spur gear on a worm shaft, which in turn drives the worm gear mounted on the camshaft. Using 3.2:1 reduction for the spur gear first stage and a 100:1 reduction for the worm and gear provides the required camshaft speed of 18.75 rpm.

Precise speed control is obtained by driving the motor with a 100-Hz square wave which is derived from a resonant fork oscillator operating at 3200 Hz ± 0.5%.

The linearity of the 15° FOV scan is primarily dependent on the accuracy of the cam profile which was held to ±0.0002-inch tolerance at fabrication. Other factors affecting this parameter are: 1) radial play of the cam follower and mirror pivot bearings, and 2) backlash in the gear train. The gear train design is such that only the worm gear stage backlash can contribute to this error. This stage is designed for a maximum backlash of 0.0005 inch. The maximum total error in scan angle which can occur from the above factor is less than 0.002° which will be repeatable with time.

The sweep rate variation is directly dependent on motor speed variation which will be ±0.5%. Over the 15° scan this is a maximum deviation of 0.075° or ±0.05°/sec.

The repeatability and predictability of the scan position, between any two points (during the 15° scan) with respect to time will be directly dependent on the sweep rate. Since the sweep variation is 0.05°/sec, or based on a 10°/sec rate, the variation is from 10.05°/sec to 9.95°/sec.

The maximum allowable error in repeatability per the specification occurs at a point in time halfway between reference points — or over an angle of 15°/8 = 1.875°, which is equivalent to 1.875°/10°/sec = 0.1875 sec.

At the minimum sweep rate, 9.95°/sec × 0.1875 sec = 1.8656° for minimum rate.

1.8750 - 1.8656 = 0.0094° variation or ±0.0094° with respect to time when measured using the nearest designated point as reference.

If the lost motion effects in the bearings, cam and gear train were assumed to be nonrepeatable, the variation with respect to time, measured from the nearest reference point, would be 0.0105°.

During systems test, mechanical jitter was traced to the scan system. This problem and its solution are discussed on page 61.

Bearings and Lubrication

The cam and follower surfaces were lubricated with "Microseal" process 100-1 per HP7-18. This is a proprietary solid-film lubricant applied by a high velocity impingement method. The material consists of a graphite base compound blended with soft metals in a liquid form which cures to a ceramic like surface. This process has been tested in vacuums of 1×10^{-8} Torr for periods of one week without appreciable change in coefficient of friction.

The steel motor pinion and the first-stage gear operated with a Fiberflas (glass cloth-melamine) idler gear lubricated with a molybdenum disulfide solid-film lubricant. The steel worm operated against a phosphorus-bronze worm gear lubricated with grease per MIL-G-3278. The entire gear train assembly is enclosed in a dust cover which prevents contamination of the optics by the lubricant, or the gear train bearings by outside contaminants.

OPTICS ANALYSIS

During the preliminary design phase of the program, several different types of optical systems were analyzed. Table 3 presents a summary of what can be expected from these systems.

When the diffraction pattern plus the geometrical image is considered, it becomes apparent that only two of the five systems have sufficiently good images. These are the double aspheric and the Wynne-Rosin systems.

Table 3. Summary of Optical Designs from Geometrical Optics (Ray Trace) Consideration

	(1) Parabolic	(2) Double Aspheric	(3) Cassegrain	(4) Dall-Kirkham	(5) Wynne-Rosin
On-Axis Image	Perfect	Perfect	0.27 mr	0.25 mr	0.1 mr
Image for 0.00522 rad	0.4 mr	<0.07 mr	0.4 mr	0.7 mr	0.13 mr
Number of Optical Surfaces	1	2	2	2	6
Nature of Surfaces	(1) Parabolic (2)	Aspheric Aspheric	Parabolic Aspheric	Aspheric Spherical	Parabolic Spherical 2 Lenses (Spherical)
Obscuration Percent of Area	10%	20%	20%	20%	20%

From a fabrication viewpoint, the Wynne-Rosin system is the simplest. However, it requires refractive materials, and it is doubtful that the available materials for operation in the 14- to 16-micron and the 20- to 35-micron regions would survive the required environmental conditions. Therefore, even though the fabrication problems involved with a double aspheric design proved to be formidable indeed (see "Optics Procurement," Section 4), it was apparent that it was the only design that would meet all the requirements.

The primary and secondary mirrors are designed to give a small geometrical image across the ±0.3° field. Figures 4 and 5 illustrate plots of computed ray trace data for three field angles. It is to be noted that the image size is approximately 0.0005 inch in diameter across the ±0.3° field, or an equivalent angular image size of 0.002°.

Due to mechanical and environmental interfaces, beryllium was selected for the mirror material. Its thermal expansion coefficient is $\alpha = 6.4 \times 10^{-6}/°F$. Steel 4140 with $\alpha = 6.15 \times 10^{-6}/°F$ was selected for the spider material. Operating over the required 50°F to 90°F temperature range, the mismatch of α's results in a change of primary-secondary

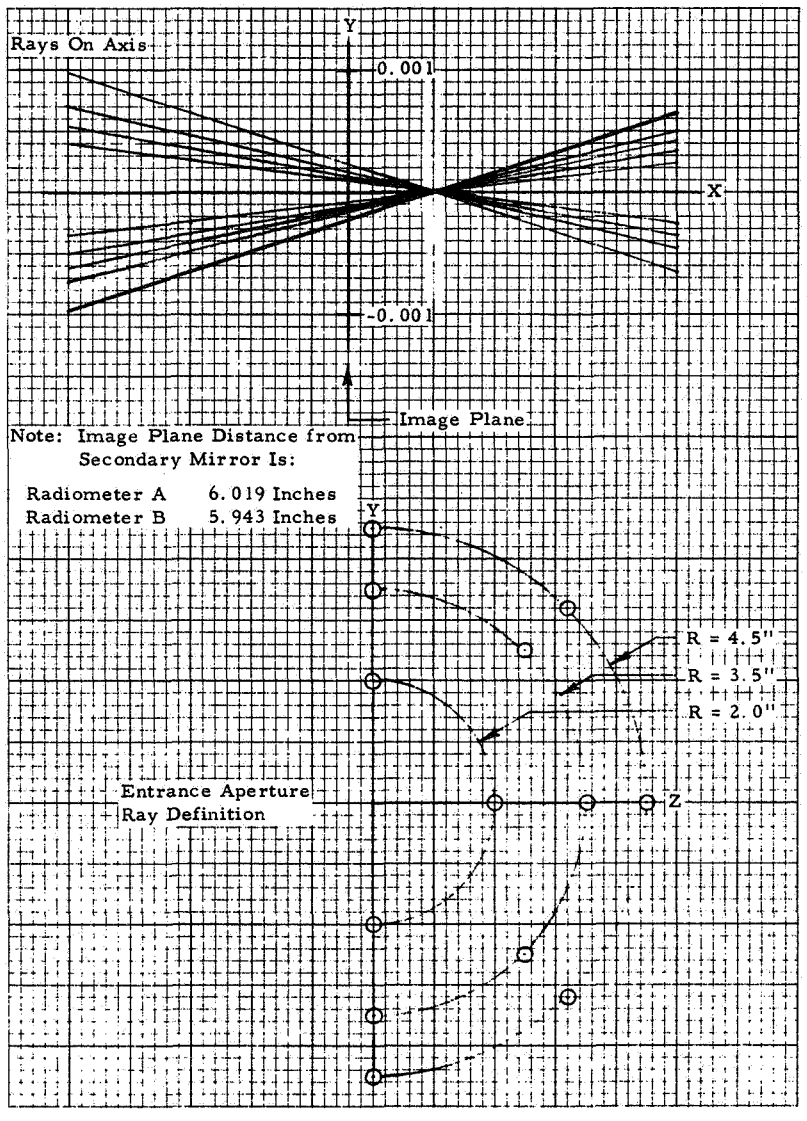

Figure 4. Optical Ray Trace

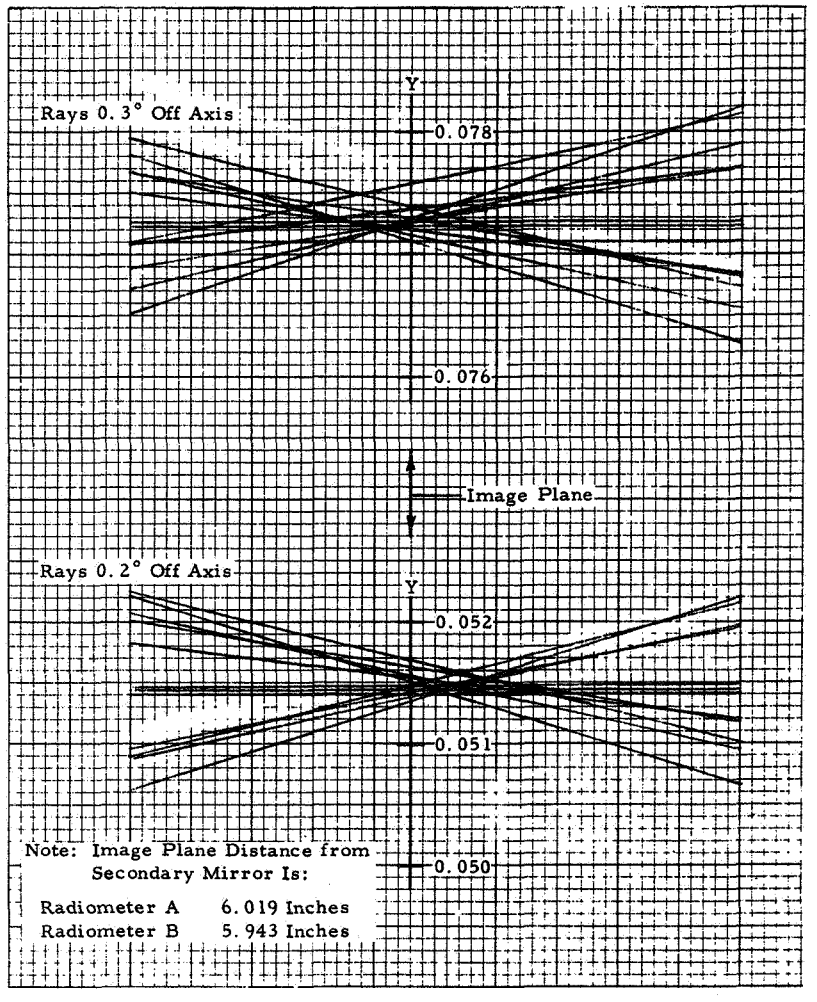

Figure 5. Optical Ray Trace

mirror separation of 0.00003 inch which is not compensated for by the corresponding change in mirror dimensions. Relating this to the optical design, the change of focus relative to the field stop is 0.00006 inch. Reference to Figures 4 and 5 shows this to be a negligible effect.

Diffraction Effect Analysis

Calculations of the diffraction pattern for the primary-secondary configuration having a 9-inch aperture with a 4-inch central obscuration have been made. Figure 6 gives the response for a geometrically perfect image from a system with obscuration $\epsilon = 0.445$ when passed across a 0.025° rectangular aperture.

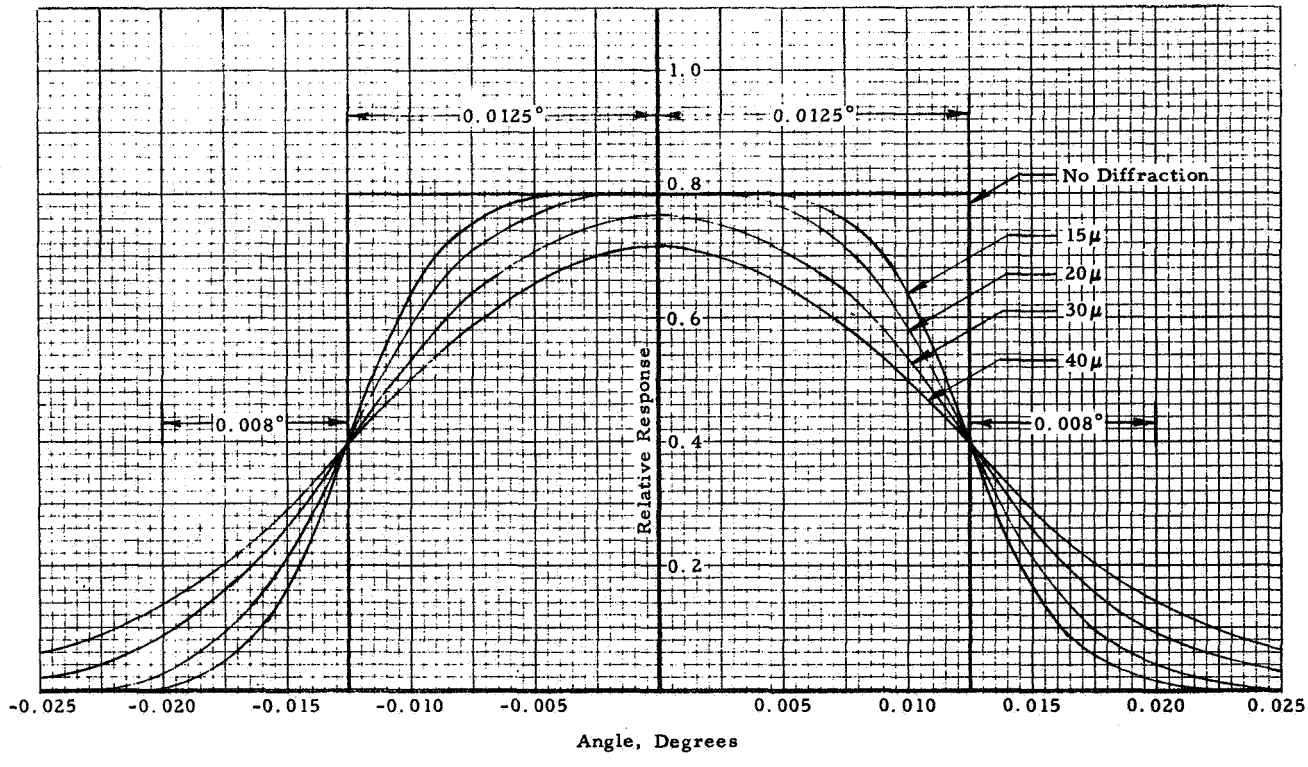

Figure 6. Effect on Response Due to Diffraction Effects with a Central Obscuration $\epsilon = 0.445$

Detector Optics

The optical filters, once installed, form a part of the detector assembly. The filter elements are sealed into a metal cap using Fuller's Resiweld epoxy. Teflon washers separate the elements, preventing the epoxy from flowing between the element surfaces by capillary action.

Sealing the filters serves two purposes:

1. It permits the more sensitive optical filter and detector surfaces to be protected from humidity by filling with dry nitrogen.
2. It protects the small apertures of the field stop from contamination.

The immersion lenses relay the radiation from the field stop onto the small detector flake. To a first approximation this is done so that the primary mirror entrance aperture is imaged onto the thermistor flake. The immersion lens and field stop aperture (long dimension) are comparable in size; therefore, the distance between them must be minimum while still preventing mechanical interference during environmental testing. The separation of 0.001 inch allows a negligible amount of energy to be lost due to incoming energy missing the immersion lens.

Optical Alignment Consideration

The Plane of Motion Specification, paragraph 3.2.1, states that "The FOV motion shall be parallel to and in the radiometer X-Y plane within ±3 minutes."

Factors that contribute to this alignment condition are:

1. Scan mirror mounting.
2. Parallelism of the plane of the primary mirror mounting pads to the Dual Radiometer-Spacecraft interface plane.
3. Centering of the central field stop aperture relative to the primary bore that positions the detector package.
4. Centering of the optical image relative to the primary mirror bore that positions the detector package in the X-Z plane.

All of these dimensions are maintained through machining tolerances. If all were to add in the same direction, 265 seconds of arc or 0.0013 radians would result. This value is in excess of the allowable alignment tolerance of 180 seconds.

To compensate for the entire misalignment would require a 0.010-inch wedge shim be placed at the primary mirror mounting pads. In actual fact, however, no problems were encountered with any of the radiometer systems.

The second alignment feature relates to optimum focusing across the field. An 8-minute wedge angle between the image plane and the field stop

plane would result in an out-of-focus condition at the edge of the field by approximately 0.0002 inch. Figures 4 and 5 show that this would result in a geometrical image blur circle increase of less than 0.0001 inch. Again, no problems were encountered in actual systems.

Design Parameters for Optical Filters and Detectors

For simplicity it is desirable that Radiometers A and B have the same primary-secondary mirror configuration. This common design assumes a given spherical aberration introduced by the optical filters. Thus, it is necessary to define the filter substrate thickness for each of the radiometers to obtain optimum spherical aberration correction for both cases.

The 20- to 35-micron filter was defined first because it introduces the greatest amount of aberration. The Optical Coating Laboratory, Inc. (OCLI), Santa Rosa, California, recommended a minimum thickness of 0.060-inch silicon substrate for the 20-micron cut-on filter. Also, to make the desired cutoff characteristic, there is a 0.100-inch thick piece of KBr. The measured response of this filter used in the F-3 system is shown in Figure 7.

The longitudinal shift introduced by the filter was calculated to be

$$\Delta S = 0.0017 \text{ inch}$$

OCLI also indicated that on the 14- to 16-micron bandpass filter three substrates were needed, namely

Ge, 0.060-inch thick
Ge, 0.060-inch thick
Irtran 4, 0.080-inch thick

These substrates resulted in a longitudinal shift of

$$\Delta S = 0.0019 \text{ inch}$$

Ray tracings indicate that equivalent images are obtained with either of the filters. Figure 7 also shows the measured transmittance for the 14- to 16-micron filter.

The complete spectral response of the entire optical system (F-3) is shown in Figures 8 and 9.

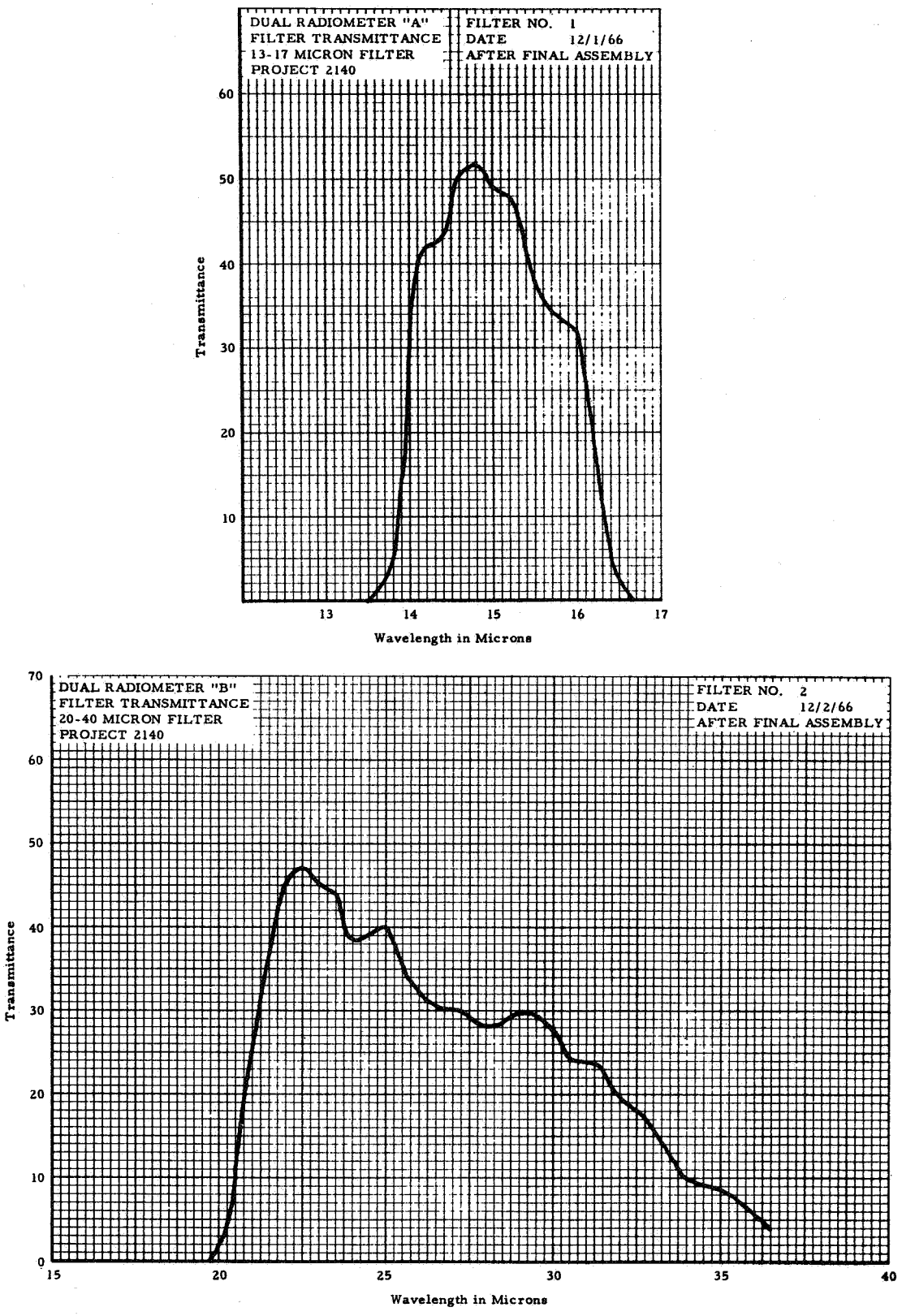

Figure 7. Spectral Filter Transmittance
F-3 Dual Radiometer

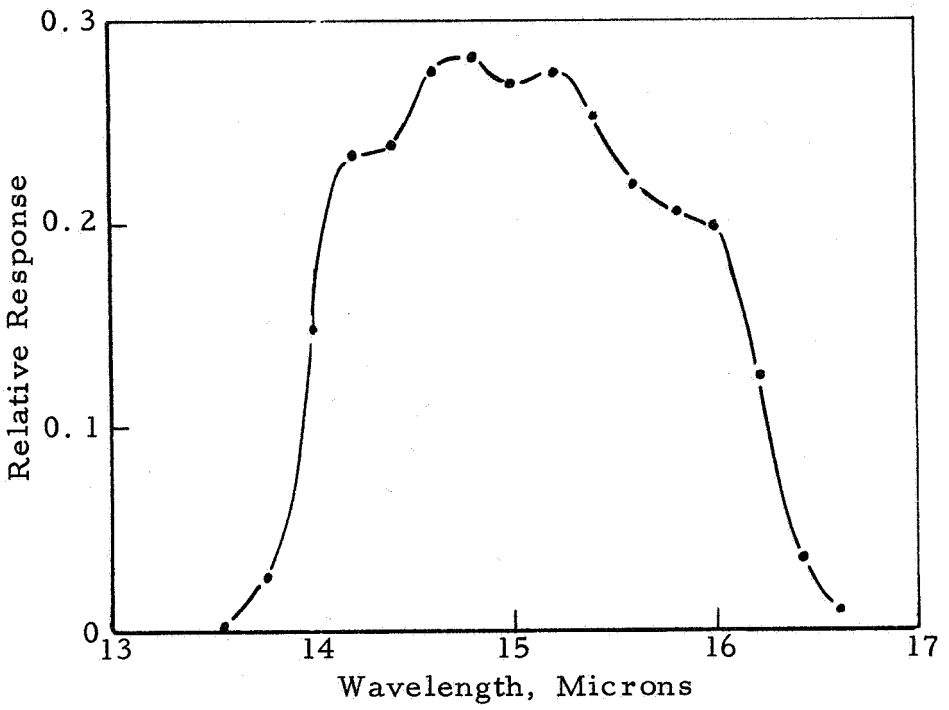

Figure 8. Spectral Response, F-3 Radiometer, 14 to 16 Microns

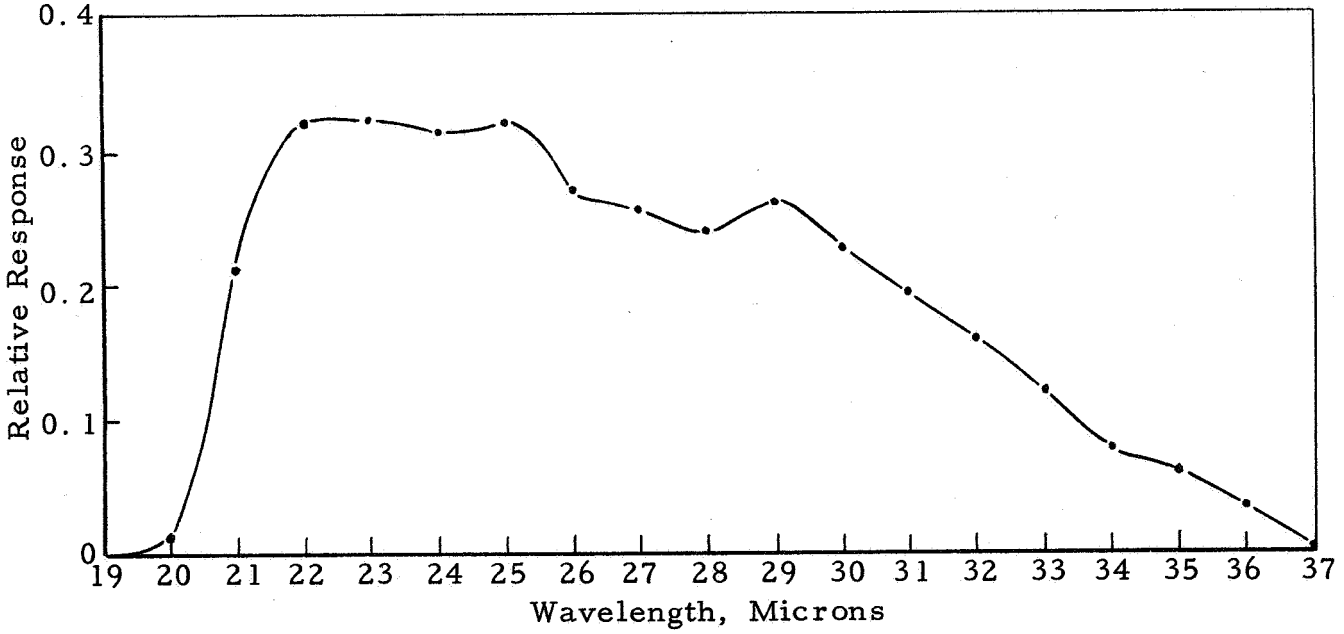

Figure 9. Spectral Response, F-3 Radiometer, 20 to 35 Microns

ELECTRONICS DESIGN

The electronics portion of the Dual Radiometer consists of ten bolometer-amplifier channels, scan position marker circuit, precision scan driver, internal calibrate circuits, and a power regulator.

Requirements for the electronics are given in Table 4.

Table 4. Electronics Design Requirements (Complete System)

Low-Frequency Response:	3 db down at 0.16 Hz ± 0.16 Hz with +6 db/octave slope.
High-Frequency Response:	3 db down at 80 Hz ± 4 Hz with -6 db/octave slope.
Plateau Response:	Plateau response will be flat to within ±0.25 db.
Gain Stability:	Gain will be stable to within ± 1.5%.
Noise Figure:	2 db or less where the noise bandwidth is that of the system.
Output Voltage Swing:	Output of the last amplifier shall be capable of swinging at least ±2 volts.*
Temperature Range:	+50°F to +90°F.

Preamplifier and Amplifier

Considerations of major importance to the design of the preamplifier were low noise, closely controlled frequency response characteristics, and gain stability with temperature.

The preamplifier consists of a field-effect transistor (FET) selected for low noise followed by two bipolar transistors. DC coupling is used with both ac and dc feedback to stabilize the gain and bias stability.

The preamplifier is followed by two additional amplifiers which, together with the preamplifier, give a total system voltage gain of 20,000.

*At the request of the Langley Research Center, this was increased to ±2.5 volts.

The second amplifier is identical to the preamplifier, while the third amplifier is modified to perform the required voltage swing. The schematic diagram for the amplifier drain is illustrated in Figure 10.

The preamplifier, consisting of Q6, Q7, and Q8, uses as the input stage an N-channel Crystalonics 2N3089A field-effect transistor, a device selected for low noise. Bias for this stage, approximately 1 volt, is provided partly by self-bias and partly by Q8 emitter current. The drain voltage is set at 7.5 volts for each preamplifier by adjusting R8 during assembly. This procedure allows for individual variations of the field-effect transistors. The following stage uses a very low-noise diffused silicon, planar transistor, a 2N3117, operated at 10 microamperes collector current. This device develops full beta at very low current and is operated with 1-volt base-to-collector voltage to allow for temperature drift and output swing while still permitting low-noise operation. Moreover, since low-current operation requires that the emitter resistor be large, the capacity necessary to provide a cutoff frequency below 0.16 Hz can be relatively low; therefore, the package size can be minimized. The third stage, connected as an emitter-follower, provides feedback current to the first stage and at the same time gives an output impedance of about 3 kilohms.

The second amplifier is functionally identical to first stage. While basically similar to the preamplifier in design philosophy, the third amplifier is modified to give a large output voltage swing. The input stage, a P-channel FET, is arranged so that the base of the second stage can operate close to ground potential. Thus, maximum collector voltage swing is possible. Nominally, about 6 volts peak-to-peak swing was obtained during breadboard tests of the amplifier. The feedback resistor, R19, is connected in a manner that will allow adjustment of the system gain without disturbing the dc biasing. This is possible because both ends of R19 are at the same dc potential.

Each of the three amplifier sections uses a FET input stage to permit operation at high input impedance so that a small tantalum coupling capacitor can be used.

Nominal closed-loop voltage gain for each of the three amplifiers was 27.

Gain Stability. - The measured stability of the breadboard amplifier (all three) was about 1% over the temperature range and with power supply variations. Because the compensated bias supply design was abandoned owing to noise problems described in a later section, the gain stability of the entire system was worse, namely about 4% change from 50°F to 90°F

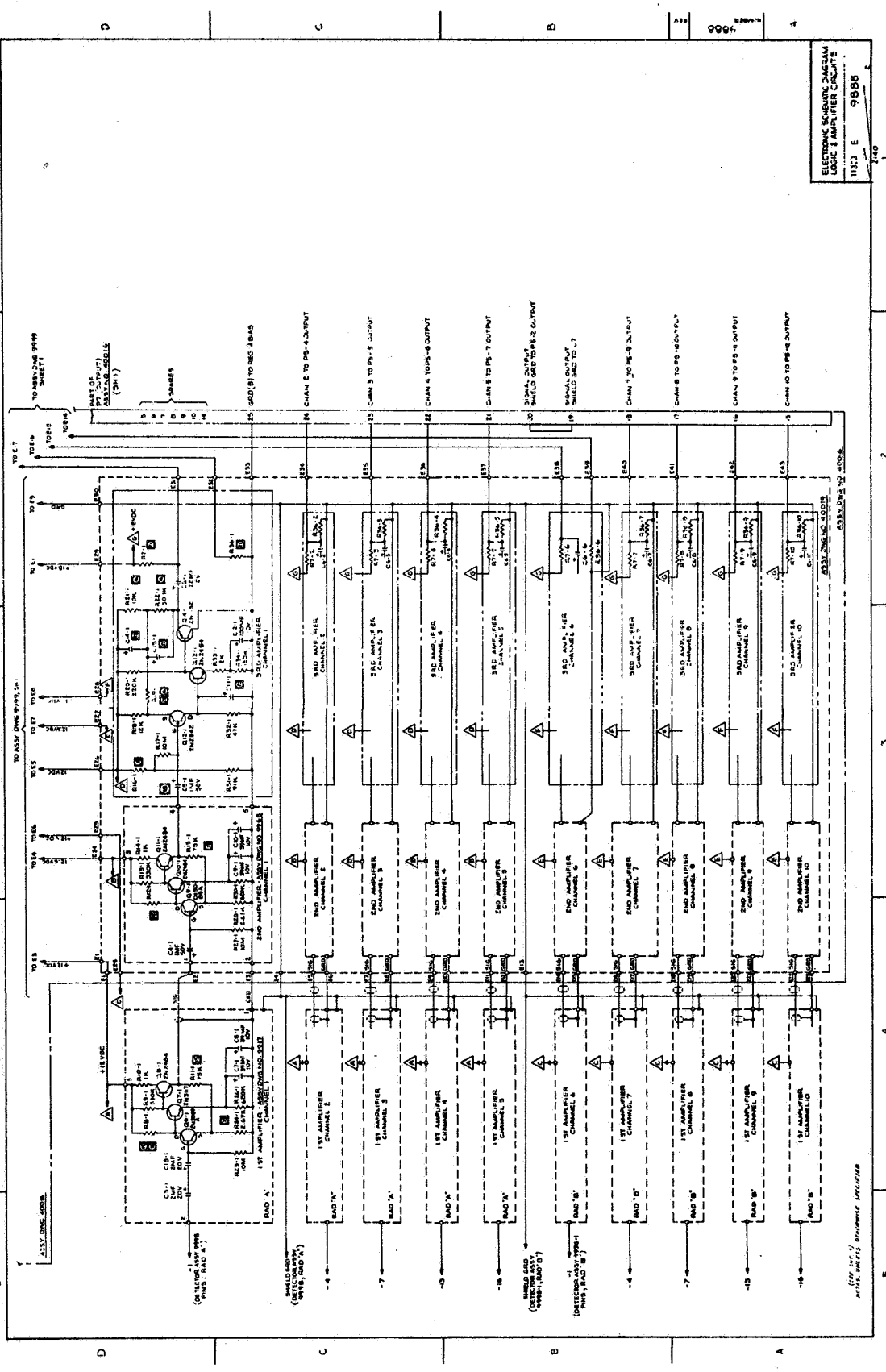

Figure 10. Amplifier Schematic Diagram

(F-2 system). However, because the system was calibrated at 10°F intervals in the range 50° to 90°F, the system gain is known to be about 1% at any temperature within the range.

Frequency Response. - The frequency response of each of the three amplifiers is designed to be flat over the frequency range 0.16 to 80 Hz. Measurements of all systems gave flatness to better than 0.5% over the above range.

Overall system high-frequency response is determined in the third amplifier by a capacitor from the base of Q13 to ground. It is selected to give a 6-db down system response at 60 Hz for the 14- to 16-micron channels and 70 Hz for the 20- to 35-micron channels. The amplifier contributes -6 db/octave slope; since the detector corner frequency is at approximately 60 to 70 Hz, the total high-frequency rolloff is -12 db/octave.

The low-frequency response is determined by the RC network at the output of the third amplifier. One resistor of this network was adjusted to give the proper low-frequency 3-db point. It should be noted that the individual amplifier response is flat down to somewhat below 0.1 Hz; below this frequency, the response begins to drop at 6 db/octave. From the system point of view, this means that although the slope of the response will be very nearly -6 db/octave at 0.16 Hz, it will increase to -24 db/octave at frequencies significantly below 0.10 Hz.

The actual adjustment of individual frequency response of each amplifier proved to be a very tedious and frustrating procedure, although once done no further problems were encountered.

Because of the variation in the time constant of the bolometers, it was necessary to carefully select the high-frequency capacitor to give the correct system response. The problem here was that C11 also was used to provide unconditional stability in the third amplifier and thus was inside the feedback loop of the amplifier. Since the system gain was adjusted by the feedback resistor of the same amplifier, it can be seen that the system frequency response was affected by gain adjustments. Obviously, it would have been better to have placed the high-frequency rolloff capacitor outside the feedback loop.

The low-frequency adjustment was equally troublesome. The combination of R7, R36 and the telemetry impedance, and C6 determined the low-frequency cut-on frequency of the system. Also, the divider R7, R36 was used to offset the output to +2.5 vdc. Consequently, these two adjustments were interdependent.

Bias Supply and Compensation Network

Considerable effort was spent in an attempt to develop a satisfactory compensated bolometer bias supply for the system. Unfortunately, however, time did not permit the solution of two severe problems — 1/f noise in the supply and immunity from line voltage variations. The result of this was that the bias supply was replaced with mercury bias batteries which proved to be a simple and reliable solution.

Sufficient consideration was not given to the 1/f noise problem when the supply was designed. Conventional chopped radiometers do not have this problem because the chopper frequency is usually out of the 1/f noise range. However, in this case the system uses no chopper and the system bandpass extends down to the 1/f region. This effect could be seen as a low-frequency wander on the output. It is felt that the correct design approach here would have been to consider the bias supply-differential amplifier and drive circuits as low-noise circuits and design them using low-noise FET stages.

Secondly, although the supply had an input regulation of better than 0.03%, changes in supply voltage were seen directly in the output as a result of the high system gain at low frequencies.

Mallory SR-3626 cells stacked to give ±43 volts were finally used. Prior to use, each battery was discharged for 5 hours at a 2-ma rate to remove the surface charge. Since mercury cells are known to become noisy when end-of-life is approached, they were replaced before 500 hours use which was about two-thirds the rated life.

Switching and Oscillator

The switching and oscillator module serves three functions: 1) to count down the resonant fork output from 3200 to 200 Hz to provide drive signal for the motor drive circuit, 2) to generate the inflight calibration pulses, and 3) to provide the scan-on, scan-off signals to the motor driver. A schematic drawing of these circuits is depicted in Figure 11.

Most of the circuit is straightforward. The calibrate circuit operates in such a way that calibrate pulses are produced whether or not the scan system is operating. When the scan is operating, the calibrate pulses are synchronized with the scan by the calibrate command pulse which occurs during the mirror turnaround at the top of the scan when the radiometers are viewing space. Presence of the calibrate command pulse inhibits the free running calibrate circuit which operates when the scan is off. Unijunction transistor, Q4, operates as a free running oscillator with a period of about 3 seconds, roughly the same as the calibrate period when the scan is on. The calibrate lamp drive voltage is a pulse of 1-volt amplitude and 50-msec duration.

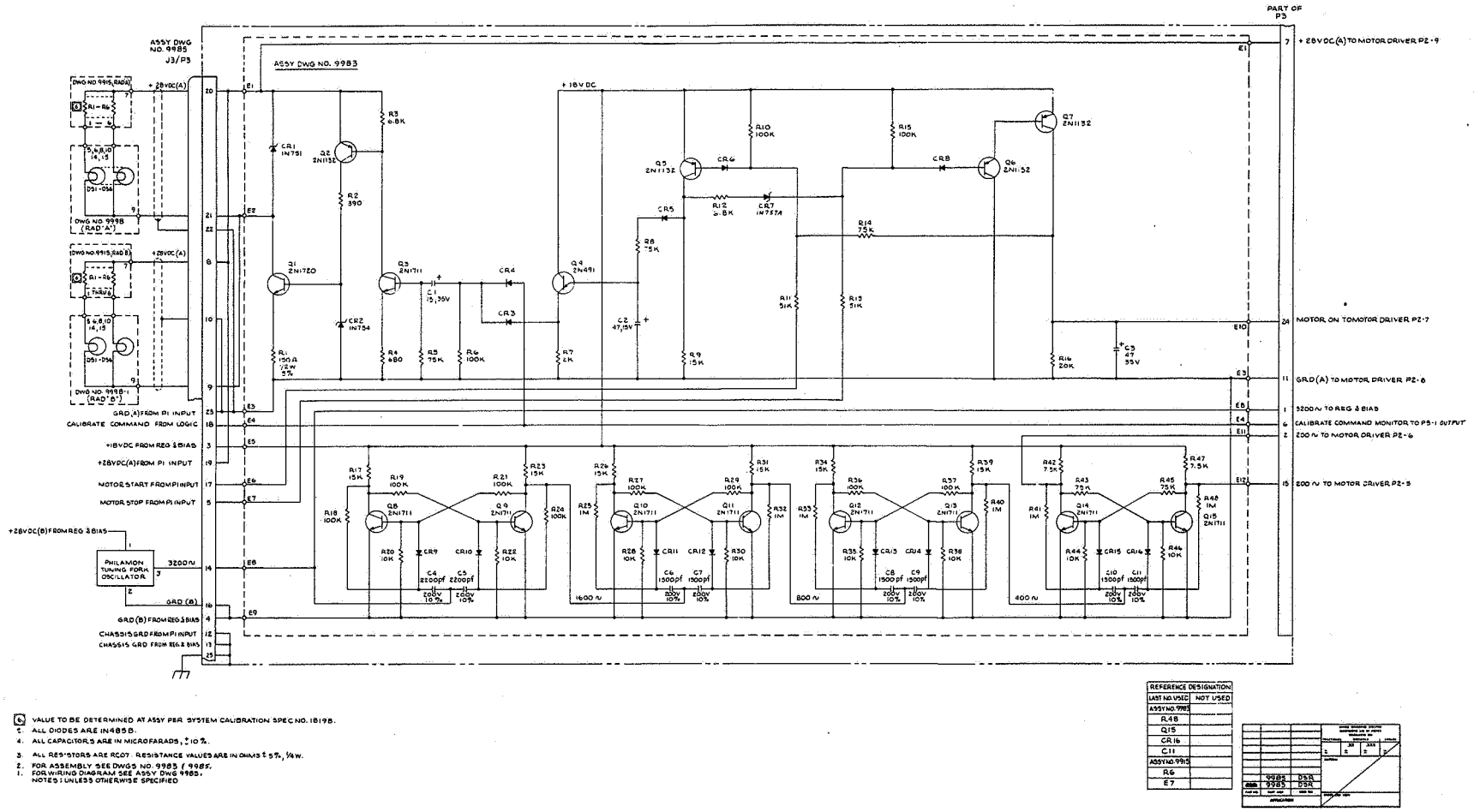

REFERENCE DESIGNATION	
LAST NO. USED	NOT USED
ASSY NO. 9985	
R48	
Q15	
CR16	
C11	
ASSY NO. 9985	
R6	
E7	

6. VALUE TO BE DETERMINED AT ASSY PER SYSTEM CALIBRATION SPEC NO. 18198.
4. ALL DIODES ARE IN4858.
4. ALL CAPACITORS ARE IN MICROFARADS, ±10%.
3. ALL RESISTORS ARE RCO7. RESISTANCE VALUES ARE IN OHMS ±5%, ¼W.
2. FOR ASSEMBLY SEE DWGS NO. 9983 & 9985.
1. FOR WIRING DIAGRAM SEE ASSY DWG 9985.
NOTES: UNLESS OTHERWISE SPECIFIED

Figure 11. Electronic Schematic Diagram, Switching and Oscillator Circuits.

Internal Calibrate System

The energy sources for internal calibration were Kay Electric Company "Pinlites" having a 3-ma current rating and a rated thermal time constant of 7 msec. Three of these lamps were mounted in a phenolic block on the back edge of the detector housing. Quartz light pipes 0.03 inch in diameter were used to conduct energy onto the bolometer immersion lenses. Figure 12 shows the arrangement of the lenses and light pipe holes.

Making this internal calibrate system operate properly was fraught with problems from the start. The most basic problem with the system was adjusting the lights in such a way that the calibrate pulse heights were equal for all five channels. Usually the center detectors were overdriven and the end detectors received very little energy. This was corrected to a degree by

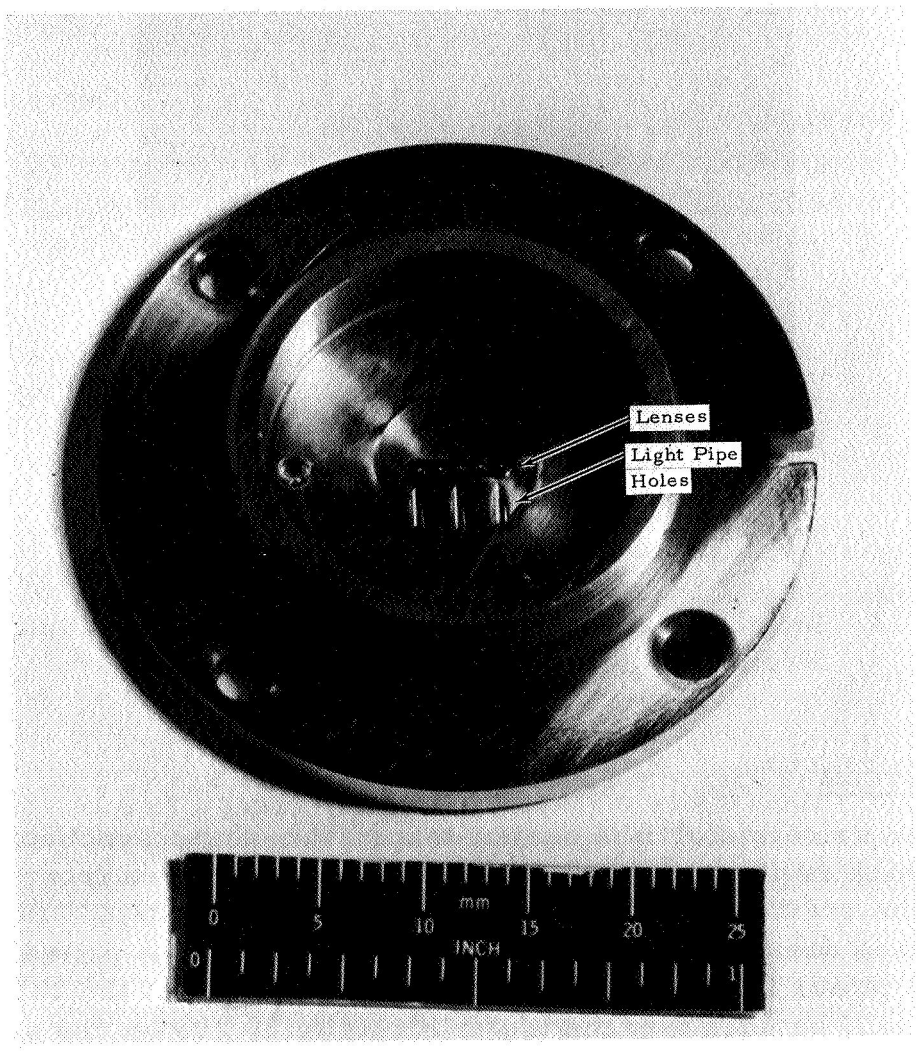

Figure 12. Bolometer Detector Array Showing Holes for Calibrate Light Pipes

adjusting the placement of the lights, and finally by a cut-and-try procedure of carefully frosting the ends of the light pipes and selectively placing small spots of Pro-Seal on the ends of the light pipes.

The calibrate pulses did not have the desired square shape and the 50-msec period; instead, they had long tails with undershoot sufficient to interfere slightly with the data. It is the writer's opinion that this problem was related to the transient response properties of the amplifiers rather than to the calibrate lamp system. That is, it is speculated that the -24 db/octave rolloff of the amplifiers below 0.05 Hz could cause an unexpected transient effect. A photo of a typical calibrate pulse output is shown in Figure 13.

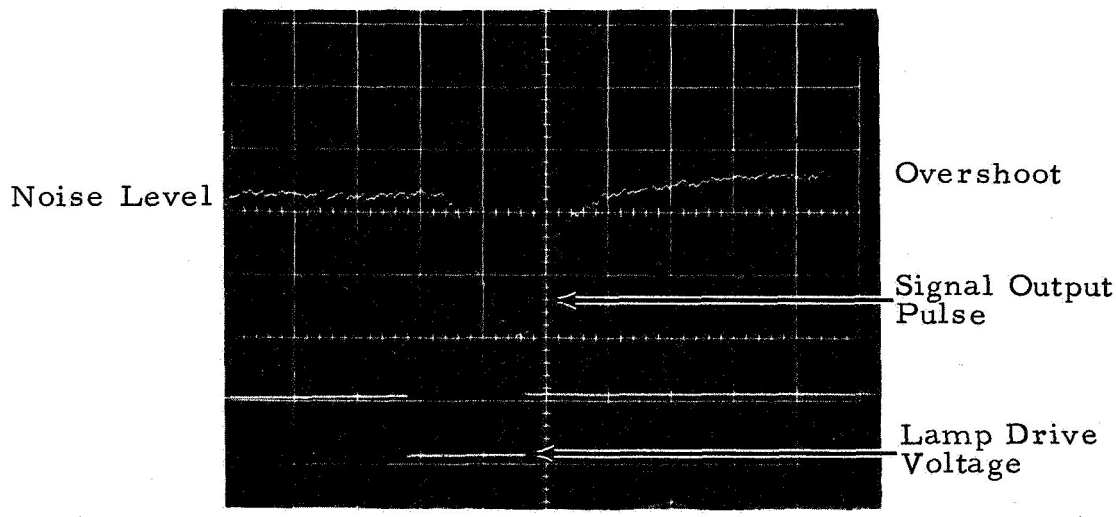

Vertical: 1 volt/cm
Horizontal: 50 msec/cm
Bottom Trace: Lamp Voltage

Figure 13. Internal Calibrate Pulse - Output of Center Detector, Prototype

Scan Drive Circuit

The scan drive motor is a center-tapped two-phase synchronous 6000-rpm motor which is driven by 100-Hz square waves derived from the 3200-Hz fork. In the previous section, "Internal Calibrate System," the count-down circuit was described briefly. The motor driver is a potted unit containing the power flip-flops. Gating is provided so that the phasing of the flip-flops will be such that the motor direction is always the same. A schematic diagram of the motor driver is depicted in Figure 14. No problems of any kind were encountered with this circuit.

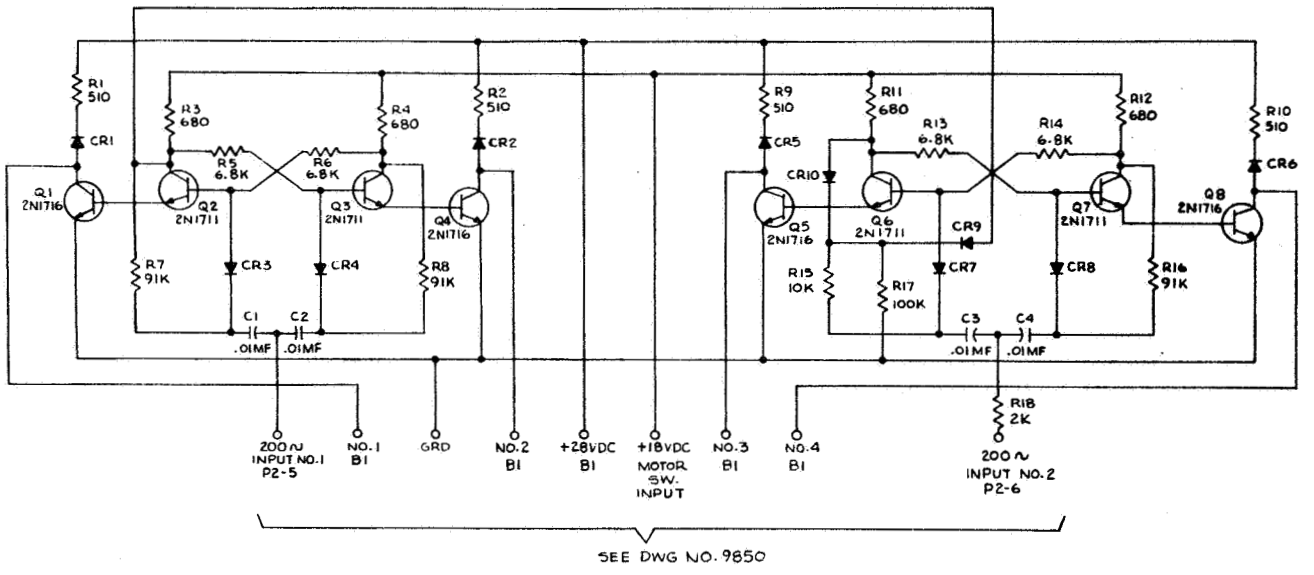

Figure 14. Schematic Diagram, Motor Driver

Position Readout Circuitry

Four equally spaced scan position pulses are provided during the linear portion of the scan. Each position has a voltage value (1, 2, 3, and 4 volts) and the sequence indicates whether the scanner is scanning up or down. This position indication is superimposed on the analog signal of the radiometer channels 1 and 6 as shown in Figure 15.

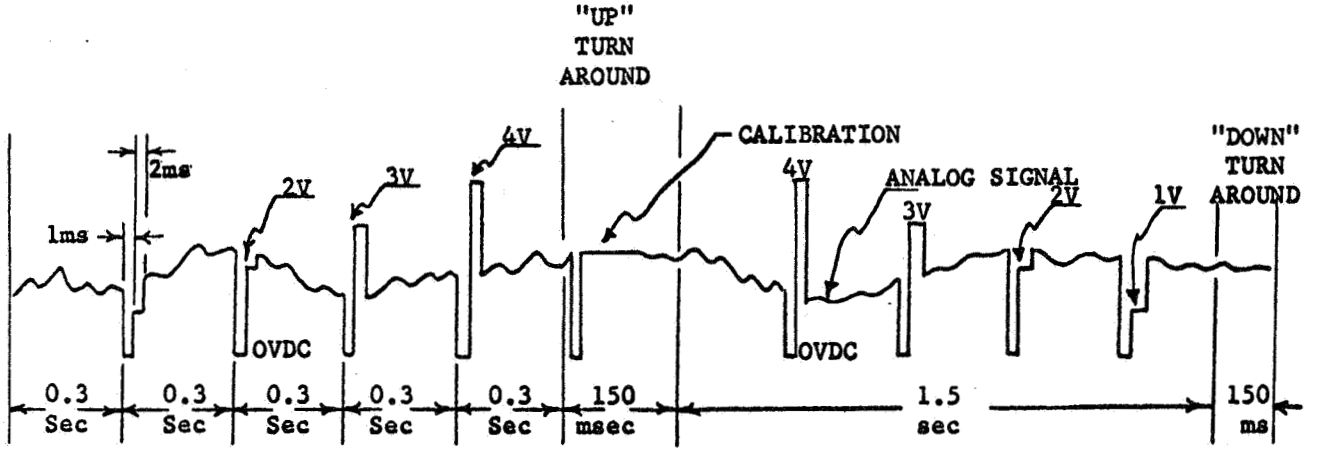

Figure 15. Channel 1 and Channel 6 Output Showing Scan Position Pulses

Position Pulse Generation. - The position pulses are initiated by a slotted disc connected to the cam that drives the scanning mirror. As the disc rotates, the slots allow light to pass from a light source to a photodiode detector. The minimum slot width is 0.030 inch at a radius of 1.625 inches with a rotation period of 3.2 seconds. The light source is two Type 15-30 "Pinlites" operating in parallel at 1.3 vdc. The system still operates normally if one lamp should fail.

The repeatability of the position readout system is dependent on the squareness of the photodiode output pulse and the level detector accuracy. The voltage pulse from the photodiode is amplified by a gain of ten making a voltage rise time slope of 6.6 volts/msec. The ±0.01° repeatability requirement of accuracy between position pulses represents an error of ±1.0 msec of scan time. The amplified pulse is passed by a threshold of 3 volts and squared by a Schmitt trigger circuit whose trigger level stability is ±39 mv over the operating temperature. Therefore, the error contributed by this portion of the electronics is about 0.006 msec. A schematic diagram of the scan logic is shown in Figure 16.

Temperature Readout Circuit

A schematic diagram of the temperature readout circuit is given in Figure 17 and a typical output curve is shown in Figure 18. Essentially, the circuit is an unbalanced differential amplifier arranged such that Q1A is cut off at 50°F and is conducting 0.5 ma at 100°F. The nearly linear output curve is due to the fact that the nonlinear characteristic of the thermistor is compensated to a degree by the nonlinear characteristic of the input voltage divider.

Power Regulator

A schematic diagram of the +18 volt regulator is shown in Figure 19. The regulator consists of Q1, Q2, and Q3. As mentioned previously, the bolometer bias supply shown on the remainder of the schematic was not used.

Further regulation for the amplifiers was provided by the regulators shown in Figure 16.

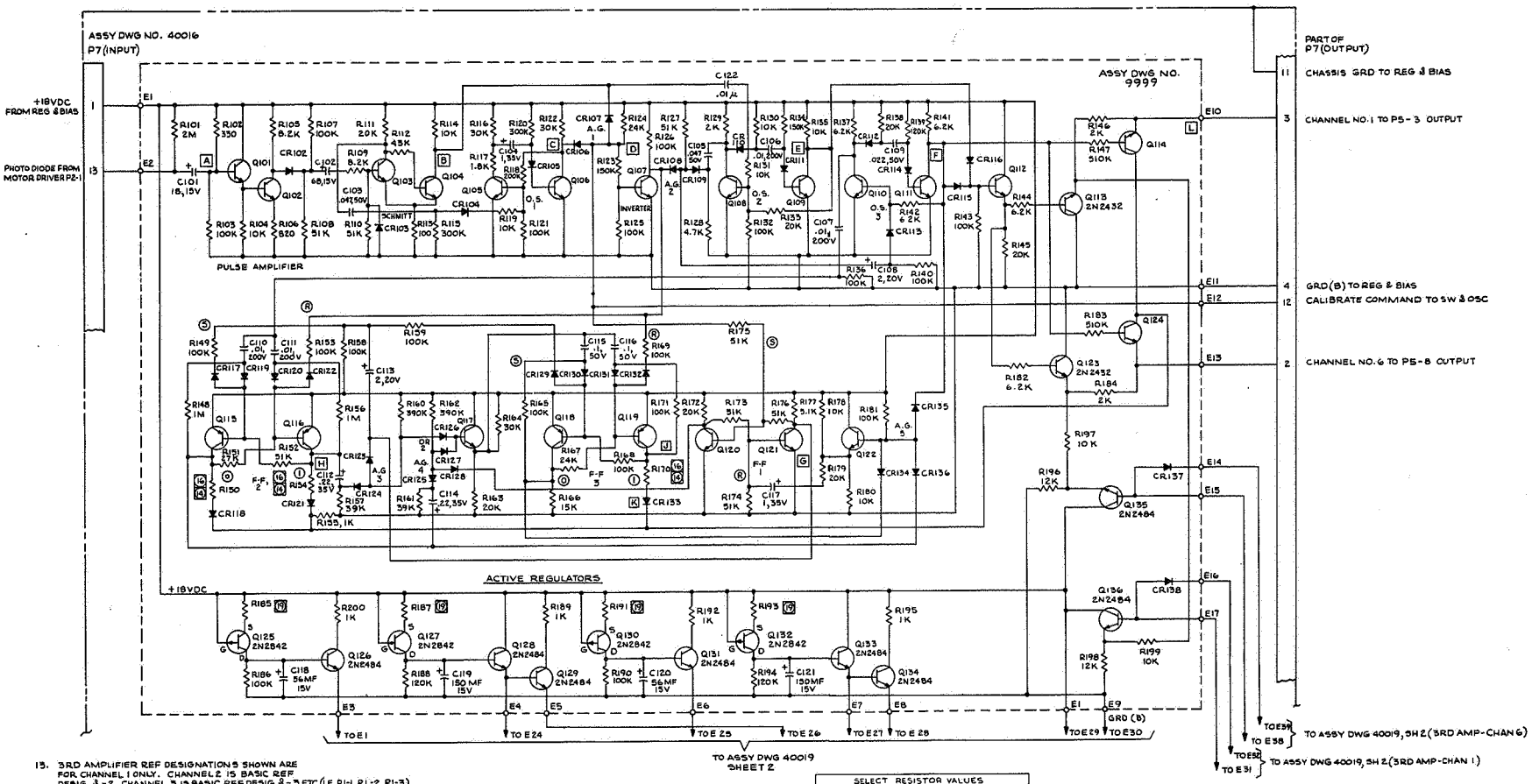

15. 3RD AMPLIFIER REF DESIGNATIONS SHOWN ARE FOR CHANNEL 1 ONLY. CHANNEL 2 IS BASIC REF DESIG & -2, CHANNEL 3 IS BASIC REF DESIG & -3 ETC. (I.E. R1-1, R1-2, R1-3)
12. TRANSISTORS: ⌐ INDICATES A 2N1711 (NPN) & ⌐ INDICATES A 2N1132 (PNP).
11. □ INDICATES WAVEFORMS SHOWN ON TIMING DIAGRAM 5BRC DWG NO. 40030.
10. Ⓡ & Ⓢ INDICATES SET & RESET AS DEFINED IN 5BRC SPEC 18210.
9. ① & ⓪ INDICATES NORMAL BINARY DESIGNATIONS FOR FLIP-FLOP (FF) STATES.
8. ABBREVIATIONS: AG = AND GATE, OR = OR GATE, FF = FLIP-FLOP & OS = SINGLE SHOT.
7. ALL RESISTORS ARE 1/4 WATT, ±5%, CARBON COMP.
6. ALL DIODES ARE IN485B.
5. APPLICABLE MIL-STDS: 12, 15 & 16.
4. ALL CAPACITOR VALUES ARE IN MICROFARADS ±10%
3. ALL RESISTOR VALUES ARE IN OHMS ±5%, 1/4 WATT
2. FOR ASSEMBLY DWG SEE DWG NO. 40016, 40019 & 9999
1. FOR WIRING DIAGRAM SEE DWG NO. 40031

NOTES: UNLESS OTHERWISE SPECIFIED

23. CAPACITOR VALUE TO BE SELECTED FROM TABLE FOR BOLOMETER FREQUENCY COMPENSATION PER REQ OF 5BRC SPEC 18198.
22. RESISTOR VALUE TO BE SELECTED FROM TABLE TO GIVE CORRECT OVERALL GAIN PER REQ OF 5BRC SPEC 18198.
21. RESISTOR VALUE TO BE SELECTED FROM TABLE TO GIVE CORRECT LOW FREQUENCY CUTOFF PER REQ OF 5BRC SPEC 18198.
20. CAPACITOR VALUE TO BE SELECTED FROM TABLE TO GIVE CORRECT HIGH FREQUENCY CUTOFF PER REQ OF 5BRC SPEC 18198.
19. RESISTOR VALUE TO BE SELECTED FROM TABLE FOR PROPER OPERATING POINT PER REQUIREMENTS OF 5BRC SPEC 18197 & 18198.
18. CAPACITOR IS SPRAGUE, TYPE 150D, CASE "A".
17. ALL CAPACITORS ARE SPRAGUE, TANTALUM, TYPE 350D OR EQUIV.
16. RESISTORS ARE 1/8 WATT, ±1%, RN60C METAL FILM.
15. RESISTORS ARE 1/10 WATT, ±1% RN55C, METAL FILM.
14. RESISTOR VALUE TO BE SELECTED FROM TABLE PER REQUIREMENTS OF 5BRC SPEC 18210.

SELECT RESISTOR VALUES							
RESISTOR	WATT	%	SELECTION				
R150	1/8	1	9.53K	10K	10.5K	11K	11.5K
R185	1/4	5	2.2K	2.4K	2.7K	3.0K	3.3K
R187	1/4	5	2.2K	2.4K	2.7K	3.0K	3.3K
R191	1/4	5	2.2K	2.4K	2.7K	3.0K	3.3K
R193	1/4	5	2.2K	2.4K	2.7K	3.0K	3.3K
R8-1	1/10	1	20K	22.1K	24.3K	27.4K	30.1K
R12-1	1/4	5	20K	22K	24K	27K	30K
R16-1	1/4	5	2.4K	2.7K	3.0K	3.3K	3.6K
R36-1	1/4	5	160K	180K	200K	220K	240K
R19-1	1/8	1	78.7K	80.6K	82.5K	84.5K	86.6K
R7-1	1/4	5	750K	820K	910K	1MEG	1.1MEG
R154	1/8	1	4.53K	4.75K	4.99K	5.23K	5.49K
R170	1/8	1	2.94K	3.09K	3.24K	3.4K	3.57K

SELECT CAPACITOR VALUES (17)							
CAPACITOR	VOLTAGE	CASE SIZE	SELECTION				
C11	35V	A	.22	.27	.33	.39	.47
C14		A					
C15		A					

REFERENCE DESIGNATION	
LAST NO. USED	NO. NOT USED
ASSY NO. 9999 (SH 1)	
R200	
Q136	
C122	
CR138	
E17	
ASSY NO. 40019 (SH 2)	
R36	R25, R29, R35
Q14	
C6	
E43	

Figure 16. Schematic Diagram, Scan Logic.

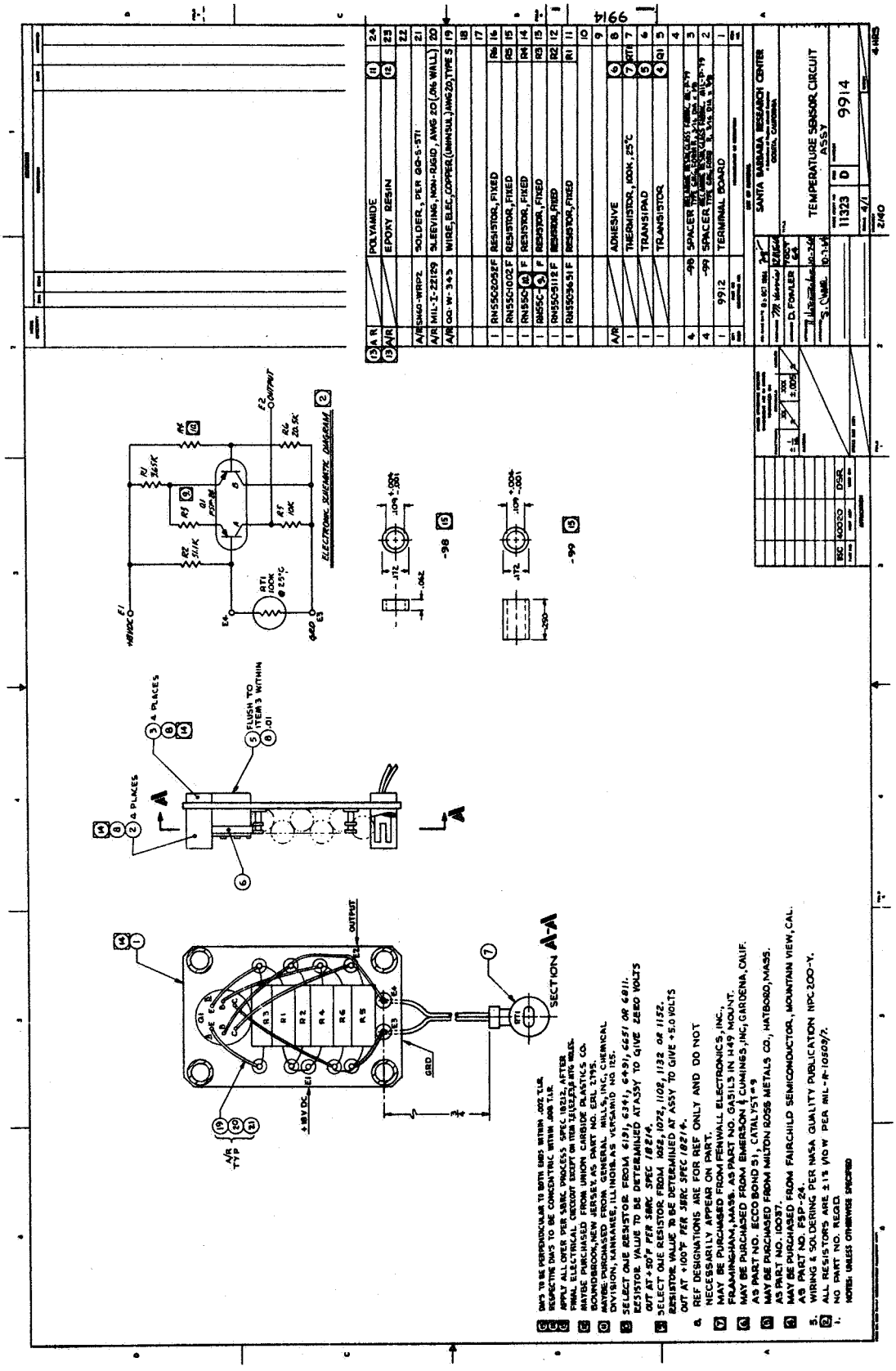

Figure 17. Schematic Diagram, Temperature Readout Circuit

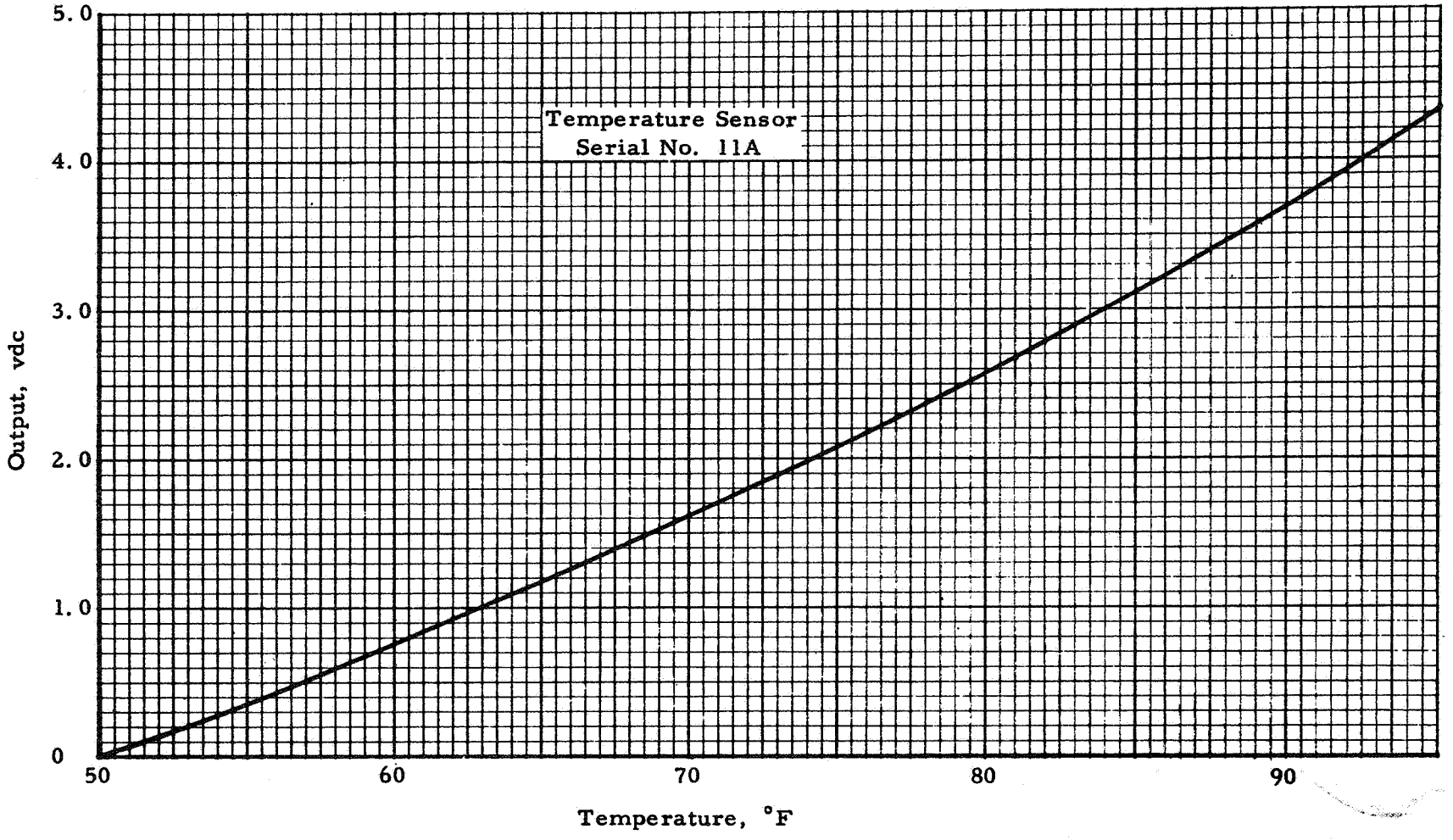

Figure 18. Calibration Curve, Temperature Sensor, Radiometer "A"

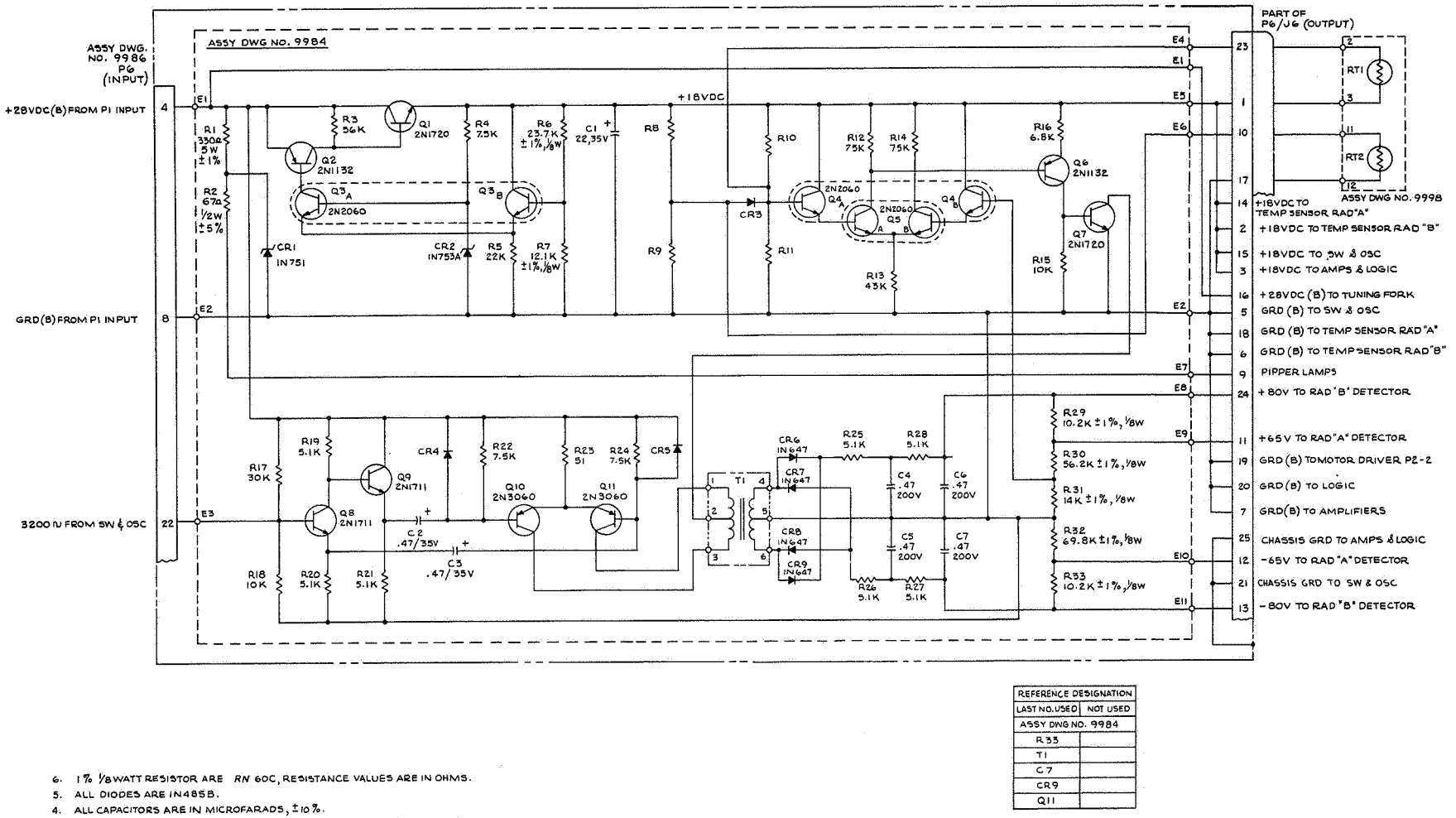

REFERENCE DESIGNATION	
LAST NO. USED	NOT USED
ASSY DWG NO. 9984	
R33	
T1	
C7	
CR9	
Q11	

6. 1% ⅛ WATT RESISTOR ARE *RN* 60C, RESISTANCE VALUES ARE IN OHMS.
5. ALL DIODES ARE IN485B.
4. ALL CAPACITORS ARE IN MICROFARADS, ±10%.
3. ALL RESISTORS ARE RC07, RESISTANCE VALUES ARE IN OHMS ±5%, ¼ WATT.
2. FOR ASSEMBLY DWG SEE NO. 9984 & 9986.
1. FOR WIRING DIAGRAM SEE ASSY DWG NO. 9986.

NOTES: UNLESS OTHERWISE SPECIFIED

Figure 19. Schematic Diagram, +18 Volt Regulator and Bias Supply.

Section 4

PROCUREMENT AND FABRICATION

Many serious problems were encountered during the fabrication phase of several subsystems. While it was realized that fabrication of true aspheric surfaces on beryllium would not be easy, the magnitude of the problems was certainly not anticipated.

Similarly, many problems were encountered with the procurement of the bolometer detector arrays; some were expected and others were not, and still others are not well understood even now.

DETECTOR PROCUREMENT

The detector package consists of a lenticular array of five separate immersion lenses which are aligned with the five elemental FOVs.

The bolometer housings were designed and built by SBRC because this afforded close control of the tight tolerances involved. Barnes Engineering Company, Stamford, Connecticut, was subcontracted to design and build the lenses and detectors and to mount them in the housings provided by SBRC. Barnes was also contracted to test and screen the bolometer arrays prior to delivery.

For Radiometer A (14 to 16 microns), the immersion lenses are AR coated germanium. For Radiometer B (20 to 35 microns), they are AR coated silicon. Both types are hyperhemispheres of 0.040-inch diameter. The detectors are 0.1×0.1 mm^2 Type 1 material. The "thin" bolometer flakes have a thickness of about 6 microns and a resistance of 4 megohms.

Immersion Lenses

Throughout the program, fabricating the small immersion lenses was a continuing problem. After trying one other vendor, Barnes contracted with Valpey Crystal Company to make the lenses. However, after the first three batches, Valpey was unable to make acceptable silicon lenses — even after the lens thickness tolerance was relaxed from ±0.0005 inch to ±0.0007 inch, and the radius of curvature from ±0.0003 inch to ±0.0007 inch. Barnes at this time was attempting to make the germanium lenses themselves and was able to make a number of these. Because of this potential bottleneck, SBRC let a time and materials contract with Cecil Mann of Montecito, California, a recognized expert in the field. After Mann had worked several weeks on

the problem, he was able to make the lenses. About the same time, Valpey had achieved a breakthrough which enabled them to make lenses also. The lenses were anti-reflection coated by the Optical Coating Laboratory, Inc. (OCLI) at Santa Rosa, California, but were rejected numerous times owing to non-uniformity of the coating. Finally, OCLI was able to arrive at a holding fixture that would coat the lens acceptably. Zinc sulfide was used on the germanium lenses and a proprietary coating was used on the silicon lenses.

Detector Housings

Later in the program it was concluded by Barnes that many of the noise problems encountered were caused by the housing design; that is, the noise was caused by leakage currents across feedthrough insulation. Therefore, they proposed to redesign and fabricate new housings — which they did. Because by this time the bias supply was no longer used, the compensating thermistors and pins could be eliminated. This allowed Barnes to make the interior cavity larger, which made interwiring problems easier. Also, instead of potting in the pins, glass-to-metal feedthroughs were used. Although these changes did not eliminate the noise problems completely, the noise did appear to be less severe with the new housings.

It was originally intended that the detector packages would be evacuated to eliminate the possibility of swish noise and leakage noise resulting from moisture and other contaminants. Because the package is sealed with epoxy adhesive around the lenses, however, there was little confidence that a true hermetic seal could be maintained inside the package. Therefore, the detectors were backfilled with dry nitrogen. No swish noise effects were observed with these detectors.

Spectral Dip Problems

All of the arrays from Barnes were sent to the Naval Ordnance Laboratory at Corona for spectral measurements prior to installation in the system. When the first spectral response curves were received, a severe anomalous dip was seen at 15 microns (see Figure 20).

Considerable time was spent trying to explain the problem in terms of interference effects, but the actual cause was that silicon had mistakenly been used for the 14- to 16-micron arrays rather than germanium. The dip was the intrinsic absorption of silicon at 15 microns.

To eliminate this problem on subsequent arrays, each of the lenses was weighed prior to mounting in the array. Silicon is roughly half as dense as germanium.

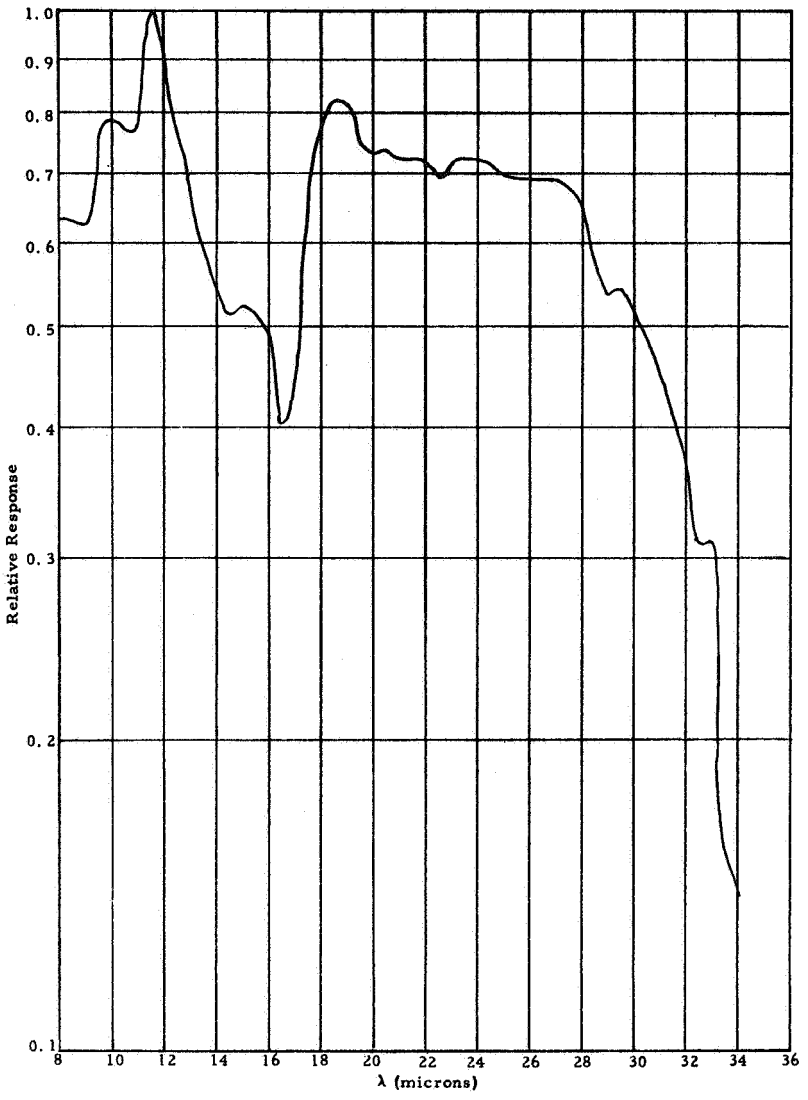

Figure 20. Spectral Response, 14- to 16-Micron Array (Germanium Immersed)

Even after the confusion over the lens material was straightened out, a dip in response at 15 microns was still present (see Figure 21). This problem was attributed by Barnes to interference effects in the selenium glass immersion material, the bolometer flake, and the blacking material.

Barnes at this time performed a study of the problem during which time a number of detector parameters were varied in an attempt to shift the spectral dip out of the 14- to 16-micron region. Barnes found that increasing the thickness of the immersion layer would shift the dip to shorter wavelength, but would shorten the time constant and hence degrade the responsivity. Barnes indicated that a 0.5-micron shift in spectral dip would cause the time constant to be reduced from 2 msec nominal to 1.3 msec.

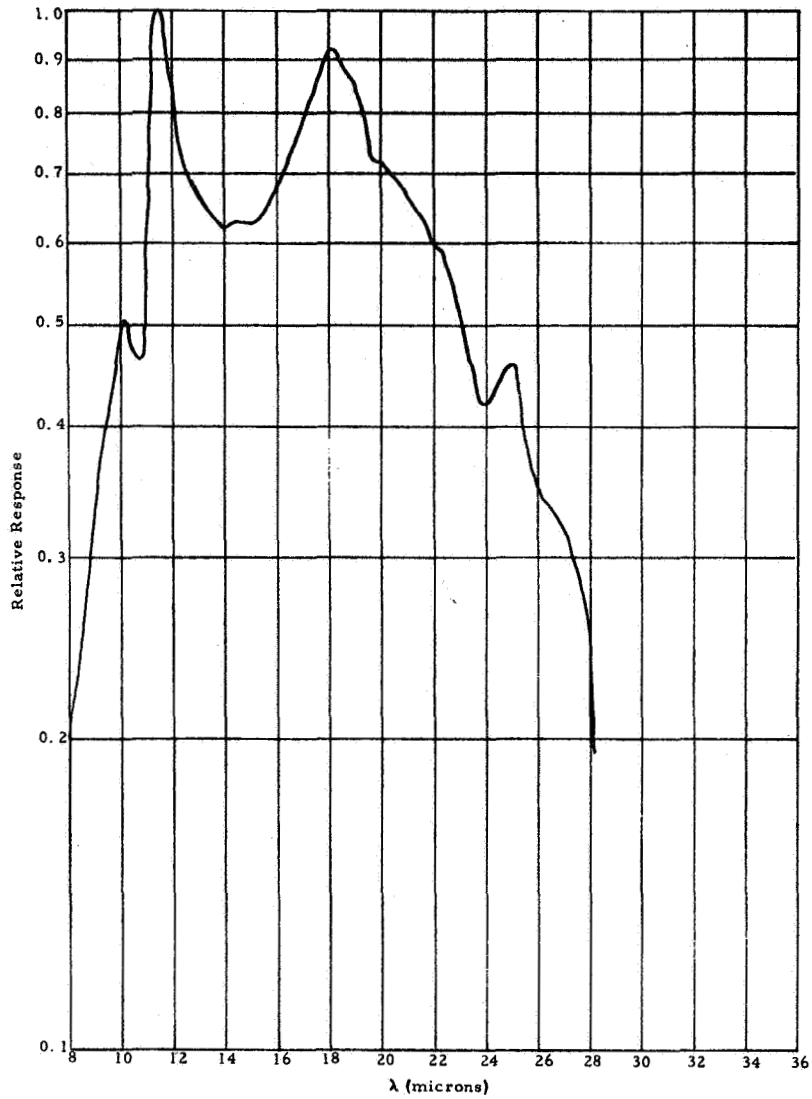

Figure 21. Spectral Response of Germanium Immersed Array S/N 5283, Channel 6

Barnes also investigated the possibility of using 10-micron thick flakes instead of the 6-micron type used normally. It was hoped that if the dip was a result of interference effects, the different layer thicknesses would shift the dip out of the region of interest (the selenium layer would be thinner for the same time constant). Data taken with the 10-micron flakes, however, showed that the shift to shorter wavelength was not enough to remove the dip from the 14- to 16-micron region.

Several other interesting results came out of this study. It was found that the 10-micron flakes immersed on germanium flats gave an entirely different response curve with little or no dip in the 14- to 16-micron region.

Barnes has no explanation for this effect other than the possibility that the convergence angle of the rays as they pass through the germanium-selenium glass interface may affect the interference pattern.

Because of the spectral dip problem, Barnes was asked to make responsivity measurements using a 14- to 16-micron filter supplied by SBRC. They found, however, that there was insufficient energy to make the measurement. All measurements were therefore made relative to an array of known performance. Array No. 5287 was removed from the F-1 system for this purpose.

Although considerable speculation was made as to the cause of the spectral dip, no cure was found by Barnes, and all of the detectors flown in the F-1 and F-2 had spectral curves similar to that shown in Figure 21.

Barnes also experimented with the effects of removing the black absorbing material from the back side of the detector flake. They found that the responsivity in the 14- to 16-micron band was not improved by adding blacking to the 10-micron thick bolometer flakes. In the case of the thinner 6-micron flakes, two applications of the APB black improved responsivity by 20% to 25% but with about 30% increase in the time constant. Without the 14- to 16-micron filter, the black improves the responsivity about 300%.

For the sake of completeness, a spectral response curve of a typical silicon immersed array is shown in Figure 22.

Noise Problems

Probably the single most disturbing difficulty encountered with the bolometer arrays was the fact that over a period of time many of the detectors would become noisy and therefore unusable.

Normal bolometers exhibit a N_B/N_O ratio* of 1.15 to 1.20, the increase over Johnson noise due to bias current noise and leakage effects. The observed effect of a detector going bad was usually a gradually increasing or occasionally a sudden increase in the N_B/N_O ratio to 2, 3, or 5 or more.

Barnes attributed the noise to leakage paths inside the detector caused by the close proximity of many detector and bias leads and leakage paths at the feedthrough pins. As previously mentioned, Barnes redesigned the

---

*N_B/N_O is the ratio of rms noise voltage with bias applied to that without bias.

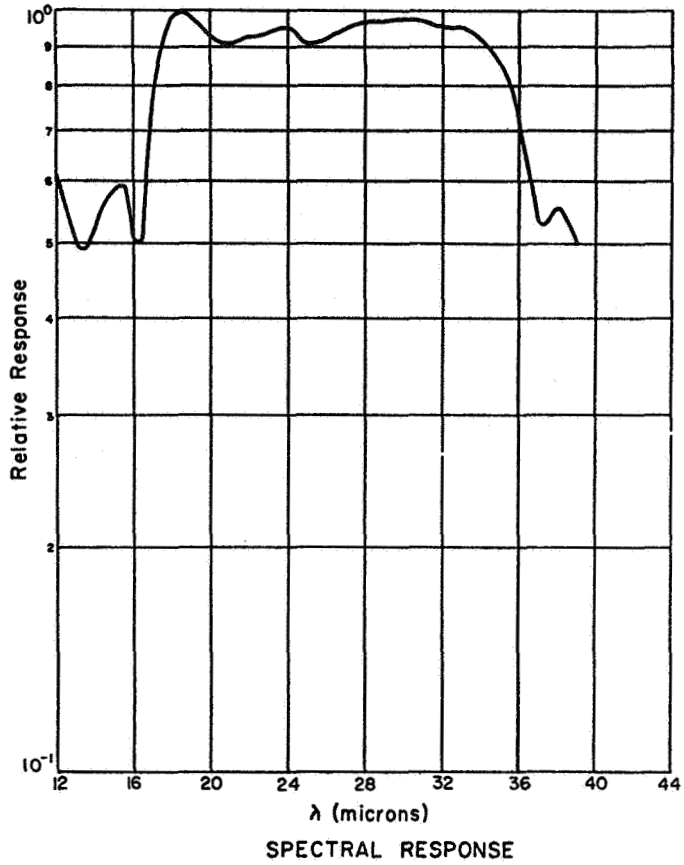

Figure 22. Spectral Response of Silicon Immersed Array S/N 5286, Channel 1

detector housing to afford more room inside the package for interconnections and replaced the epoxy feedthroughs with a glass-to-metal type. These features appeared to help the problem to a degree but did not solve it entirely.

Finally, in an attempt to eliminate those detectors that might go bad later, a 200-hour burn-in test was specified during which the N_B/N_O ratio was measured periodically. It was further specified that the N_B/N_O ratio could not be greater than 1.50 at the end of the test. Furthermore, the increase in N_B/N_O ratio during the last 100 hours could not exceed 20%. As a further check on the condition of the bolometers, the N_B/N_O ratio was periodically measured during systems tests and was then plotted to see if any trends would develop. A typical curve taken from the F-1 report is depicted in Figure 23 where failures actually occurred. The upward trends were much more pronounced than shown in the figure.

In retrospect, it is felt that many of the problems experienced with the bolometers on this project were a result of the specialized nature of the

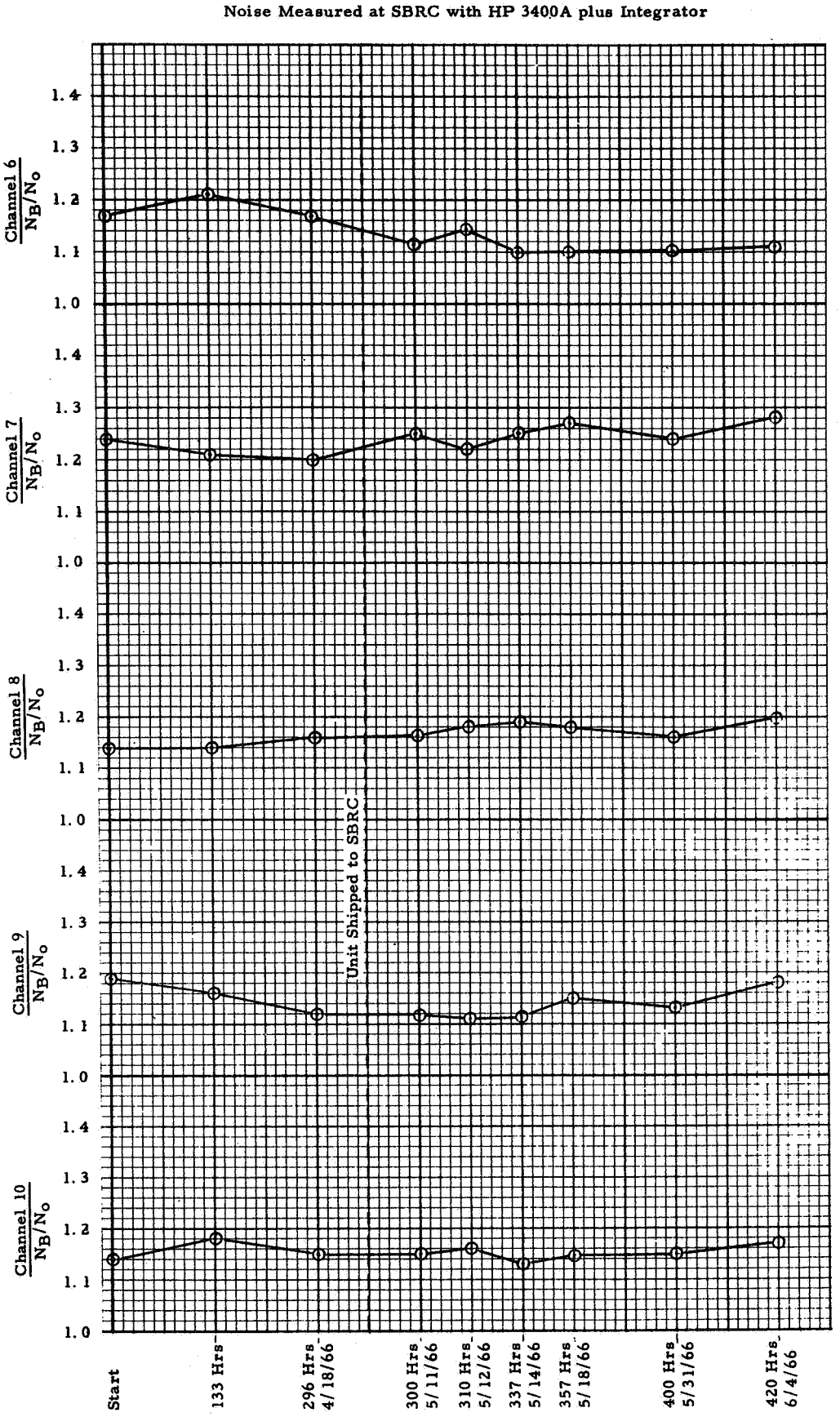

Figure 23. N_B/N_o Ratio for Radiometer "A" (14 to 16 microns) Detector S/N 5283, F-1

multielement arrays employing extremely small lenses in close proximity. Problems of this nature probably would not have been encountered had the detectors been of ordinary construction.

OPTICS PROCUREMENT

Optical Element Finishing

The design of the Dual Radiometer optics required three beryllium optical elements. The aspheric primary mirror, the aspheric secondary, and the flat scan mirror were to be fabricated of electroless nickel-plated beryllium. The differences in fabrication technique and complexity require that these elements be discussed separately.

Machining Beryllium

The beryllium primary and secondary mirror blanks were machined with an aspheric profile. The specified surface was to be within ±0.0005 inch of the nominal aspheric shape. Speedring Corporation, Warren, Michigan, had no difficulties with these parts. The machined aspheric profile was within ±0.0003 inch of the desired profile. Thus, machining of beryllium proved to be no problem.

Scan Mirror Finishing. - The major steps in fabrication of the flat scan mirror are listed below:

1. Machine beryllium blank to size and shape.
2. Apply a thin copper plating to the beryllium surface approximately 0.001 inch thick.
3. Lap the copper plating flat.
4. Apply an electroless Ni plating approximately 0.006 inch thick.
5. Lap the nickel reasonably flat.
6. Mount mechanical parts on the mirror blank (pivot shaft, counter weight, and follower arm).
7. Polish the nickel surface to specified tolerances.
8. Apply reflective coating of aluminum and protective coating of SiO.

The copper plating is used to provide a uniform surface to which the nickel can be more uniformly applied. The copper is soft and will "flow" during lapping to fill any voids. This is intended to provide a base that can be plated with freedom from pits.

Step 5 above is performed to examine the plating before the mechanical assembly is started.

Many parts were found to have an excessive number of pits in the nickel plating. This required that the plating be chemically removed and Steps 2 through 8 repeated. In several instances, as the optical polish was nearing completion, the nickel plating wore through. Again it was necessary to repeat Steps 2 through 8.

The optical vendor expressed considerable difficulty in polishing the first scan mirrors, and these distorted severely during the vacuum deposition of aluminum and SiO. Test of mirror flatness in a temperature chamber showed a temperature distortion of the scan mirror under the follower arm assembly. The differential expansion of the beryllium scan mirror and the aluminum follower arm produced a distortion corresponding to about 15 fringes of helium light. Minor modification of the holding mechanism (nylon jacketed screws) alleviated the problem. This also eliminated the distortion during vacuum coating and allowed the optical polishing to proceed in a more reasonable fashion.

During acceptance tests on the mirrors at SBRC, reflectance tests were made on witness mirrors which had been coated concurrently with the scan mirrors. It was discovered that several mirrors had a peculiar absorption band around 16.5 microns. This was traced to a vendor error in coating the mirrors with MgF_2 instead of the specified SiO. Reflectance values are shown in Figure 24. This absorption phenomenon is reported elsewhere in the technical literature.* Scan mirrors with this absorption would clearly be objectionable for the short wavelength channel, though not objectionable in long wavelengths. Rather than rework the mirrors with the attendant loss of time and reliability, the MgF_2 coated mirrors were used for the long-wavelength radiometers.

The scan mirrors, as accepted at SBRC, were of excellent quality and they passed the procurement specification in all respects. The mirror surface was almost free of pits and scratches. This does not imply that future procurement would be much easier. The vendor (Herron Optical) had nearly as much trouble with the final scan mirror as with the first scan mirror. However, good quality flats can be purchased if one has the time and money.

---

*M. Laikin, Appl. Opt. 2, 91 (1963).

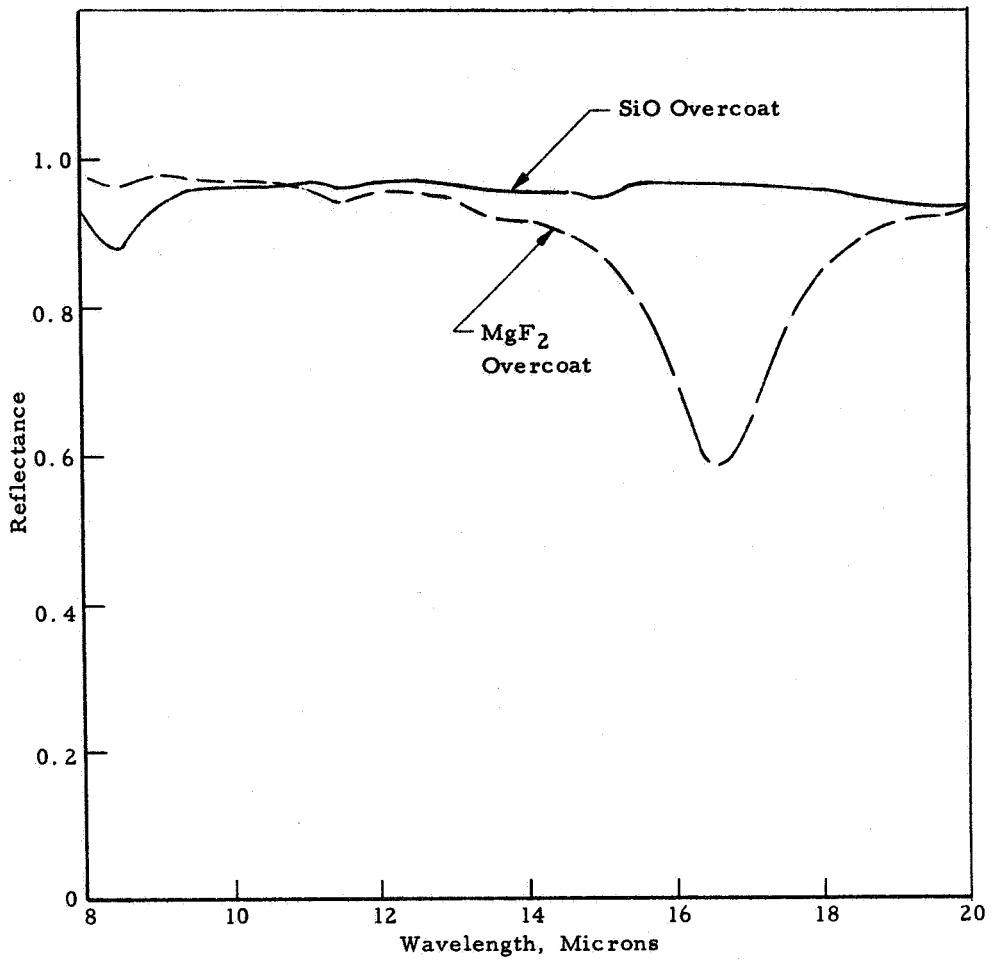

Figure 24. Reflectance, Herron Optical Sample Mirrors

The Primary Mirror. - The primary mirror of beryllium was 9 inches in diameter and required an aspheric surface. The aspheric curve was machined into the beryllium blank. The nickel was plated directly onto the beryllium and optical polishing followed. Many parts had excessive pitting and had to be stripped and replated. Severe problems were encountered in keeping the optical surfaces a true surface of revolution; this required more replating. Table 5 summarizes the history of each primary mirror along with the plating variations tried in an attempt to get suitable platings.

It is not clear from the table in what order the mirrors were fabricated. No particular order was involved. Texas Instruments worked on each mirror in turn until either the part was successfully completed or until the part was rejected for rework.

The fact that the S-1 system was completed with relative ease compared to the others is fortuitous.

Table 5. Summary of Primary Mirror History

System S-1

Sept 1964	SBRC issued purchase order to Texas Instruments (TI) of Dallas, Texas.
Oct 1964	S-1 plated by Electro-Coating, Inc., of Emoryville, California.
Dec 1964	Primary mirror completed.
Jan 1965	Pyrex secondary mirror completed.
Mar 1965	Began silicon secondary mirror.
May 1965	Silicon secondary mirror completed.
Aug 1965	Completed system shipped to SBRC.

All plating was electroless nickel unless otherwise stated. Nominal thickness was 0.005 to 0.008 inch (unless otherwise stated).

System S-2

Sept 1964	SBRC issued purchase order to TI.
Oct 1964	S-2 plated by Electro-Coating, Inc. Rejected by TI after visual inspection - pits. Chemically stripped by Metal Surfaces of Bell Gardens, California. Plated by Metal Surfaces. In process. During grinding nickel plating wore through.
Nov 1964	Chemically stripped by Metal Surfaces. Plated by Metal Surfaces.
Dec 1964	In process at TI.
Feb 1965	Nickel stripped by heat treatment at United Heat Treat (UHT) of Fort Worth, Texas.
Mar 1965	Plated by Metal Surfaces. Plating porous throughout layer.
Apr 1965	Chemically stripped by Metal Surfaces. Plated by Metal Surfaces. In process - did not work well. Plating stripped by heat process, UHT.
May 1965	S-2 remachined at Speedring of Warren, Michigan.

Table 5. Summary of Primary Mirror History (Cont)

System S-2 (Cont)	
June 1965	Plated at Metal Surfaces, used spin process. In process.
July 1965	Still exhibited soft spots and imperfections after three weeks in process.
Aug 1965	Stripped by UHT via heat treatment. Plated by Metal Surfaces with 0.002-inch copper plating. Machined at J&R Machine Shop of Fort Worth, Texas, using aspheric template. Plated by Metal Surfaces with 0.003-inch nickel plating; plating rejected - excessive bubbles. Stripped by Metallurgical Consultants of Montebello, California. Plated by Anadite of South Gate, California, with 0.006-inch nickel. Machined at J&R; exhibited some bubbles and hairline cracks. Tried spot plating at Confederate Supply in Arlington, Texas after J&R machining - no improvement noted. Anadite stripped and replated with 0.004-inch Ni layer. Plating flaked off during machining at J&R.
Sept 1965	Stripped and replated by Anadite. Heat treated to a lower Rockwell number. Machined at J&R, plating flaked off. Anadite stripped and replated.
Oct 1965	Machined at J&R; surface was too far off-axis. Anadite stripped and replated.
System S-2 never was successfully completed.	
System S-3	
Sept 1964	SBRC issued purchase order to TI.
Oct 1964	Plated by Metal Surfaces.
Nov 1964	Part rejected - plating quality, surface pits.
Jan 1965	Plated by Metal Surfaces via spinning process; during process part was severely etched. Sent to SBRC for evaluation.

Table 5. Summary of Primary Mirror History (Cont)

System S-3 (Cont)	
Mar 1965	SBRC sent mirror blank to TI with instructions to work as is, if possible. Plating too uneven.
May 1965	Stripped by UHT via heat treatment. S-3 remachined at Speedring.
June 1965	Plated at Metal Surfaces using spin process; Metal Surfaces had rejected a plating job and had stripped part chemically and replated. Plating rejected by TI.
Aug 1965	Plating stripped via heat treatment by UHT. Plated by Metal Surfaces. Rejected by TI. Stripped and plated by Anadite. Machined by J&R.
Sept 1965	Stripped and replated by Anadite. Machined by J&R. In process. S-3 primary completed.
Oct 1965	Could not complete a secondary to this primary.
Nov 1965	Stripped and replated primary by Anadite. Machined by J&R.
Dec 1965	Completed primary.
Jan 1966	Silicon secondary completed.
Feb 1966	System delivered.
System S-4	
Sept 1964	SBRC issued purchase order to TI.
Nov 1964	Plated by Metal Surfaces with 0.002-inch thickness nickel. Coating too thin, broke through during grinding.
Dec 1964	Chemically stripped by Metal Surfaces. Plated by Metal Surfaces with 0.005- to 0.008-inch thickness; had not been properly stripped and was etched. Shipped to SBRC for evaluation. SBRC shipped part back to TI with authorization to use it.

Table 5. Summary of Primary Mirror History (Cont)

System S-4 (Cont)	
Jan 1965	Stripped by Metal Surfaces. An attempt to polish beryllium directly was made (not successful). Plated by Metal Surfaces.
Feb 1965	Dial indicator showed uniform surface. In process.
Mar 1965	Completed primary mirror. Completed silicon secondary.
May 1965	Shipped completed system to SBRC.
System S-5	
Sept 1964	SBRC issued purchase order to TI.
Dec 1964	Plated by Metal Surfaces. Special heat treat to improve optical finishing properties.
Feb 1965	Asymmetrical polishing.
Mar 1965	Stripped by UHT via heat treatment. Plated at Metal Surfaces using spin coat process.
Apr 1965	Part rejected for porosity problems. Stripped via heat treatment by UHT.
May 1965	S-5 remachined at Speedring.
June 1965	Plated by Metal Surfaces using spin coat process.
July 1965	In process. Rejected because of porosity problems.
Aug 1965	Stripped by UHT via heat treatment. Plated by Metal Surfaces - 0.002-inch thick copper and 0.003-inch nickel. Machined at J&R. Rejected because of excessive bubbles in outer 1 inch. Stripped by Metallurgical Consultants. Anadite of California plated part with 0.006-inch nickel layer. Machined at J&R, exhibited some bubbles and hairline cracks. Remachined to get underneath bubbles; bubbles opened up.

Table 5. Summary of Primary Mirror History (Cont)

System S-5 (Cont)	
Sept 1965	Stripped and replated by Anadite. Heat treated to a lower Rockwell hardness. Machined at J&R. Completed S-5 primary.
Oct 1965	Completed silicon secondary.
Nov 1965	Shipped completed system to SBRC.
System S-6	
Sept 1964	SBRC issued purchase order to TI.
Oct 1964	Plated by Metal Surfaces. Plated part rejected.
Dec 1964	Stripped and plated by Metal Surfaces.
Mar 1965	Stripped by UHT. Plated by Metal Surfaces using spin process.
Apr 1965	Rejected because of porosity problems.
May 1965	Stripped by UHT. S-6 remachined at Speedring.
June 1965	Plated by Metal Surfaces. In process.
July 1965	Rejected due to porosity problems.
Aug 1965	Plated by Metal Surfaces - 0.002-inch thick copper and 0.003-inch thick nickel. Machined at J&R. In process. Completed S-6 primary mirror.
Sept 1965	Completed S-6 silicon secondary mirror.
Nov 1965	Shipped completed system to SBRC.
System S-7	
Sept 1964	SBRC issued purchase order to TI.
Oct 1964	Plated by Metal Surfaces.
Nov 1964	In process. Plating was so uneven the tools would not center.

Table 5. Summary of Primary Mirror History (Cont)

System S-7 (Cont)	
Dec 1964	Stripped and plated with copper by Metal Surfaces. In process, ground and polished copper.
Feb 1965	Plated with thin nickel layer over polished copper. In process, went through the nickel layer. Stripped and plated by Metal Surfaces with nickel using spin coat process. In process.
Mar 1965	Completed S-7 primary.
Apr 1965	Completed S-7 silicon secondary.
May 1965	Shipped completed system to SBRC.
System S-8	
Sept 1964	SBRC issued purchase order to TI.
Oct 1964	Plated by Metal Surfaces.
Nov 1964	Measured surface variations after plating; variations of the order of 0.008 inch were found.
Dec 1964	Improvement of polishing characteristics was attempted via heat treatment. In process.
Jan 1965	Second heat treatment to improve polishing characteristics. Stripped by TI.
Feb 1965	Polished bare beryllium. Plated by R&L Plating of Dallas, Texas; part was etched by R&L due to a wrong P-H factor.
Mar 1965	Ground beryllium to remove etch marks.
May 1965	S-8 remachined at Speedring.
July 1965	Plated by Metal Surfaces using spin coat process. In process.
Aug 1965	Completed S-8 primary mirror. Completed S-8 silicon secondary mirror.
Aug 1965	Completed system shipped to SBRC.

The fabrication of an aspheric optical surface requires polishing with a tool that has very small surface area, whereas either a spherical surface or a flat surface can be polished with a tool having large surface area.

In the opinion of the optical vendor, minor variations existed in the hardness of the nickel plating. The small polishing tool used would tend to dig deeper in the softer portion of the surface, and destroy the surface of revolution.

In an effort to get some control over this problem, several approaches were tried as given below:

1. Several plating companies were tried, but none seemed greatly superior.
2. The mirror blank was rotated during the plating process. This seemed to produce some improvement.
3. After plating, the parts were given a heat soak to control the nickel hardness.
4. After plating, the parts were mounted in a tracer lathe and the aspheric surface machined to be a true figure of revolution. However, polishing could later destroy the figure.

Parts were accepted which fell somewhat short of the original procurement specification. Most of the parts did not meet the blur circle requirements and had more than the specified number of pits and blemishes. Despite these apparent problems, systems tests showed that all of the radiometric requirements for the instrument were satisfied. In retrospect, it is felt that the procurement specification for the optics was more stringent than necessary.

Secondary Mirror Finishing. - The secondary mirror has an aspheric surface which is machined in the beryllium blank. The beryllium is plated directly with electroless nickel. It is not possible to use a quick lapping method as was done on the flat scan mirror due to the aspheric shape of the secondary.

The secondary mirror is finished only after the aspheric primary is completed, and the two can be tested together. Small, precise changes on the secondary mirror are made to achieve proper system performance. The nickel is a very hard material that is difficult to polish. Because of variations in the hardness of the plating, soft spots would tend to polish through to the base metal. With this combination of adverse features, the vendor (Texas Instruments) asked if it would be possible to substitute some other material.

The material for the secondary mirror was changed to silicon which is readily available, lightweight, strong, and has very satisfactory optical polishing characteristics.

It would be satisfying to say that eventually the secret of fabricating good mirrors was found. However, at the completion of the task, no clear indication is evident of how to fabricate high-precision nickel-plated beryllium aspheric mirrors.

Conclusion. - Electroless nickel plated beryllium is not recommended for use on a mirror substrate in cases where the optical surfaces have aspheric figuring and high numerical aperture.

Testing Aspheric Primary-Secondary Mirror

The primary mirror was tested during fabrication via a Foucault knife edge test. An auxiliary spherical corrector lens was designed and built, such that, when the primary mirror had the proper aspheric figure, the combination (primary-corrector lens) was free of spherical aberration.

Actually, during fabrication the primary mirror was worked until the blur circle was of the order of 0.0005 inch rather than a null condition.

After the primary mirror was completed, the secondary mirror was matched to the primary using the end item optical system primary-secondary mirror mounts and spider. Since the "nominal" aspheric primary-secondary mirrors formed a null system, the Foucault's knife edge test was used as an in-process method to indicate how the secondary mirror should be optically worked.

As one of the final acceptance tests for the completed optical telescope assembly, image quality was measured on axis, half and full field angles. After the image quality tests and alignment tests were made on the completed assembly, it was never disassembled.

Telescope Performance

Blur circle measurements were performed by measuring the percentage of a beam of collimated light which was focused to pass through a small aperture. The blur circle measured at off-axis positions was essentially the same as that for on-axis radiation for each optical system.

It should be noted that all the optical systems deviated from the procurement specification by varying amounts. Figure 25 shows the blur circle performance for the F-1 telescopes. Off-axis performance is shown in Table 6.

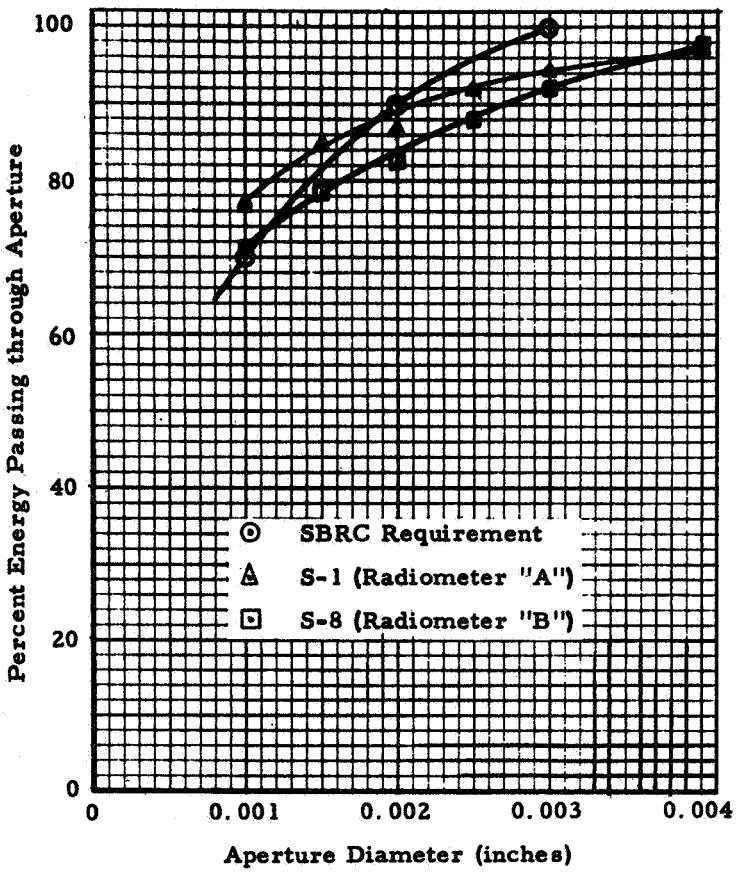

Figure 25. Test Results to Define Blur Circle of Optical Systems for On-Axis Radiation

Table 6. Blur Circle Measurements

Aperture Diameter (inches)	% Transmission System S-1 (Radiometer "A")			% Transmission System S-8 (Radiometer "B")		
	On Axis	0.15° Off Axis	+0.3° Off Axis	On Axis	0.15° Off Axis	+0.3° Off Axis
0.010 (nominal 100%)	100	100	100	100	100	100
0.004	97	97	95.5	97.6	96	97
0.003	94.5	92.2	92	92	92.2	92
0.0025	92	91	90	88	90	89
0.002	87	84.5	84.5	82.5	82.2	84
0.0015	85	82.3	82	78.5	78.8	79
0.001	77.3	75.5	74.3	71	70.2	72
0.025	103	104.5	104	105	105	103

PROCUREMENT OF MECHANICAL ITEMS

Isolation Mount

The payload stage rocket motor for the Dual Radiometer was a rough burning unit. It was expected to cause vibrations approaching 40g (0 to peak) along the vertical (Z axis) in the 525- to 625-Hz frequency range and one-sixth of this in the horizontal (X and Y) directions. Because of spacecraft structural limitations, the 20-inch high radiometer frame which supported a 38-lb star mapper had to be base mounted. The fragility level of the star mapper required that the vibration amplification through the radiometer frame to the star mapper be limited to 1:1 in the critical 525- to 625-Hz frequency range.

The radiometer frame had to be stiff and would probably have maximum vibration amplification in this frequency range. Therefore, it became evident very early in the design that a vibration isolation mount would be required. The following major technical problems had to be overcome in the design of the mount.

1. The radiometer, being base mounted, required a noncenter-of-gravity type mount. This would have to be designed to be stable during the payload vehicle 280-rpm spin.

2. The spacecraft was expected to have resonances below 40 Hz. Therefore, the natural frequency of the isolation system would have to be kept between 40 and 500 Hz. Due to the noncenter-of-gravity mounting, two coupled natural frequencies would occur along the horizontal axes (X and Y), the rocking mode and the lateral translation mode. If the lower mode frequency is kept above 40 Hz, the upper frequency will be above the upper limit and vice versa. To solve this problem would require very close control of the spring rates of the mount in various directions. Also because the radiometer was to be mounted inside the spacecraft, the rocking mode excursions would be limited severely.

3. The mount had to be stiff enough to return the instrument to the proper relationship with the spacecraft mounting platform (0.03°) after launch vibration to accurately measure the horizon gradient. Also, because the spacecraft would be stored horizontally, the hysteresis of the mount had to be low enough so that the instrument would return to its correct alignment after long time loading.

SBRC Specification 18192 was written to describe the requirements of the mount, and the Cal-Val Research and Development Corporation in Burbank, California, was selected as the vendor after competitive bidding. The mount as described was to be relatively stiff (resonant at 100 Hz, transmissibility of 2.5) and isolation was to be obtained by using an elastomer in shear.

The delivered mounts did not meet the specifications in that the rocking mode frequencies were too low (13 and 28 Hz in the Z and Y axes, respectively) and the mount did not return the instrument to true position after prolonged loading in a cantilevered position. A review of the vendor's certified calculations showed that their assumptions for the effective spring constants and the ratio of vertical-to-lateral spring rate were incorrect. The actual ratio of dynamic to static spring rate for the elastomer was 7:1 versus a predicted 4:1. This caused the stability of the mount to be marginal during vehicle spin.

Six machined springs (rate of 5000 lb/in) were designed by SBRC and added to the isolation mount. The springs raised the rocking mode frequencies to an acceptable level (but not above 40 Hz) and enabled the mount to maintain optical alignment with respect to the spacecraft to within the required accuracy. The modified mount provided less than 0.5 transmissibility in the critical input frequency range and was shown to be stable at spin rates over 400 rpm.

Section 5

PERFORMANCE

SCAN LINEARITY MEASUREMENTS

The performance of the scan drive system is critical to the definition of the earth's horizon gradient because spatial resolution depends on the scan position repeatability angle being no larger than the field of view.

Similarly, if for purposes of analysis the scan is assumed linear, the actual departure from linearity must be known.

Therefore, scan position marker pulses have been provided which are superimposed on Channels 1 and 6 by the circuitry described in "Scan Drive Mechanism" and "Internal Calibrate System, " Section 3.

Test Setup

The F-2 system measurements are described since they are the most comprehensive of the flight models.

Measurement of the scan linearity to the required accuracy was not successful on the prototype and F-1 models. The basic reason for the difficulty was that the slow rise and fall time of the radiation output pulse made it difficult to obtain accurate measurements. Measurements were made by taking the time from the calibrate command pulse to a certain point on the leading and trailing edges of the output pulse. The center of this pulse, and hence the scan position at that instant of time, was determined by splitting the time difference between leading and trailing edges. A threshold and squaring circuit was used to generate the counter start-and-stop pulses. The major inaccuracy lay with the shape of the radiation pulse. The rise time of the pulse is limited by the high-frequency rolloff of the amplifiers. That is, for a cutoff frequency of 60 Hz, the 10% to 90% rise time would be about 7 msec. To meet specifications, the position of the center of the pulse must be known to 1 msec or better. Moreover, the pulse is not symmetrical but has a longer fall than rise time which causes the center of the pulse to be displaced at least 1 msec. In addition, noise on the base line of the output signal causes uncertainties in the threshold level which causes further small errors.

It was clear from the foregoing problems that a new technique had to be developed. The method finally used involved two parts. The first was an infrared measurement similar to that already described except that the threshold and squaring circuit was not used. Instead, the pulse itself was

amplified and the position pulse was superimposed on the radiation pulse so that the leading edge of the position pulse coincided with the peak of the radiation pulse. The test setup for the measurement is shown in Figure 26. The data were taken with the radiometer lying on its side and leveled to gravity. The offset of the alignment pads was accounted for in these measurements.

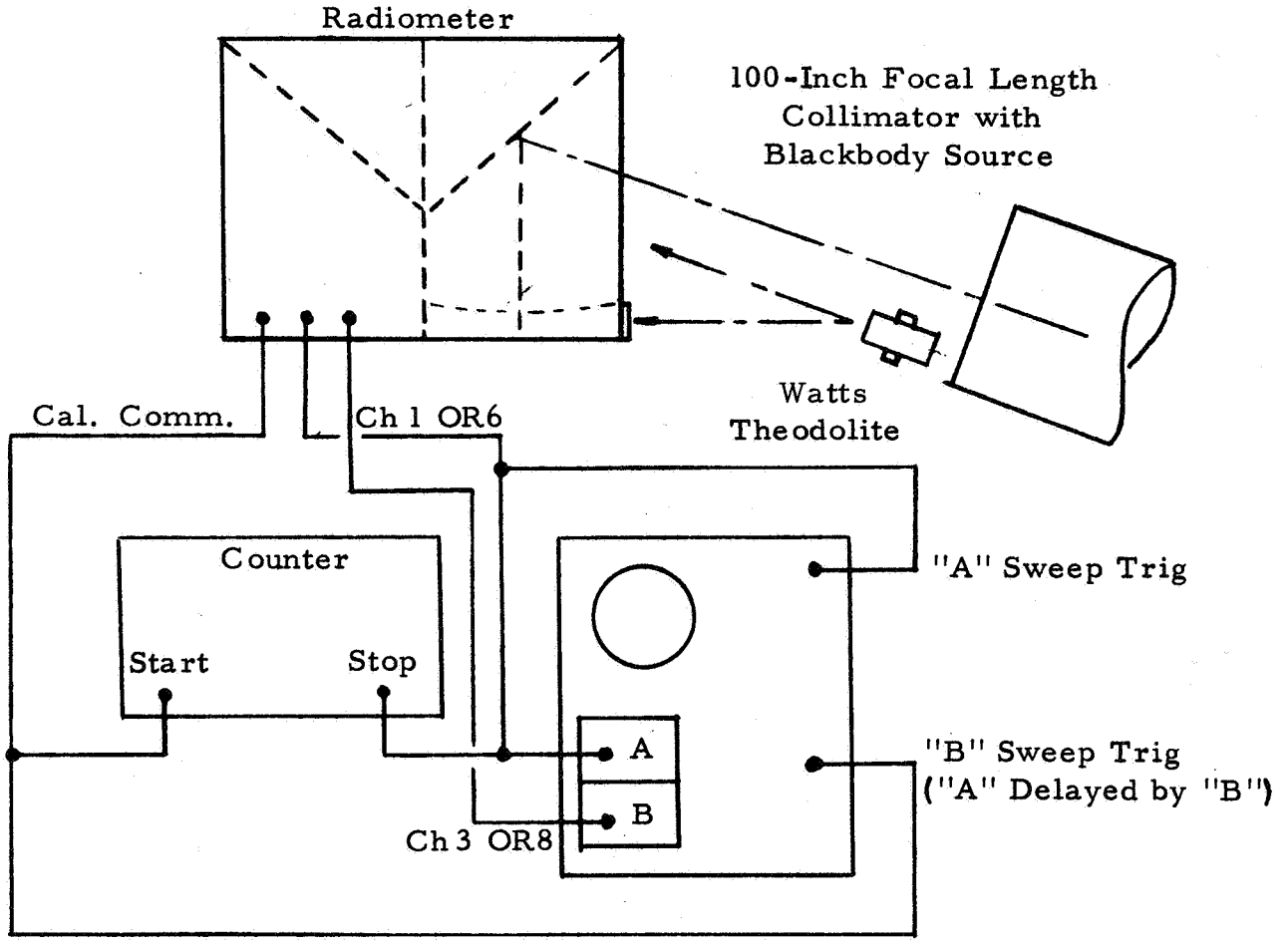

Figure 26. Infrared Scan Linearity Test Setup

It soon became apparent that part of the original problem with the scan linearity measurements was jitter in the time readings readout of the counter. An investigation of this revealed that the source of the jitter was mechanical backlash and end play in the scan drive gear train. Various remedies were tried including new gears and shims. Finally, a teflon friction drag was devised which was installed so as to apply a constant preload to the output shaft. This reduced the jitter from 4-5 msec to about 1-2 msec.

When the pre- and post-environmental data were compared, an angular error of about 3 minutes of arc was noticed. It was recalled that after the pre-environmental measurements but before flight acceptance tests were run, the rubber spider supports for the secondary mirror were installed. The supports deflected the secondary mirror enough to account for some of this error because after removing the supports the error was reduced to about 1.5 minutes.

To confirm this the supports were reinstalled, scan measurements were made and the unit was subjected to a second shock and vibration test, after which it was measured again. A comparison of these two sets of data point by point is given in Table 7. For the readings given in the table, ten counter readings were averaged. The jitter is the time spread between the maximum and minimum readings.

Another way of looking at the data is to fit a least-squares straight line through the four points and then compare the slopes and intercepts. This has been done in Table 8.

The second technique employed was called the "strobe" method. The idea here was to remove the optical filters and to fire a strobe lamp into the aperture of the radiometer coincidentally with one of the position pulses. By adjusting the angle of a theodolite viewing into the aperture properly, the center slit in the aperture mask could be seen if the theodolite angle was exactly equal to the scan depression angle for the particular position pulse being measured.

The advantage of this scheme is that the delay time of the radiometer electronics is removed from the measurement and the depression angle corresponding to each position pulse can be obtained.

A schematic arrangement of equipment is shown in Figure 27. As before, the delay sweep feature of the Tektronix type 545 scope was used to gate out all but the desired position pulse. Because of the delay involved in driving the relay which in turn fired the strobe, it was necessary to employ two counters. The first (A) counter started with the calibrate command and stopped on the position pickoff pulse. The second counter started on the leading edge of the position pickoff pulse and stopped on the sync return from the strobe. The delay times of the strobe firings were converted to angles (because of the known scan rate). The results were then subtracted from the down-scan angles and were added to the up-scan angles. This is so, because on the down scan the delay causes an angle to be read which is larger than it should be to correspond to the "A" counter reading. On the up scan the angle corresponding to the delay time is added to the scan angle readings.

Table 7. F-2 Infrared Scan Data Before and After Flight Acceptance Testing

Radiometer "A"		Before Second Environmental Test		After Second Environmental Test			
Position Pulse No.		Corrected Time (sec)	Corrected Angle (D, M, S)	Corrected Time (sec)	Corrected Angle (D, M, S)	Error (arc sec)	Maximum Jitter (10 Readings) (msec)
1	Down	0.2888	16°48'16.5"	0.2889	16°47'56"	-20.5	1.96
2		0.6646	20 33 26	0.6645	20 33 3	-23.0	1.75
3		1.0395	24 18 10	1.0391	24 17 55	-15.0	1.95
4		1.4136	28 3 0	1.4138	28 2 57	-3.0	2.00
5	Up	1.8899	28 50 42	1.8899	28 50 33	-9.0	1.04
6		2.2648	25 5 38	2.2648	25 5 43.5	+5.5	1.82
7		2.6395	21 20 53	2.6394	21 20 38	-15	1.58
8		3.0136	17 35 47	3.0132	17 35 27	-20	1.93
Radiometer "B"							
1	Down	0.2888	16 39 57.5	0.2890	16 40 31	+33.5	1.64
2		0.6643	20 25 21.5	0.6643	20 25 28.5	+7.0	1.96
3		1.0388	24 10 14.5	1.0394	24 10 43.5	+29	1.82
4		1.4137	27 55 9	1.4138	27 55 14.5	+5.5	1.43
5	Up	1.8901	28 38 55.5	1.8903	28 38 45.5	-13	1.39
6		2.2646	24 53 35.5	2.2647	24 53 55.5	+20.0	1.93
7		2.6392	21 8 46.5	2.6392	21 8 43	-3.5	2.21
8		3.0135	17 23 40.5	3.0135	17 23 37.5	-3.0	1.96

Table 8. Least Squares Fit to Infrared Scan Data

Radiometer	Before Second Environmental Test			After Second Environmental Test		
	Intercept (sec)	Slope (sec/deg)	σ (sec)	Intercept (sec)	Slope (sec/deg)	σ (sec)
A Down	-1.3919	+10.003	2.902×10^{-4}	-1.3904	+9.9982	2.185×10^{-4}
A Up	+4.7719	-9.9906	2.598×10^{-4}	+4.7697	-9.9833	4.253×10^{-4}
B Down	-1.3771	+9.9957	5.83×10^{-5}	-1.3778	+9.9954	3.064×10^{-4}
B Up	+4.75	-9.9835	2.25×10^{-4}	+4.7496	-9.9809	1.394×10^{-4}

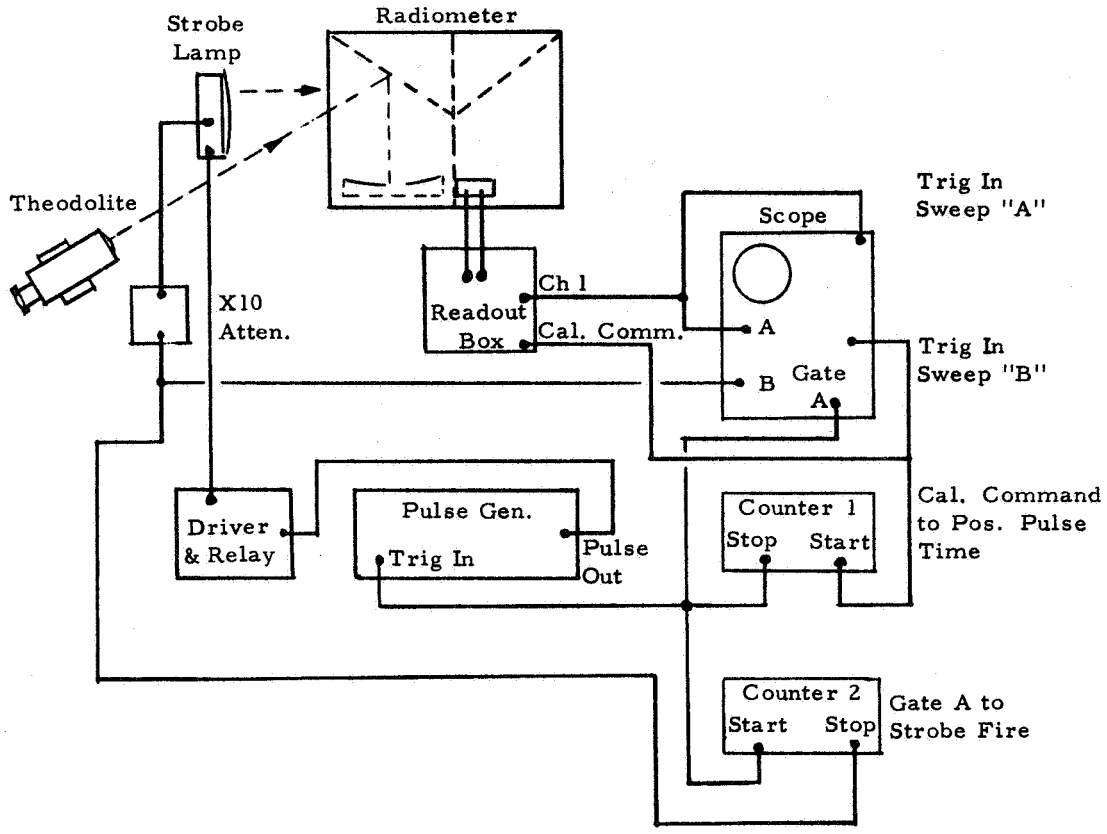

Notes: 1. On time base "B" stability of trigger critical for long delays.

2. Set delay (A delayed by B) to obtain approximate time of position pulse. Then "A" time base will trigger on falling edge of desired position pulse.

Figure 27. Equipment Arrangement, Strobe Method

To minimize angular errors arising from defocusing and aberration effects, glass blanks instead of filters were used again for these measurements. Also, the theodolite was translated for each reading so that the same portion of the telescope aperture was used each time. Several sets of data were taken as a check on repeatability but comparison of data before and after environment was not made since removal of filters to make the measurement might have invalidated the final calibration. Therefore, in Table 9, below, the scan data taken by the strobe method are compared to the infrared scan data taken prior to flight acceptance testing. Three runs were averaged to obtain the strobe readings in the table, but the spread of the three angle readings was less than 20 seconds in all cases.

Table 9. Comparison of Strobe Scan Data to Infrared Scan Data

Radiometer "A"	Strobe Method		Infrared Method		
Position Pulse	Time (sec)	Angle (D, M, S)	Time (sec)	Angle (D, M, S)	Angle Difference (M, S)
1	0.28917	16°46' 0.3"	0.2856	16°44'33"	+1'27"
2	0.6643	20 31 2	0.6609	20 29 46	+1 16
3	1.0393	24 15 43	1.0372	24 14 29	+1 14
4	1.4141	28 0 26	1.4132	27 59 10	+1 16
5	1.8901	28 45 13	1.8888	28 47 22	-2 9
6	2.2649	25 0 23	2.2632	25 2 27	-2 4
7	2.6395	21 15 14	2.6374	21 17 29	-2 15
8	3.0137	17 30 26	3.0119	17 32 55	-2 29
Radiometer "B"					
1	0.2890	16 39 43.4	0.2885	16 38 43	+1 0
2	0.6643	20 24 58.3	0.6640	20 23 48	+1 10
3	1.0392	24 9 53.3	1.0390	24 8 48	+1 5
4	1.4142	27 55 1	1.4144	27 53 37	+1 24
5	1.8901	28 34 59	1.8898	28 37 28	-2 29
6	2.2643	24 50 5	2.2646	24 52 31	-2 26
7	2.6396	21 4 58.4	2.6390	21 7 47	-2 49
8	3.0140	17 19 50	3.0135	17 22 34	-2 44

Because of the delay in the electronics, it is to be expected that the strobe angle readings would be larger than the infrared measurements on the down scan and smaller on the up scan. The table shows this to be true, but a bias appears to be present. That is, the angular difference should be equal for up and down scans. It is clear for reasons already mentioned, however, that there can easily be a bias to the angular strobe readings (tilt of glass blanks, etc.) amounting to as much as 1 arc minute. The use of the blanks and translation of the theodolite preserves only the relative accuracy of the readings.

Also, the fact that symmetrically opposite pairs of pulses, 1 and 8, 2 and 7, etc., are not at the same depression angle will have further biasing effect but since it is the same for infrared readings and strobe readings it will not affect the calculation of the electronic delay.

Therefore, the electronic delay is equal to the time associated with one-half the sum of the angle differences for each pair of pulses. Table 10 gives these values which are then averaged to produce a delay associated with each radiometer. This value cannot be assumed for all channels, however, but must be scaled according to the frequency and phase response.

Table 10. Calculation of Electronic Delay

Radiometer "A" (14-16μ)		Radiometer "B" (20-40μ)	
Position Pulse Pair	Delay (msec)	Position Pulse Pair	Delay (msec)
1 and 8	3.28	1 and 8	3.11
2 and 7	2.92	2 and 7	3.30
3 and 6	2.75	3 and 6	2.92
4 and 5	2.83	4 and 5	3.24
Avg Delay (msec)	2.94	Avg Delay (msec)	3.14

INFRARED FIELDS OF VIEW

Test Setup

The FOV measurements shown here for the F-3 system were made in a straightforward manner using a 100-inch focal length collimator and a chopped blackbody source operating at about 700°C. Because the image at the focal plane of the radiometer was substantially smaller than the aperture stop, the system S/N ratio was low. Therefore, a synchronous demodulator having an equivalent bandpass of 0.2 Hz was used to enhance the S/N ratio by a factor of roughly 25.

Three scans were made across the 0.025° dimension for each FOV, one across the center and one across each half-power point. One center scan was made across the 0.10° dimension. The center scan for each dimension is presented together on one sheet and the half-power scans on another. The angular displacement of the half-power points from the center is also indicated (see Figures 28 and 29).

The 0.025° plots were made using a 0.005 X 0.080 inch aperture in the collimator oriented with the long dimension and centered on the 0.10° FOV dimension.

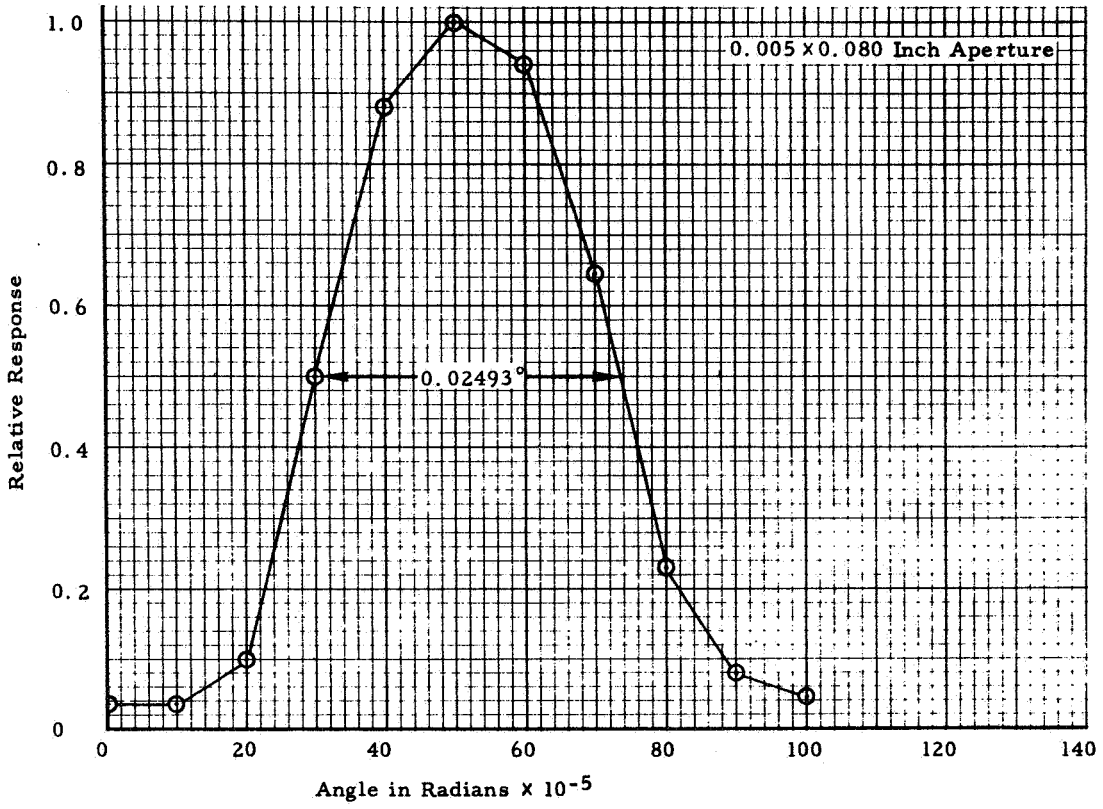

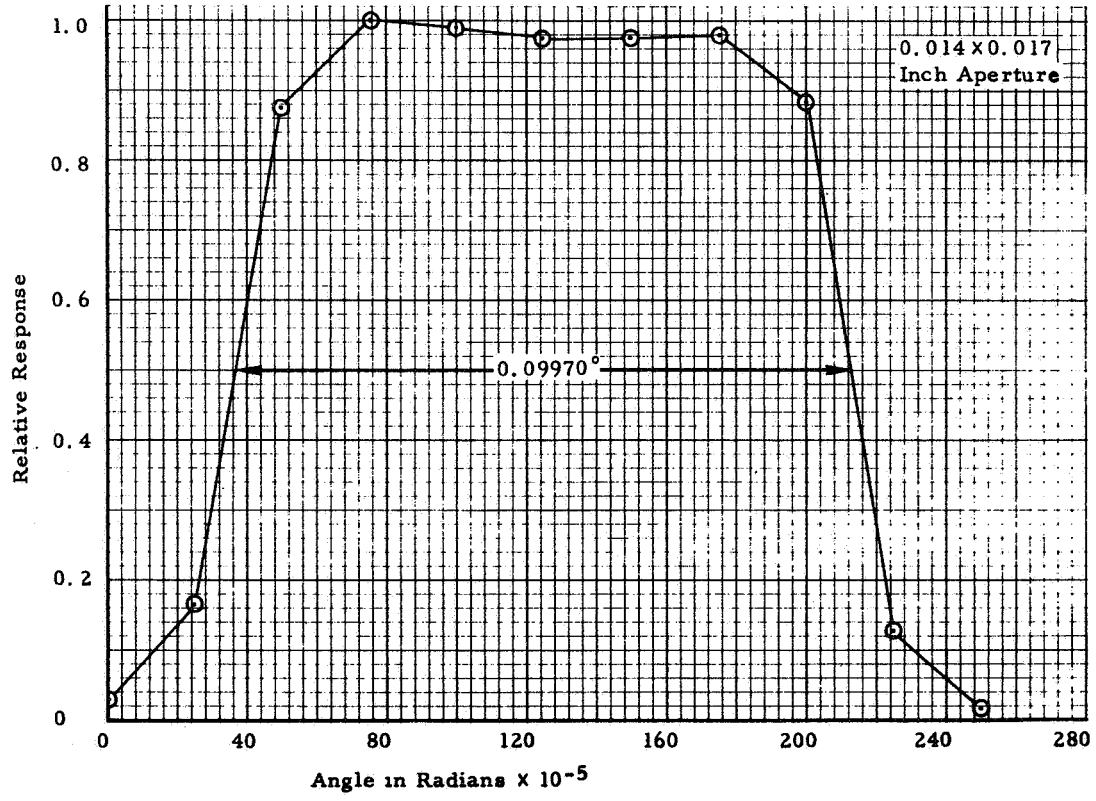

Figure 28. Infrared Fields of View, Channel 1, 0.025° Dimension and 0.10° Dimension, Center Scan

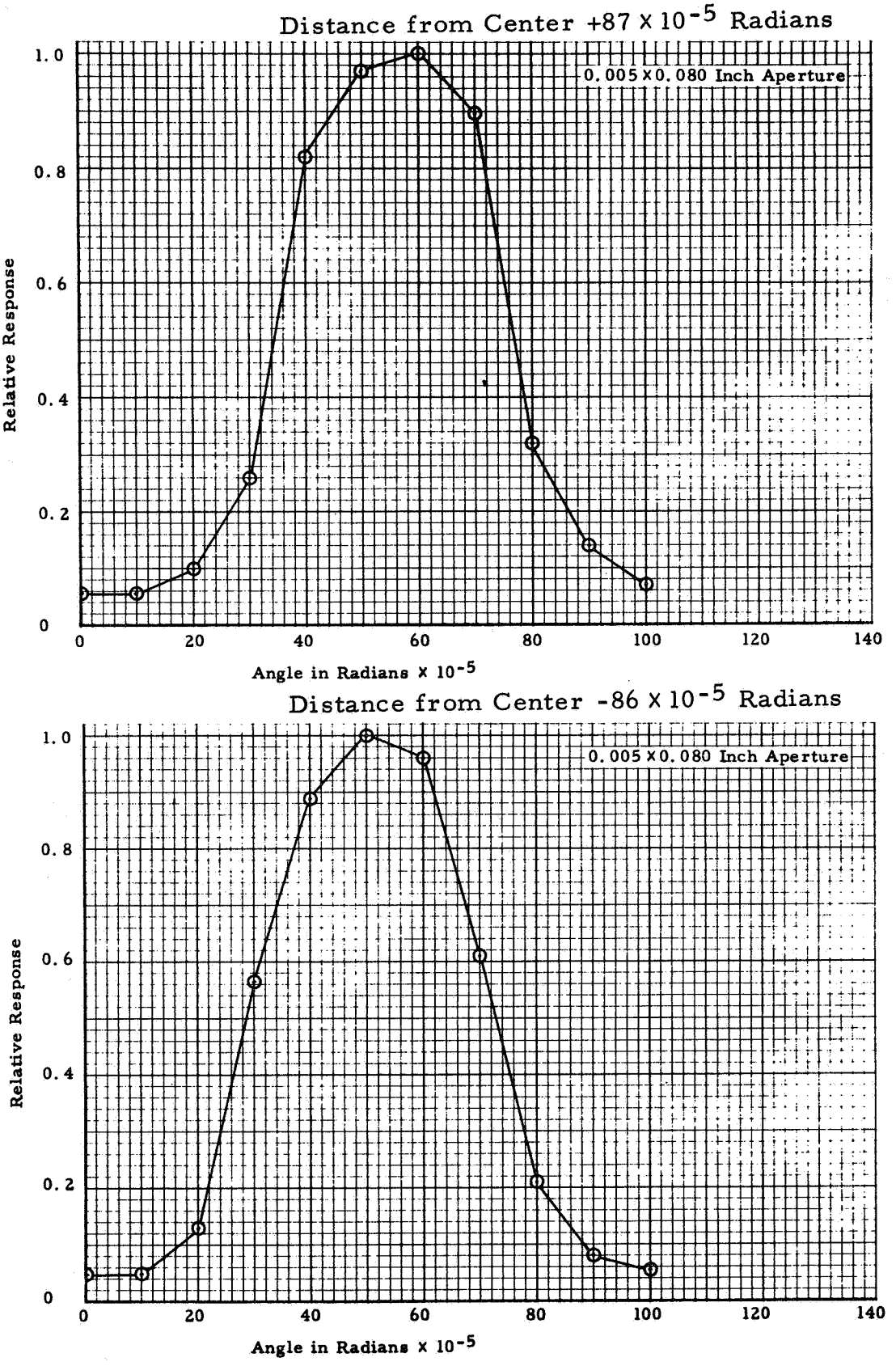

Figure 29. Infrared Fields of View, Channel 1, 0.025° Dimension, ± Half-Power Point Scans

The 0.10° plots were made using a 0.014 x 0.017 inch aperture with the long dimension aligned with the center of the 0.025° FOV dimension. Since mechanical alignment of the collimator could not be maintained for these runs it was necessary to measure the angular displacement by viewing the aperture stop directly with the theodolite.

Results of Tests

The requirements for the narrow FOV are that the width at the 50% response points be less than 0.025° and that the 5% points be less than 0.008° away from the 50% points.

Although measurements for only one channel are shown, the narrow 0.025° dimension was well within ±0.005° in all cases.

The skirts did not have the required steepness although this system appeared to be better in this respect than either the F-1 or F-2 systems.

The 0.10° FOVs for the 14- to 16-micron channels (Radiometer A) were somewhat narrower than specified owing to the acceptance angle in the germanium immersion lenses. The 0.10° dimensions of the 20- to 35-micron channels (Radiometer B) were within the specification.

Table 11 summarizes the half-power FOVs for both Radiometers A and B. Also shown in Table 11 are indicators of skirt steepness for the 0.025° center scans. The larger of the two values of transmission at the two skirts is indicated for 0.008° away from the half-power points.

The slight non-uniformities of the flat tops of the 0.10° FOVs are attributed to defects in the antireflection coatings on the immersion lenses. Microscopic examination of these lenses before assembly showed some crazing and pitting of the spherical surfaces.

Table 11. Half-Power Point Widths and Percent Transmissions

Radiometer "A"				Radiometer "B"			
Channel	Half-Power Point Width 0.1° Dimension (degrees)	Half-Power Point Width 0.025° Dimension		Channel	Half-Power Point Width 0.1° Dimension (degrees)	Half-Power Point Width 0.025° Dimension	
		Width (degrees)	% Transmission (at 0.008°)			Width (degrees)	% Transmission (at 0.008°)
6	0.07879	0.02424	11.2	1	0.09970	0.02493	12
7	0.08308	0.02458	8.5	2	0.09632	0.02458	13
8	0.08308	0.02475	9	3	0.10030	0.02458	12
9	0.08308	0.02538	9	4	0.099086	0.02458	11.5
10	0.08394	0.02579	10	5	0.09884	0.02412	11.5

FREQUENCY AND PHASE RESPONSE

Test Setup

The test setup used for the measurement of the F-3 frequency and phase response was identical to that used for the prototype F-1 and F-2 models. The technique was to modulate a Kay Electric Company "Pinlite" directly with a Hewlett-Packard Model 202A sine-wave generator. A dc biasing circuit was added so that frequency doubling was not present in the lamp output. By removing the optical filter and placing the lamp within 1/4 inch of the detector sufficient energy was available beyond 1.8 microns to pass through the immersion lenses and give a full output signal.

Since the output of the lamp falls off rapidly above 10 Hz, a reference photodiode was mounted next to the lamp so that the lamp output could be kept constant with increasing frequency.

The original specification requirement was that the high frequency system response would be 6 db down at 80 Hz. However, after radiometric calibration of the prototype and F-1 units it was found that a reduction in the bandwidth was needed to improve the S/N ratio. Accordingly, the -6 db point was set at about 60 Hz for the 14- to 16-micron channels and 70 hz for the 20- to 35-micron channels.

For the phase response measurements, the reference photodiode output was used to drive the horizontal amplifier of an oscilloscope while the vertical amplifier was driven by the radiometer output. The result was an elliptical Lissajou figure which was measured by the slide-back technique* to produce the phase response plot which, together with the frequency response curve, is shown in Figures 30 and 31.

At the higher frequencies the phase measurements were difficult to make owing to low available signal. Thus, the higher frequency points show irregularities in some cases.

The method described using a modulated "Pinlite" proved to be a far superior technique to that originally attempted; namely, using a mechanically chopped blackbody. A sine wave was produced by making an eccentrically mounted circular chopper which modulated a narrow slit. An ordinary bladed chopper could not be used because of the harmonics produced by the square-wave chop. Unless a wave analyzer were used, the harmonics would produce an error in the output. The major difficulty with the mechanical system was providing speed control over three orders of magnitude (0.1 to 100 Hz).

---

*Refer to page 76 for a description of the slide-back technique.

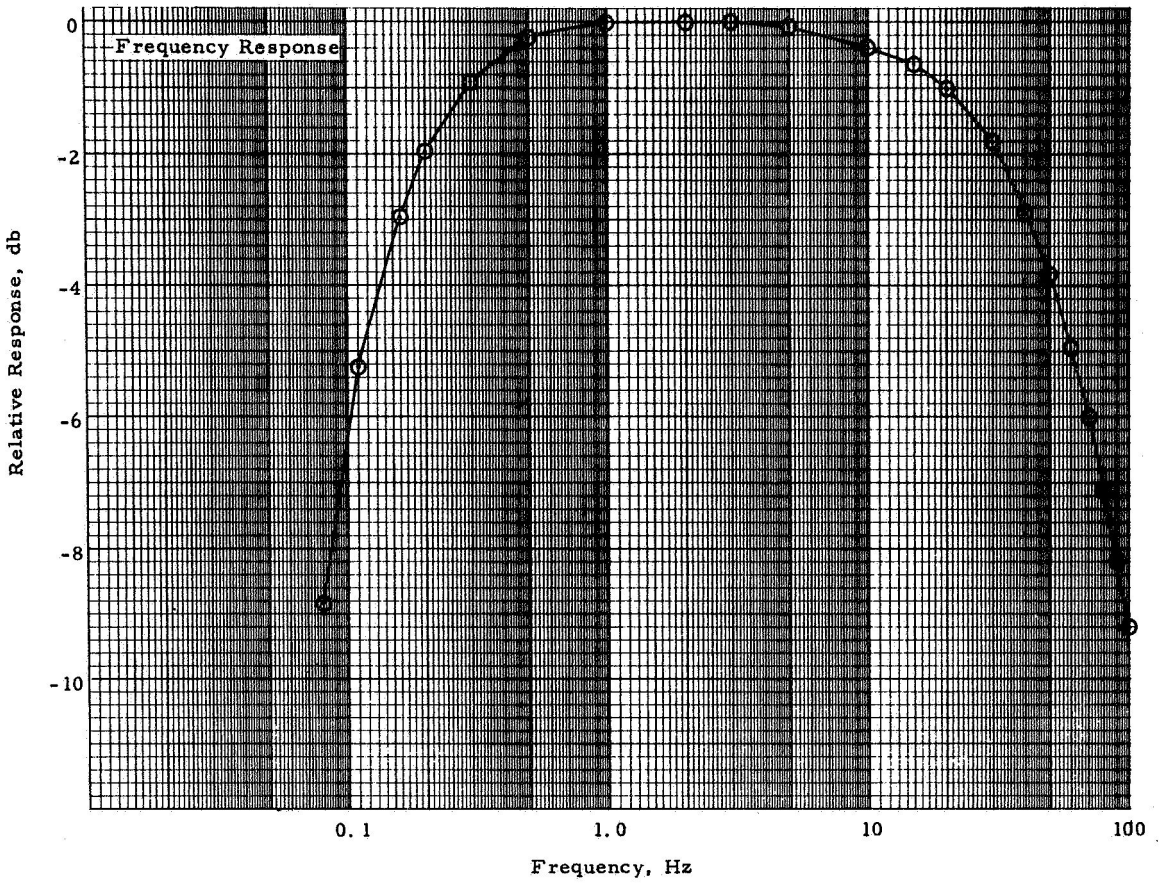

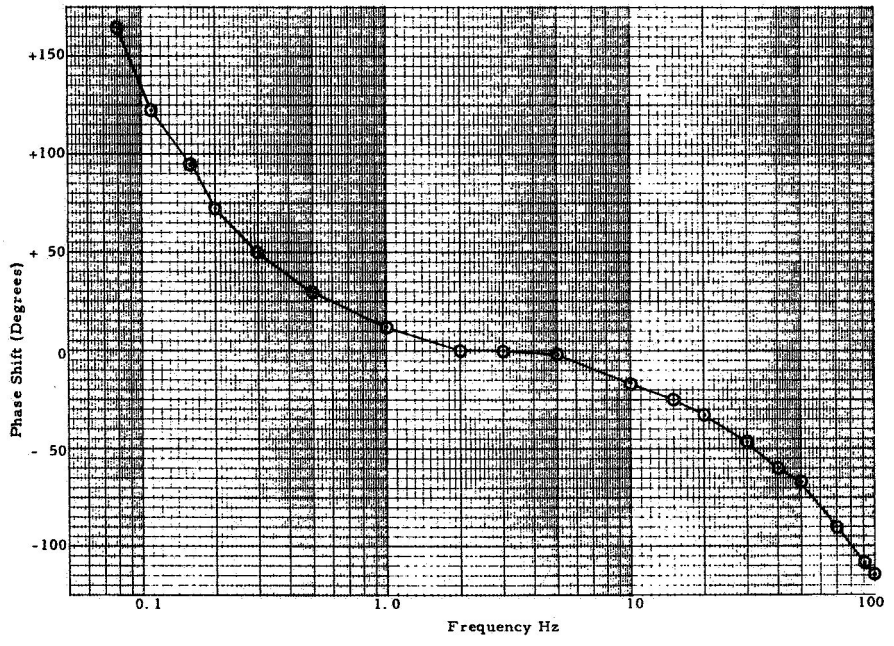

Figure 30. Frequency Response and Phase Shift, 20- to 35-Micron Channel, F-3

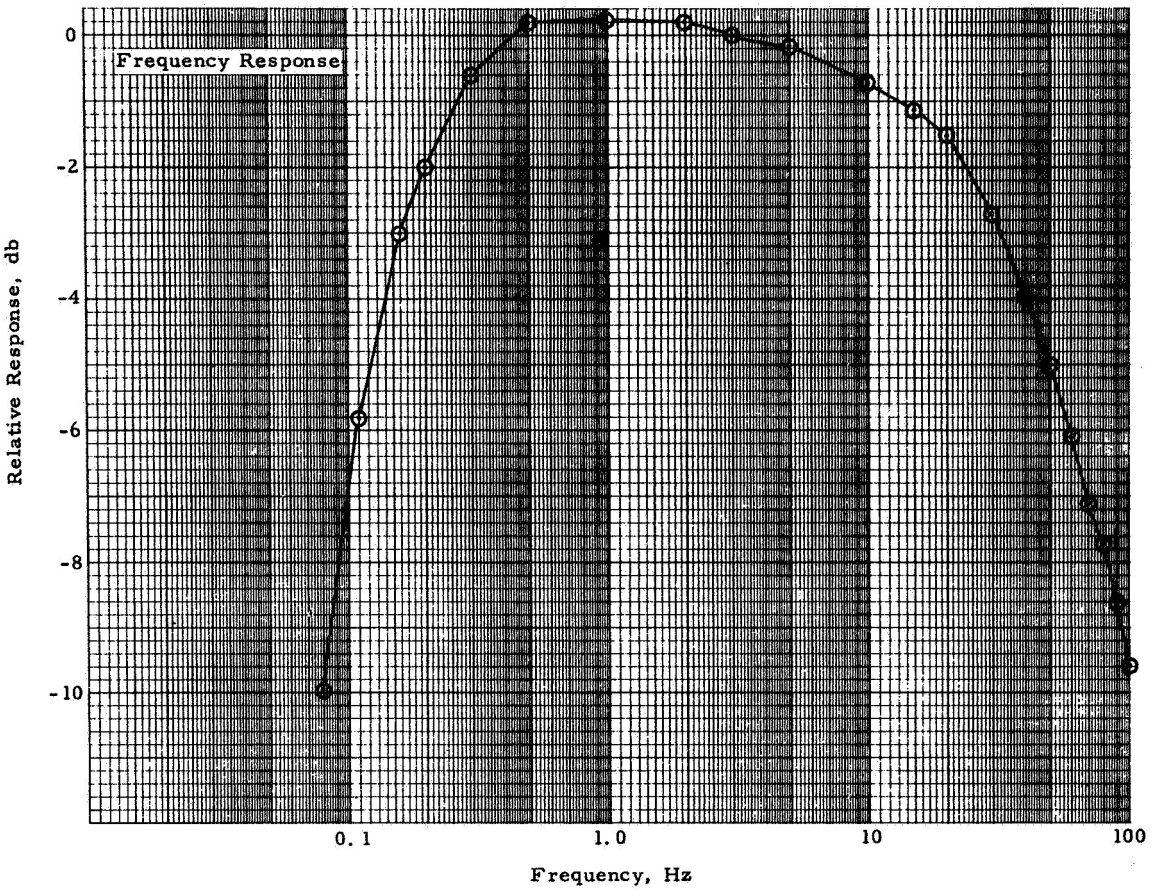

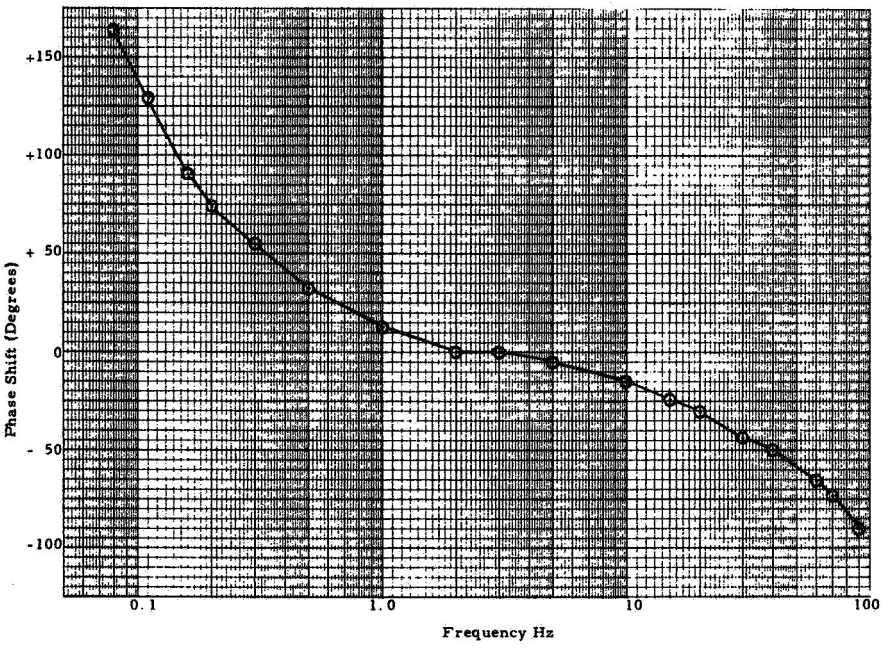

Figure 31. Frequency Response and Phase Shift, 14- to 16- Micron Channel, F-3

INTERNAL CALIBRATION

The method of inflight calibration was described earlier in this report in Section 3. In this section the calibrate pulse heights actually obtained on the F-2 system are given.

The lamps are driven from the forward voltage drop of a silicon diode connected through a resistor and transistor switch to the +28 volt line ("A" spacecraft battery). In this configuration, the output of the lamps was a fairly sensitive function of the supply voltage, but this connection was necessary to prevent switching transients from getting into the amplifier channels through the +18 volt regulator. Measurements of this dependence are shown in Table 12. The output of the system is essentially independent of variations on the "B" 28-volt battery because of internal regulation and filtering. A summary of the calibrate pulse amplitudes measured on the F-2 system is given in Table 13.

Table 12. Changes of Calibrate Pulse Output with Power Supply Variations

Supply Voltage (volts)	Percent Change in Output, Channel 3 (volts)	Percent Change in Output, Channel 8 (volts)
26	-4.8	-7.0
28 (nom)	0	0
30	+5.7	+6.2

Table 13. F-2 Radiometer, Calibrate Pulse Amplitudes

Radiometer "A" (14-16μ)		Radiometer "B" (20-40μ)	
Channel	Pulse Amplitude (volts)	Channel	Pulse Amplitude (volts)
6	1.833	1	1.317
7	0.801	2	1.031
8	1.721	3	2.135
9	1.073	4	1.130
10	2.173	5	1.355

RADIOMETRIC CALIBRATION

Technique and Equipment

The calibration technique employed may be called the extended source method although the approach was somewhat indirect. Three well known types of calibration could have been used.

1. Distant small source method
2. Extended source method
3. Jones method (small source located near the radiometer which, under proper alignment conditions, will uniformly irradiate the detector).

Method 2 was felt to be the best calibration technique in this case because it would approximate the actual conditions under which data is taken.

The ideal method of obtaining a radiometric calibration is to have the radiometer FOV alternately filled by radiation from two blackbody cavities at different known temperatures. In this case, the size of the radiometer aperture, 9 inches, and the speed at which the chopping must be performed eliminated the use of large extended source blackbodies.

Instead, an optical relay system of a Cassegrain type was selected. The primary mirror is a first surface parabolic reflector and the secondary mirror surface is spherical. The optical relay system quality is such that the blackbody cavities completely fill the radiometer FOV. Since the focal length is approximately 35 inches, the radiometer field aperture stops when projected in the blackbody cavity opening subtends 1.0 inch as a maximum value. This includes magnification between the systems, the aberrations of the optical relay system, and fabrication tolerances of the optical components. The central obscuration of the calibrator optics is smaller than that for the radiometer.

The two blackbodies are capable of being independently cooled to LN_2 temperature or heated if desired. A motor driven mirrored chopper alternately reflects radiation from the two blackbodies into the aperture of the radiometer. An additional folding mirror is used so that there is an equal number of mirror reflections for both the "space" look and the "earth" look. Thus, providing that the chopper and folding mirror are at the same temperature, no error in calibration will be introduced by optical losses of the calibrator. A photo of the calibrator assembly is shown in Figure 32.

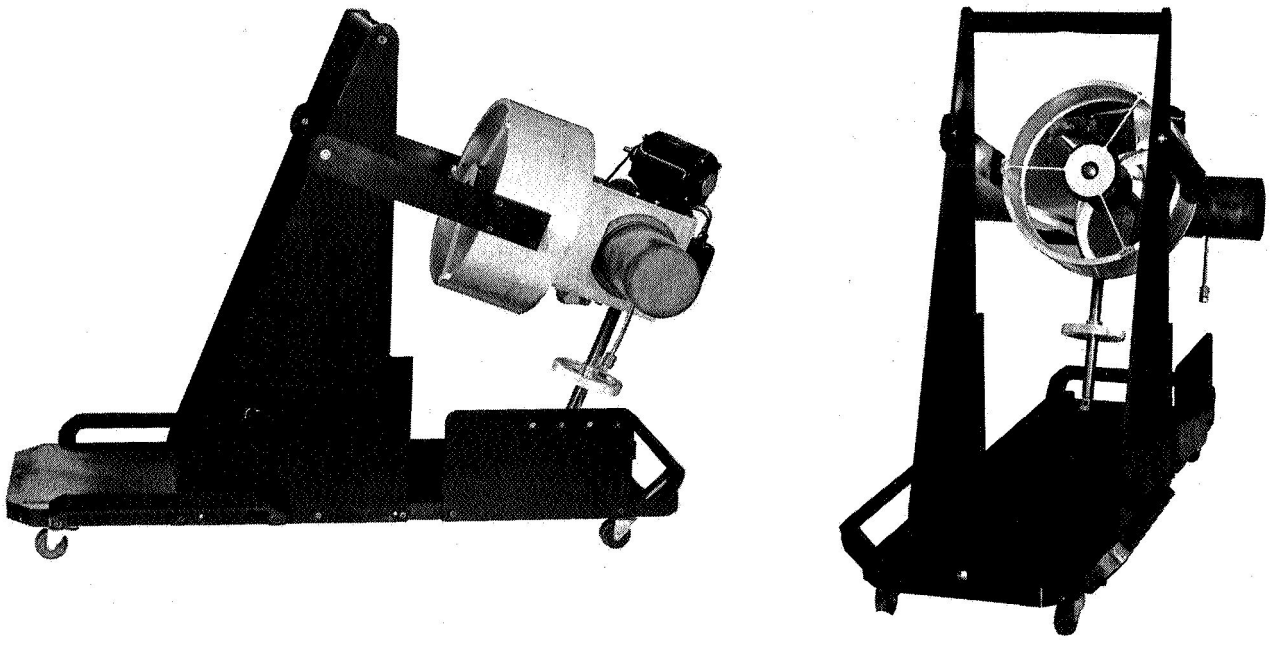

Figure 32. Radiometric Calibration Fixture

The procedure during a calibration run was to flow LN_2 through both blackbodies until the lowest possible temperature was obtained. The null output of the radiometer was observed to ensure that the FOVs were truly centered on the blackbodies and not on surrounding structure. Then, while the LN_2 flow was maintained to the "space" blackbody, the LN_2 to the "earth" blackbody was turned off and the temperature drifted upward. Data were taken at eight or nine points between the temperatures of 130°K and 250°K. Also, runs were made at each of five instrument temperatures in the range 50°F to 90°F.

Calibration of the F-2 and F-3 systems was performed at the Hughes Aircraft Space Systems Laboratory in El Segundo, California. The F-1 system was calibrated at Wyle Laboratories in El Segundo.

At Hughes a 7-foot diameter bell-jar vacuum system was used which was equipped with actively controlled thermal shrouding on the walls as well as on the top and bottom of the chamber. The thermostatically controlled Lexol piped through the shrouds provided temperature control of the unit by radiative transfer to within 2° to 3°F of any desired temperature between 50°F and 90°F. The chamber was designated as Class 4 which sets certain

standards for cleanliness. As a minimum, the chamber was washed internally and baked out prior to use.

The data described in this report were taken on the F-2 system because it is the most comprehensive data for any of the units.

Output Voltage Measurement

Two methods of signal voltage measurement were used: recording on a multitrack FM tape machine, and direct measurement using an oscilloscope and digital voltmeter "slide-back" technique.

Tape Recordings. - Tape recordings were made using an Ampex ten-channel FM subcarrier tape machine. The recordings were taken simultaneously with the measurements using the "slide-back" technique. This was intended as a backup technique to provide a positive record of the calibration data. Tape speed of 30 inches per second and a carrier frequency of 54 kHz were used for all channels. Flutter and wow compensation was not employed. The input impedance of all channels was greater than 10 megohms except for the pre-environmental runs. For these, because of a misunderstanding, the input impedance was 100 Kohms. This impedance was sufficiently low to cause a sizable decrease in output of Channels 1 and 6. This was so because the emitter followers used in the position pulse circuitry had an output impedance of about 15 Kohms. The other channels had much lower output impedances.

Calibration runs were made of the recording equipment at the beginning of the radiometer calibration and at 4-hour intervals during the calibration. The first of these was done by applying a sine-wave voltage to the input of the machine from 0 to 2.5 volts peak-to-peak amplitude so that linearity could be assessed. The remaining calibrations were performed with 2.5-volt peak-to-peak inputs only.

Data recording on tape was performed at every blackbody temperature and voice annotation was used for identification.

"Slide-Back" Measurement Technique. - This method is used for all calibration data measurement. It consists of displaying the radiometer output waveform, a square wave with droop, on one trace of a dual trace oscilloscope. On the other, a square wave of much higher frequency is presented. The square wave is generated by a free-running multivibrator relay circuit which switches between ground and a dc voltage produced by a battery-helipot arrangement. The voltage at the wiper arm of the helipot is monitored by a digital voltmeter. Amplitude coincidence of the two waveforms is produced by adjusting the helipot so that the square wave bisects the noise top and bottom on the output signal waveform.

Because the radiometer output waveform has droop, the peak-to-peak value is not read. Instead, the peak-to-"break" value is read out.

The technique has the advantage that noise present on the signal can be averaged out by eye. Also, of course, the accuracy of the scope is not involved since it is used only as a visual coincidence indicator. Temperature sensor voltages are read directly with the digital voltmeter.

It should be explained at this point that the calibration was arranged to simulate as nearly as possible the actual conditions to be expected when the radiometer is in space scanning across the earth horizon gradient. Thus, the mirror chopper speed was set at 5 Hz (300 rpm) so that the dwell time of 100 msec would approximate the time of a horizon crossing.

Test Results

Five calibration runs were made on radiometer "B" (20 to 35 microns) and four on "A" (14 to 16 microns). Because of the large volume of data, it is not presented point by point in this report. Instead, each run consisting generally of eight points was processed on a digital computer and the least squares straight line fit and standard deviation of the points was determined. The results of these computations are given in Tables 14 and 15.

Table 14 gives the data taken at 80°F instrument temperature and Table 15 shows the data taken at other instrument temperatures.

Both tables give the slope, zero irradiance intercept, standard deviation and the maximum deviation from the straight line fit. Also, the percent change in slope and the initials of the person taking the data are given. Because of discrepancies in the scan data the unit was given two shock and vibration tests. Runs labeled "TS A" and "last" were taken following the second exposure. The runs are identified as follows:

PRE Pre-environmental; the first run.

REV Also pre-environmental but with the sense of the blackbodies reversed.

POST After the first shock and vibration tests were performed.

TS A After the second shock and vibration test. During the "Pre," "Rev" and "Post" runs, a broken wire in the cable disabled the radiometer "B" temperature sensor which necessitated using the "A" sensor for all runs. For the "TS A" and "Last" runs this was corrected, but the "A" sensor was used for the "TS A" radiometer "B" run to check consistency with previous data.

LAST After the second shock and vibration test. Appropriate temperature sensors were used.

Table 14. F-2 Calibration Data - Least Squares Fit at 80°F Instrument Temperature

Run By	Channel	Run Type	Intercept (mv)	Slope (mv/flux)	σ (mv)	Maximum Deviation (mv)	% Slope Change
HH	1	PRE	+14.84	4297	9.6	15.7	
HH		REV	+1.60	4284	11.18	15.3	
HH		POST	+14.78	4526.4	6.47	11	
AHS		TS A	No Good, Bad Connection				
HH		LAST	+29.6	4719.2	10.6	17.2	
HH	2	PRE	+15.85	5076	13.6	22.7	+2.222
HH		REV	-6.54	5076.8	4.15	5.44	+2.272
HH		POST	+14.2	4912.3	7.56	10.4	-1.052
AHS		TS A	+8.39	5005.3	21.8	42.1	+0.831
HH		LAST	+28.7	4964	6.99	12.1	0
HH	3	PRE	+1.31	4985.5	3.73	7.29	+2.476
HH		REV	+10.7	4885.8	13.69	17.8	+0.427
HH		POST	+10.18	4807	8.48	15.3	-1.206
AHS		TS A	+9.55	4876.6	16.2	30	+0.238
HH		LAST	+16.4	4865	10.7	17	0
HH	4	PRE	+3.13	4953.8	6.99	11.8	+1.325
HH		REV	+5.19	4869.9	5.85	10.5	-0.392
HH		POST	+13.28	4803.9	9.69	22.9	-1.771
AHS		TS A	+6.57	4934.2	14.2	31	+0.924
HH		LAST	+22.4	4889	4.47	8.29	0
HH	5	PRE	+11.49	5032.8	8.46	16.5	+2.469
HH		REV	+2.65	4999.4	5.39	7.80	+1.789
HH		POST	+4.03	4900	6.94	14.6	-0.234
AHS		TS A	+19.8	4913.5	9.74	17.4	+0.040
HH		LAST	+31.8	4911.5	9.09	14.0	0
AHS	6	PRE	+2.822	10810	21.3	42.4	
AHS		REV	-23.9	10821	5.88	9.8	
AHS		POST	+17.3	11323	18.1	32.6	
AHS		LAST	-6.98	11732	21.14	36	0
AHS	7	PRE	+10.69	13802	14.96	24.6	+4.205
AHS		REV	-45.4	14145	16.9	23.5	+6.795
AHS		POST	+14.0	13160.8	14.38	35.3	-0.639
AHS		LAST	-0.64	13245	18.3	31	0
AHS	8	PRE	-15.2	13439	14.7	22.6	+5.61
AHS		REV	-45.88	13333	14.44	20.4	+4.384
AHS		POST	-1.986	12782	5.72	11.0	+0.0704
AHS		LAST	+4.27	12773	14.6	21.4	0
AHS	9	PRE	-12.36	13786	20.87	46.7	+3.07
AHS		REV	-52.8	13672	18.2	27.6	+2.2
AHS		POST	+26.5	12746	11.1	19.75	-4.94
AHS		LAST	-16.1	13375.8	9.59	14.4	0
AHS	10	PRE	-21.74	12761	19.7	24	+4.61
AHS		REV	-52.45	12540	21.5	35.3	+2.80
AHS		POST	-17.2	11971	17.97	31.45	-1.894
AHS		LAST	-7.167	12197.8	9.4	14.0	0

Table 15. F-2 Calibration Data - Least Squares Fit at Various Instrument Temperatures

Run By	Temperature (°F)	Channel	Run Type	Intercept (mv)	Slope (mv/flux)	σ (mv)	Maximum Deviation (mv)	% Slope Change
HH	50	1	PRE	+16.96	4342	12.2	20.6	
HH	50		LAST	+16.8	4837.5	8.8	12.5	
HH	60		PRE	+13.7	4451.8	9.9	10.52	
HH	60		LAST	+32	4830.6	9.75	24	
AHS	70		PRE	-16.25	4417.1	6.04	9.7	
AHS	70		LAST	-6.22	4849.8	5.6	8.8	
AHS	90		PRE	+15.53	4004.9	11.69	22.6	
HH	90		LAST	+32.75	4557	7.8	13	
HH	50	2	PRE	+19.3	5186.4	16.3	24.1	+0.526
HH	50		LAST	+19.9	5213.7	10.68	22	
HH	60		PRE	+12.5	5246.9	13.8	29.45	-1.39
HH	60		LAST	+33	5174.9	7.36	11.0	
AHS	70		PRE	-2.63	5195	22.2	31	-2.008
AHS	70		LAST	+19.6	5092.7	14.5	20	
AHS	90		PRE	+3.187	4800	8.39	15.4	-0.292
HH	90		LAST	+23.1	4786	9.1	16	
HH	50	3	PRE	+17.2	4993.8	9.63	15.97	-0.242
HH	50		LAST	+18.5	4981.7	7.37	14	
HH	60		PRE	+8.89	5064	18.76	26.2	-2.43
HH	60		LAST	+32.9	4944	8.88	22	
AHS	70		PRE	-10.1	5072.6	15.2	37.1	-3.52
AHS	70		LAST	+28.1	4900	13.5	21	
AHS	90		PRE	+6.485	4703	7.9	16.65	-0.879
HH	90		LAST	+21.4	4662	12.3	26.8	
HH	50	4	PRE	+2.2	5008	11.67	19.1	+0.636
HH	50		LAST	+23.3	5039.9	1.89	4.0	
HH	60		PRE	+8.45	5022.5	17.78	40.7	+1.204
HH	60		LAST	+20.3	5083	7.2	11.0	
AHS	70		PRE	-19.6	5058.5	8.47	16.47	-1.435
AHS	70		LAST	+13.44	4986.9	14.2	30	
AHS	90		PRE	+0.065	4718.6	5.99	10.0	0.0
HH	90		LAST	+20	4718.7	14.7	28	
HH	50	5	PRE	+22.9	5033.6	5.33	7.7	+0.623
HH	50		LAST	+28.1	5065	5.88	14	
HH	60		PRE	+25.06	5082	24.89	57.4	+1.062
HH	60		LAST	+30.6	5136	8.9	17	
AHS	70		PRE	-7.65	5098.9	11.8	19.3	-1.855
AHS	70		LAST	+20.7	5006	16.8	32	
AHS	90		PRE	-0.795	4774	6.046	10.77	-0.251
HH	90		LAST	+28.9	4762	11.3	19	

Run By	Temperature (°F)	Channel	Run Type	Intercept (mv)	Slope (mv/flux)	σ (mv)	Maximum Deviation (mv)	% Slope Change
HH	50	6	PRE	+21.6	10778.9	10.55	22.8	+
HH	50		LAST	+22.1	11896	11.5	22	
HH	60		PRE	+1.37	11292	12.7	19.1	+
HH	60		LAST	+49.6	11899	20		
AHS	70		PRE	-5.01	11040	22.2	35.6	+
HH	70		LAST	+38.8	11870	15.86	23	
HH	90		PRE	+15.2	10613	13.3	21.1	
AHS	90		LAST	+7.04	11359	13.7	22	
HH	50	7	PRE	+20.5	13997	19.3	34.4	-4.229
HH	50		LAST	+51.67	13429	14	31	
HH	60		PRE	+15.8	14316	15.3	31.9	-3.334
HH	60		LAST	+42.7	13854	10.8	15	
AHS	70		PRE	-3.83	14065	11.44	26.3	-4.619
HH	70		LAST	+44	13444	17.8	36	
HH	90		PRE	+30.89	13472	16.3	27	-3.447
AHS	90		LAST	-3.14	13023	28.2	48	
HH	50	8	PRE	+24.1	13025	16.7	38	-0.393
HH	50		LAST	+43	12974	12.8	26	
HH	60		PRE	-0.916	13630	10.58	18.1	-1.617
HH	60		LAST	+25	13413	7.3	13.5	
AHS	70		PRE	-10.4	13602	8.45	14.7	-3.959
HH	70		LAST	+36.6	13084	9.81	23.3	
HH	90		PRE	+12.3	12974	17.11	33.3	-2.707
AHS	90		LAST	-9.5	12632	21.4	36	
HH	50	9	PRE	+18.6	13413	26.7	58.1	+0.387
HH	50		LAST	+29	13465	10.5	19	
HH	60		PRE	+18.1	13834	14.17	25.4	-0.835
HH	60		LAST	+47	13719.4	15.02	27	
AHS	70		PRE	-14.5	13840.9	6.587	12.4	-0.369
HH	70		LAST	+8.8	13790	20.4	29	
HH	90		PRE	+28.1	13333	22.2	33.0	-4.19
AHS	90		LAST	+12	12797	14	22	
HH	50	10	PRE	+13.03	11568	16.8	37.5	+1.106
HH	50		LAST	+28.6	11696	14.8	28	
HH	60		PRE	-12.64	12382	7.5	12.8	-2.098
HH	60		LAST	+42.6	12127.5	11.9	25	
AHS	70		PRE	+7.46	12328	8.51	16.9	-0.751
HH	70		LAST	+31	12236	8.8	14	
HH	90		PRE	+4.39	12210	21.91	55.6	-2.933
AHS	90		LAST	+0.90	11862	6	11	

The results of the F-2 calibration can be summarized as follows. See Tables 14, 15, and 16.

Table 14. - This table gives the changes in calibration resulting from environmental stress. Effects of temperature were minimized because all runs were made at 80°F. All gain (slope) changes are compared to the "last" readings. Slope changes for Channels 1 and 6 were omitted owing to loading effects described earlier.

1. Radiometer B (Channels 1 through 5) shows generally less scatter (smaller σ) than Radiometer A, which is to be expected from the higher S/N ratio of Radiometer B.

2. Both radiometers have standard deviations considerably smaller than the rms value of the noise which was about 50 millivolts (mv) for Radiometer A and 20 mv for Radiometer B. This is a good indicator of the value of the reading technique because the peak-to-peak noise actually seen on the scope is about 200 mv for Radiometer A and 80 mv for Radiometer B.

3. All intercepts are consistent from channel to channel, both as a result of temperature changes and as a result of environmental stress, indicating that a common causal factor exists such as the power supply, or perhaps the calibrating fixture itself.

4. Clearly, an apparent shift in calibration occurred between the "Pre" and "Last" runs. The shift was consistently larger in Radiometer A than Radiometer B. On the other hand a reasonably small change was observed for the two runs "post" and "last."

Table 15. - This table presents a summary of results taken at instrument temperatures other than 80°F. Complete temperature runs (50°F to 90°F) were made only on the "pre" and "last" runs. The data have been arranged so that readings taken at the same instrument temperature can be compared. As can be seen, not all the gains changed a similar amount or in the same direction.

Table 16. - This table gives F-2 data arranged to show the temperature dependence of the calibration independent of environmental stress. Two sets of data are compared however; "pre" and "last."

The bolometer responsivity is, of course, temperature dependent. Because of the finite input impedance of the preamplifier the responsivity is not a perfectly monotonic decreasing function of increasing temperature. Rather, the responsivity curves tend to be double-valued with a peak in the 60°F to 70°F range. Originally, when the 10-micron thick thermistor flakes

Table 16. F-2 Calibration Data Arranged to Show Temperature Effects

Channel	Temperature (°F)	Slope (Gain)				
		"Pre"	% Change Max. to Min.	"Last"	% Change Max. to Min.	% Change "Pre" to "Last"
Radiometer B	50	5,186		5,214 Max.		
	60	5,247 Max.		5,175		
2	70	5,195	8.5%	5,093	8.25%	1.97%
	80	5,076		4,964		
	90	4,800 Min.		4,786 Min.		
Radiometer B	50	4,994		4,982 Max.		
	60	5,064		4,944		
3	70	5,073 Max.		4,900	6.4%	3.44%
	80	4,986	7.3%	4,865		
	90	4,703 Min.		4,662 Min.		
Radiometer B	50	5,008		5,040		
4	60	5,023		5,083 Max.		
	70	5,059 Max.		4,986		1.44%
	80	4,954	6.75%	4,889	7.1%	
	90	4,719 Min.		4,719 Min.		
Radiometer B	50	5,034		5,065		
	60	5,082		5,136 Max.		
5	70	5,099 Max.		5,006	7.25%	1.82%
	80	5,033	6.4%	4,911.5		
	90	4,774 Min.		4,762 Min.		
Radiometer A	50	13,997		13,429		
	60	14,316 Max.		13,854 Max.		3.3%
7	70	14,065	5.9%	13,444	6.0%	
	80	13,802		13,245		
	90	13,472 Min.		13,023 Min.		
Radiometer A	50	13,025		12,974		
	60	13,630 Max.		13,413 Max.		1.6%
8	70	13,602	4.8%	13,084	5.8%	
	80	13,439		12,773		
	90	12,974 Min.		12,632 Min.		
Radiometer A	50	13,413		13,465		
	60	13,834		13,719		
9	70	13,841 Max.		13,790 Max.		0.37%
	80	13,786	3.7%	13,376	7.25%	
	90	13,333 Min.		12,797 Min.		
Radiometer A	50	11,568 Min.		11,696 Min.		
	60	12,382		12,126	4.4%	
10	70	12,328	9.4%	12,236 Max.		1.09%
	80	12,761 Max.		12,198		
	90	12,210		11,862		

were considered for this application the calculated change in responsivity was 3% from the maximum to minimum value. The thermistors actually used, however, were a thinner 6-micron thick high resistance type, the temperature dependence of which was undetermined but probably was higher than the 10-micron type. About 1 to 1.5% can be attributed to the electronics. In any event, Table 16 shows that the maximum change in system gain is in the 6 to 8.5% range. Changes this large were not expected but show fairly good consistency between channels. The changes for Channels 9 and 10 are atypical and unexplained.

The last column of the table gives the change in gain at the point of maximum gain between "pre" and "last" or at 70°F if the maxima did not occur at the same temperature. However, the apparent changes in calibration resulting from environmental stress appeared to be smaller at or near the maximum gain temperature than at 80°F (see Table 14).

Signal-to-Noise Considerations

The results of the first calibration measurements performed on the 14- to 16-micron radiometer revealed that the radiometric sensitivity of the system was a factor of 2 below the specified value. This loss of sensitivity was attributed to the following factors:

1. Responsivity loss of detector from that specified in proposal: 1.33. This is because the increased responsivity of the 4-megohm flake compared to the original 2.5-megohm flake was more than offset by the increase in Johnson's noise.
2. In the proposal, 80 Hz was used as the system noise bandwidth. The actual equivalent noise bandwidth is 125 Hz for a system having a response 6 db down at 80 Hz with a -12 db/octave slope. The loss factor is 1.25.
3. The IFOV in the long dimension was 0.07° instead of 0.10°. The reasons for this are explained on page 69. The loss factor is 1.43.

The product of these factors is 2.37.

Modifications were made to the system to improve the S/N ratio. They are as follows:

1. The electrical bandpass was narrowed from 80 Hz to 70 or 60 Hz depending on the radiometer. The expected improvement was 1.07 or 1.16. The actual reduction in noise, as measured on a Flow true rms meter, was 1.73.

2. The bias supply (32.5 volts) was replaced with mercury batteries (40.5 volts). This change gave several advantages:

   a. Increase in responsivity: factor of 1.25.

   b. Improvement in noise. The bias supply contributed 1/f noise to the system (see Monthly Report No. 13, page 11). Mercury batteries do not appear to have this problem. The measured improvement in system noise was 1.16.

   c. The battery supply eliminates line regulation problems associated with the original supply.

Total improvement should therefore be:

$$1.73 \times 1.25 \times 1.16 = 2.52$$

Error Analysis of the F-2 Radiometric Calibration

Two classes of errors will be explored in this analysis:

1. Repeatability Errors
   a. Spectrometric Measurements
   b. Subjective Reading Errors
2. Absolute Calibration Errors
   a. Errors in Emissivity of Blackbody Sources
   b. Errors in Temperature Measurements
   c. Absolute Systematic Reading Errors.

1. Repeatability Errors

a. Spectrometric Measurements. - Three types of errors can be associated with the spectrometer:

1) Spectrometer Wavelength Calibration Error. - The wavelength calibration is based on atmospheric absorption bands which afford a calibration accuracy of ±0.1 micron. Errors of this magnitude are not considered significant.

2) Amplitude Calibration Errors. - Reflectance and transmission measurements are made by calibrating the output meter to full scale with the test item out of the beam. With the test item in the beam, the reflectance (or transmittance) is measured. Thus, the absolute accuracy is minimal and for this analysis is negligible.

3) Repeatability Errors. - A Perkin-Elmer Model 112 Spectrometer with a cesium bromide prism was used for all reflectance measurements. The stated repeatability accuracy of the instrument is ± 1%, but at wavelengths beyond 20 microns, the lack of available signal reduces the accuracy. Similar errors exist for the filter transmission measurements, and although witness filters were not available for reference, extensive humidity testing of filters from the same lot was done with no observable degradation in transmission within the spectrometer accuracy.

The expression describing the output of the radiometer as a function of the optical parameters is

$$V = K_1[\rho_1\rho_3\rho_4 H_{BB} + (1 - \rho_1)\rho_3\rho_4 H_{M_1} - (1 - \rho_2)\rho_3\rho_4 H_{M_2} - \rho_2\rho_2\rho_4 H_{BB_o}] \underbrace{\rho_P\rho_S T_F R_D}_{\text{Radiometer}} \quad (1)$$

where ρ_1 = reflectance of the fixed folding mirror in the calibrator

ρ_2 = reflectance of the rotating chopping mirror in the calibrator

ρ_3 = reflectance of the primary mirror in the calibrator

ρ_4 = reflectance of the secondary mirror in the calibrator

H_{BB} = blackbody irradiance from the target blackbody

H_{BB_o} = blackbody irradiance from the cold reference blackbody

H_{M_1} = blackbody irradiance from the fixed folding mirror

H_{M_2} = blackbody irradiance from the rotating chopping mirror

K_1 = system gain constant

ρ_P, ρ_S, T_F and R_D refer respectively to the reflectance of the radiometer primary and secondary mirrors, the filter transmission, and finally the detector responsivity.

If $H_{M_1} = H_{M_2}$ and $\rho_1 = \rho_2$, then

$$V = K_1\rho_1\rho_3\rho_4(H_{BB} - H_{BB'_o})\rho_P\rho_S T_F R_D \quad (2)$$

Now, if it is assumed that the spectrometer has a repeatability error of ± 1%, it can be seen that the total error would be approximately

$$\epsilon_r \cong \pm\sqrt{n\Delta^2\rho} = \pm\sqrt{3\%}$$

from the reflectance measurements of the three optical surfaces in the calibrator. Relative response measurements are sufficient for the mirrors in the radiometer because only a determinable scale factor is involved.

An error of ± 1% is assigned to the combined spectral measurements of the filter and the detector array. Only errors in wavelength calibration are considered.

$$\epsilon_{fd} \cong \pm 1\%$$

In actual practice it has been found that because the LN_2 pipes in the calibrator are routed close to the fixed mirror, its temperature is considerably lower than that of the rotating mirror. Thus,

$$H_{M_1} \neq H_{M_2}$$

and equation (1) applies.

The temperature of the fixed mirror was measured during calibration but it was impractical to measure the temperature of the moving mirror. Instead, the temperature of nearby supporting structure was assumed for the mirror. However, no specific error could be assigned to this effect.

The total error attributed to spectrometric measurements is therefore:

$$\epsilon \cong \sqrt{\epsilon_r^2 + \epsilon_{fd}^2} = \sqrt{4\%}$$

b. Subjective Repeatability Errors. - Owing to the low S/N ratio of the system, it is felt that the largest source of repeatability error is in the reading of the waveform from the face of the oscilloscope. As presented on the scope, the peak-to-peak noise is about 200 mv or 8% of full output for the 14- to 16-micron radiometer and 100 mv or 4% for the 20- to 35-micron radiometer. The task is to read the peak-to-break value of a 5-Hz square wave by superimposing a chopped dc voltage on the waveform so as to bisect the noise top and bottom. This can be done fairly successfully in spite of the noise because of the integrating ability of the eye. Typical standard deviations for individual runs are about 1% of full scale for the 14- to 16-micron radiometer and 0.5% for the 20- to 35-micron radiometer.

Although the consistency of data is good for each run when the conditions are constant, it is felt that errors can result from reading the data differently at different times. For example, the vertical sensitivity of the scope is always set at 0.5 volt/cm which means that the smallest division

(2 mm) is equal to 100 mv. The trace width, depending on the lighting conditions and focus, can correspond to as much as 25 mv. Parallax and nontracking of the two preamplifiers can account for another 25 mv. Thus, these two effects combined could amount to a 2% change in slope. In general, the error is proportional to noise so that reading errors on the 14- to 16-micron radiometer are about twice those on the 20- to 35-micron side.

Errors of 1 to 2% between runs taken by one operator and another can be regarded as repeatability errors when comparing runs taken by each man.

Total repeatability errors in reading data points, then, are

$$\epsilon_{read(repeat)} \cong \pm 2 \text{ to } \pm 4\%$$

2. Absolute Calibration Errors

a. Errors in Emissivity of Blackbody. - The parameters of the blackbodies are specified to give an effective emissivity of 0.995. These specifications were followed exactly during the design and fabrication of the blackbodies. Moreover, the condition of the surface within the cones was checked periodically to ensure that the paint was not chipped or otherwise damaged.

Assuming that both blackbodies are identical, as they indeed appeared to be, the absolute calibration error is

$$\epsilon_{BB} = \pm 0.5\%$$

b. Errors in Temperature Measurements. - Blackbody temperatures were measured with copper-constantan thermocouples imbedded in the blackbody close to the tip of the conical cavity. One thermocouple was provided for the reference blackbody (reflected from the fixed mirror) and two for the variable body (reflected from the moving mirror). One continuous piece of thermocouple wire was used from the junction to the potentiometer bridge. No solder joints or connectors of any kind that might have acted as thermocouples were used.

The calibration of the thermocouples was checked at two points (LN_2 and ice bath) prior to installation in the blackbodies. The reference junctions were placed in an ice bath (0°C). Thermocouple No. 1 was mounted in the blackbody referenced to the rotating mirror. The measuring instruments utilized were a Leeds and Northrup direct reading potentiometer and a Honeywell millivolt bridge. The readings in Table 17 were recorded for the thermocouples indicated. Each reading was checked for repeatability.

Table 17. Thermocouple Readings Before Mounting in Blackbody

Thermocouple No.	Ice Bath (+32°F)		LN_2	
	Honeywell Bridge (mv)	Leeds & Northrup Potentiometer (°F)	Honeywell Bridge (mv)	Leeds & Northrup Potentiometer (°F)
1	-0.020	+32.1	-5.496 (-323.2°F)*	-322.5
2	-0.020	+32.0	-5.501 (-323.8°F)*	-324.0
3	-0.012	+32.0	-5.501	-324.0

*Read from published table.

The data were compared with standard published Copper versus Constantan Thermocouple Conversion Tables prepared by the Leeds and Northrup Company. There was a minus (-) 0.020 mv offset in the data from the published data, which was observed at both LN_2 and ice bath temperatures. This was assumed to be a constant offset over the entire temperature range, and a calibration curve was drawn (with 0.020 offset) parallel to a curve generated from the published data.

The thermocouples were mounted in the blackbodies and the blackbodies installed in the calibrator. LN_2 was transferred through the blackbodies and the readings in Table 18 were taken after appearance at LN_2 transfer and stabilization.

Table 18. Thermocouple Readings After Mounting in Blackbody

Thermocouple No.	LN_2	
	Honeywell Bridge (mv)	Leeds & Northrup Potentiometer (°F)
1	-5.394	-312
2	-5.446	-318
3	-5.449	-318

As is noted in the above data, the readings are consistently higher than the previous readings with the thermocouple junction alone, before insertion into the blackbody. The reason for not being able to achieve LN_2 temperature is due to the heat loss in the calibrator assembly. Lower temperatures were attained when testing the prototype and F-1 units as compared to the F-2 radiometer. Probable causes of this are due to the following changes made in the blackbody assemblies.

1) The original stainless steel blackbody cavity inlet and exhaust tubing was replaced with copper tubing because of leak problems at the copper blackbody-stainless steel tubing joint. Evidently the copper tubing provided an appreciable heat loss path from the blackbodies.

2) The original thermocouple wire was replaced with larger diameter wire providing another possible heat loss path. The original smaller diameter wire was very fragile for the application, regularly breaking and requiring repair.

Prior to recalibration of F-2, the blackbody corresponding to the rotating mirror was removed from the calibrator and the temperature calibration at LN_2 checked. LN_2 was poured into the cavity and between the cavity and vacuum wall until stabilization was achieved. After stabilization, the temperature readout was performed. The following is a listing of the readings which agree within 5/8°C of the original. The difference possibly is a heat loading path of air as opposed to the condition with just the thermocouple alone.

Thermocouple No. 2	-5.495 mv
Thermocouple No. 3	-5.491 mv

In terms of errors in irradiance, the two cases shown in Table 19 can be assumed: minimum calibration temperature (130°K for 20- to 35-micron radiometer and 150°K for 14- to 16-micron radiometer), and maximum calibration temperature (250°K for both).

Table 19. Irradiance Error Corresponding to a Temperature Error of 1°C

Temperature (°K)	14- to 16-Micron Radiometer (%)	Temperature (°K)	20- to 35-Micron Radiometer (%)
150	±4.8	130	±3.9
250	±1.88	250	±1.11

ϵ_T = 1°C is assumed for temperature error.

The values stated in Table 19 are percentages of the total irradiance in the spectral band at the indicated temperature. Thus, in terms of the 14- to 16-micron radiometer output voltage, an error of about 10 mv would be present at the low end of the curve and about 50 mv at the 2.5-volt level, which means that the slope of the curve has changed essentially 2%. It is clear, then, that relatively minor changes in temperature measurement can produce sizable absolute calibration errors.

c. Absolute Systematic Reading Errors. - Most reading errors would fall into the repeatability error category. One not in this area is the effect of reading the noisy square wave signal differently at high and low levels. The intent is to read the voltage excursion from the peak of the waveform to the break. However, owing to the noise it is difficult to tell where the break is at low signal levels. The tendency is to read the peak-to-peak values at low signal levels which, when combined with the upper, correctly read points, causes the least square line to have a slightly lower slope and slightly positive intercept. Since the droop in the chopped waveform is about 10% owing to the low-frequency rolloff, the signals in the range 0.20 to 0.5 volt could be as much as 20 to 50 mv too high.

It can also be expected that there is a consistent bias in the data resulting from other subjective effects. For example, it has been found that for two identical runs, one operator has read data points about 1 to 2% higher than another. (The higher value is for the 14- to 16-micron radiometer.) Hence, one can only assume that absolute errors are at least this amount. Absolute reading errors, then, are

$$\epsilon_{read} \cong \pm 2\%$$

The errors discussed in the foregoing discussion are summarized in Table 20.

Table 20. Summary of Errors

Paragraph	Error Type	14- to 16-Micron Radiometer (%)	20- to 35-Micron Radiometer (%)
1a	Spectrometric Errors	±2	±2
1b	Subjective Reading Errors	±4	±2
Total	Repeatability Errors	±4.47	±2.83
2a	Blackbody Emissivity Errors	±0.5	±0.5
2b	Temperature Errors	±1.88	±1.1
2c	Reading Errors	±2	±1
Total	Absolute Errors	±2.8	±1.56
Total	Repeatability and Absolute Errors	±5.28	±3.23

NATIONAL AERONAUTICS AND SPACE ADMINISTRATION
WASHINGTON, D.C. 20546

OFFICIAL BUSINESS

FIRST CLASS MAIL

POSTAGE AND FEES PAID
NATIONAL AERONAUTICS AN
SPACE ADMINISTRATION

POSTMASTER: If Undeliverable (Section 15
Postal Manual) Do Not Ret

"The aeronautical and space activities of the United States shall be conducted so as to contribute . . . to the expansion of human knowledge of phenomena in the atmosphere and space. The Administration shall provide for the widest practicable and appropriate dissemination of information concerning its activities and the results thereof."

—NATIONAL AERONAUTICS AND SPACE ACT OF 1958

NASA SCIENTIFIC AND TECHNICAL PUBLICATIONS

TECHNICAL REPORTS: Scientific and technical information considered important, complete, and a lasting contribution to existing knowledge.

TECHNICAL NOTES: Information less broad in scope but nevertheless of importance as a contribution to existing knowledge.

TECHNICAL MEMORANDUMS: Information receiving limited distribution because of preliminary data, security classification, or other reasons.

CONTRACTOR REPORTS: Scientific and technical information generated under a NASA contract or grant and considered an important contribution to existing knowledge.

TECHNICAL TRANSLATIONS: Information published in a foreign language considered to merit NASA distribution in English.

SPECIAL PUBLICATIONS: Information derived from or of value to NASA activities. Publications include conference proceedings, monographs, data compilations, handbooks, sourcebooks, and special bibliographies.

TECHNOLOGY UTILIZATION PUBLICATIONS: Information on technology used by NASA that may be of particular interest in commercial and other non-aerospace applications. Publications include Tech Briefs, Technology Utilization Reports and Notes, and Technology Surveys.

Details on the availability of these publications may be obtained from:

SCIENTIFIC AND TECHNICAL INFORMATION DIVISION

NATIONAL AERONAUTICS AND SPACE ADMINISTRATION

Washington, D.C. 20546